

University of Warsaw
Faculty of Mathematics, Informatics and Mechanics

Piotr Minakowski

Fluid Model of Crystal Plasticity - Mathematical Properties
and Computer Simulations

PhD dissertation

Supervisors

prof. dr hab. Piotr Andrzej Gwiazda

Institute of Applied Mathematics and Mechanics
University of Warsaw

prof. RNDr. Josef Málek, CSc., DSc.

Mathematical Institute
Charles University in Prague

June 2015

Author's declaration:

aware of legal responsibility I hereby declare that I have written this dissertation myself and all the contents of the dissertation have been obtained by legal means.

June 1, 2015

date

.....

Piotr Minakowski

Supervisors' declaration:

the dissertation is ready to be reviewed

June 1, 2015

date

.....

prof. dr hab. Piotr Andrzej Gwiazda

.....

prof. RNDr. Josef Málek, CSc., DSc.

Abstract

Looking at severe plastic deformation experiments, it seems that crystalline materials at yield behave as a special kind of anisotropic, compressible, highly viscous fluid. In the presented approach the plastic behaviour of crystalline solids is treated as a highly viscous material flow through an adjustable crystal lattice.

The main purpose of this dissertation is to investigate model of a plastic flow of a highly viscous fluid that describes the ultrafine structure formation induced by severe plastic deformation. The idea behind is to apply and further develop methods known from fluid mechanics to modelling crystal solids.

We first provide the thermodynamic description of a fluid like - Eulerian model of crystal plasticity. The model derivation is based on the application of the Gibbs potential to obtain a rate type stress strain constitutive relation. The result is compared to the approaches of traditional plasticity.

The second part of this thesis is devoted to the mathematical analysis of a simplified problems originating from the visco-elastic model derived to describe flows of crystal plastic materials. Even after simplifications, neglecting the plastic effects, the problem seems to be difficult to establish local-in-time existence of a smooth solution and the existence of a weak solution. We propose a regularisation of the stress evolution equation and prove the global-in-time existence of a weak solutions, in the case of two dimensional bounded domain, for general initial data. The results, obtained by the Galerkin method, hold true for the periodic case.

We then give a thorough description of the numerical methods used in the dissertation. Necessary tools in order to discretize the fluid model of crystal plasticity both in space and time, such that: triangulation of a domain, proper finite dimensional spaces and time discretization schemes, are recalled. The discrete system resulting from the weak formulation of the considered system is solved by means of the Newton's method.

Further the results of numerical simulations are reported. Performed simulations aim to justify that the presented approach is capable of capturing large strains in typical experimental settings. We give a detailed description of performed numerical simulations. Two different deformation settings were considered: uniaxial compression and channel extrusion. In the case of a simple compression we deal with a free boundary problem. For this reason we employ the Arbitrary Lagrangian Eulerian (ALE) approach in the sense that we use the Eulerian formulation on a moving mesh which captures the free boundary. As a test example we analyse a plane strain compression in a channel die and an uniaxial compression of a pillar-shaped sample. The second case focuses on 2-turn equal channel angular pressing (ECAP) in two dimensions. We take advantage of the Eulerian formulation and obtain high strains in a single 2-turn ECAP pass.

Keywords

crystal plasticity, large deformations, constitutive theory, weak solution, global existence, crystal plasticity finite elements

AMS Mathematics Subject Classification

74-XX, 74A20, 74E15, 74S05, 35D30, 65M60

Acknowledgements

Hereby I thank all who have supported my efforts to write this work.

I would like to express my deep gratitude to both of my supervisors, Professor Piotr Andrzej Gwiazda, and Professor Josef Málek for their inspiring leadership and enthusiastic encouragement.

I am very grateful for the hospitality that I met at the Charles University in Prague, where I spent two years of my Ph.D. studies. In particular, I thank prof. RNDr. Jan Kratochvíl, and doc. RNDr. Martin Kružík, Ph.D. for their advice in mathematical modelling and RNDr. Jaroslav Hron, Ph.D. for help with the numerical simulations.

Moreover, I am very thankful to Professor K.R. Rajagopal who shared with me his expertise in the modelling of plastic materials.

I would like to thank sincerely to all of my colleagues from the Faculty of Mathematics, Informatics and Mechanics, University of Warsaw and the Faculty of Mathematics and Physics, Charles University in Prague for the fruitful discussions and the unique and friendly atmosphere they created. I was fortunate to work with Jan Burczak, Ph.D. who served as an aid to mathematical analysis.

Moreover, I would like to acknowledge the support of the following projects and grants: International Ph.D. Projects Programme of the Foundation for Polish Science operated within the Innovative Economy Operational Programme 2007-2013 (Ph.D. Programme: Mathematical Methods in Natural Sciences), the National Science Centre (Poland) grant *Numerical simulations of severe plastic deformations by flow model of crystal plasticity*, no. 2012/07/N/ST1/03369, and the Grant Agency of Czech Republic grant: *Modelling of ultra-fine deformation substructure causing enhance strength of materials*, no. P107/12/0121.

Podziękowania

Dziękuję wszystkim, którzy wspierali moje wysiłki w pisaniu rozprawy doktorskiej.

Chciałbym wyrazić głęboką wdzięczność dla moich promotorów: profesora Piotra Andrzeja Gwiazdy oraz profesora Josefa Máłka za ich ciągle zachęcanie mnie do pracy, niezliczone cenne uwagi oraz konstruktywną krytykę na każdym etapie badań.

Jestem bardzo wdzięczny za gościnność, której doświadczyłem na Uniwersytecie Karola w Pradze, gdzie spędziłem dwa lata podczas studiów doktoranckich. W szczególności dziękuję profesorowi Janowi Kratochvílowi oraz profesorowi Martinowi Kružíkowi za pomoc w modelowaniu matematycznym. Podziękowania dla profesora Jaroslava Hrona za współpracę przy symulacjach numerycznych.

Ponadto dziękuję bardzo profesorowi K.R. Rajagopalowi, który podzielił się ze mną swoją wiedzą z zakresu modelowania materiałów plastycznych.

Serdecznie dziękuję wszystkim koleżankom i kolegom z Wydziału Matematyki, Informatyki i Mechaniki Uniwersytetu Warszawskiego oraz Wydziału Matematyki i Fizyki Uniwersytetu Karola w Pradze za owocne dyskusje i wyjątkowo przyjazną atmosferę, którą stworzyli. Miałem szczęście pracować z doktorem Janem Burczakiem, który służył pomocą w analizie matematycznej.

Ponadto, chciałbym podziękować za wsparcie otrzymane w ramach następujących projektów i grantów: Międzynarodowy Program Projektów Doktoranckich Fundacji na rzecz Nauki Polskiej w ramach Programu Operacyjnego Innowacyjna Gospodarka 2007-2013 (Ph.D. Programme: Mathematical Methods in Natural Sciences), Narodowe Centrum Nauki grant: *Symulacje numeryczne dużych odkształceń plastycznych przy pomocy modeli plastycznego płynięcia*, nr 2012/07/N/ST1/03369 oraz Agencja Grantowa Republiki Czeskiej grant: *Modeling of ultra-fine deformation substructure causing enhance strength of materials*, nr P107/12/0121.

Contents

Introduction	13
0.1 Origin of the problem	13
0.2 Techniques for severe plastic deformation processing	14
0.2.1 Equal-channel angular pressing	14
0.2.2 High-pressure torsion	14
0.3 Framework and outline of the thesis	15
0.3.1 Modelling of large deformation crystal plasticity	15
0.3.2 Mathematical analysis of a rate-type fluid model arising from crystal plasticity	16
0.3.3 Numerical methods and simulations	17
0.4 Potential applications	18
0.5 List of Notations	18
1 Mathematical modelling	21
1.1 Continuum Mechanics	21
1.1.1 Kinematics	21
1.1.2 Lagrangian and Eulerian description	22
1.1.3 Balance equations	23
1.2 Elasto-Visco-Plasticity	27
1.2.1 One-dimensional mechanical analogues	28
1.2.2 Viscoelasticity	29
1.2.3 One dimensional plastic element	29
1.2.4 Elasto/visco-plasticity	30
1.2.5 Generalization of one-dimensional models	31
1.3 Constitutive theory	32
1.3.1 Multiplicative decomposition of the deformation gradient	32
1.3.2 The additive decomposition of the velocity gradient	34
1.3.3 Stress-strain dependence	35
1.3.4 Gibbs potential approach - stress dependence	35
1.3.5 Elasticity	38
1.4 Crystal Plasticity	39
1.4.1 The evolution of the lattice	40
1.4.2 Single Crystal Hypothesis	41
1.4.3 The flow rule and hardening	42
1.4.4 The second law of thermodynamics	43
1.4.5 Implicit constitutive relation	43
1.5 Maximization of the rate of entropy production	45
1.5.1 Incompressibility	46
1.6 Non-dimensional scaling	47

1.6.1	Typical scales of the problem	50
1.7	Formulation of the problem	51
2	Mathematical analysis of a rate-type fluid model	53
2.1	Problem formulation	53
2.2	Overview of the known results	54
2.2.1	Visco-elastic fluids	54
2.2.2	Euler equation	55
2.3	Existence of a global weak solution	58
2.3.1	A priori estimates	58
2.3.2	Galerkin approximation	63
2.3.3	Uniform estimates	64
2.3.4	Estimate of the time derivative	64
2.3.5	Limit passage	65
2.3.6	L^p -estimates	66
2.3.7	Higher order local estimates	68
2.4	Regularization by $\Delta \mathbf{S}$	69
2.4.1	A priori estimates	69
3	Finite Element Formulation	73
3.1	The mesh	74
3.2	Space discretization	74
3.3	Time discretization	76
3.4	The discrete problem	76
3.4.1	The Newton solver	78
3.5	The choice of finite element space	78
3.5.1	Stress evolution stabilization	81
3.6	Arbitrary Lagrangian-Eulerian approach	81
3.6.1	Balance equations in the ALE coordinates	82
3.7	Implementation	83
4	Numerical examples	85
4.1	Plane strain compression of a single crystal	85
4.1.1	Channel-die compression	85
4.1.2	Finite element formulation	88
4.1.3	Three step algorithm	88
4.1.4	Comparison with experimental data	89
4.1.5	The influence of the rate sensitivity	89
4.1.6	Influence of initial angle of lattice rotation	90
4.1.7	Activity of slip systems	91
4.1.8	Stress-strain behaviour	92
4.2	Micropillar compression	93
4.2.1	Slip systems	94
4.2.2	Finite element formulation	95
4.2.3	Two step algorithm	95
4.2.4	Experimental Results	96
4.2.5	Results	96
4.3	2-turn Equal Channel Angular Extrusion	101
4.3.1	Evolution of slip systems	101

<i>CONTENTS</i>	11
4.3.2 Initial-boundary Value Problem	102
4.3.3 Finite Element Formulation	103
4.3.4 Results	104
5 Conclusions	107
List of Figures	111
A Functional spaces and technical lemmas	113
A.1 Definition of functional spaces	113
A.2 Bases consisting of eigenfunctions of an elliptic operator	113
A.3 Embedding theorems	114
A.4 Inequalities in Sobolev spaces	115
A.5 Compactness result	115
A.6 Ordinary Differential equations	116
B Analysis of two dimensional system	119
C Lagrangian and Eulerian coordinates	123
D Stress–strain dependence, the Helmholtz potential approach	125
E Frame-indifference principle	127
F Examples of the rate of entropy production	129
Bibliography	131

Introduction

0.1 Origin of the problem

The title of the thesis is Fluid Model of Crystal Plasticity - Mathematical Properties and Computer Simulations. The topic arises from the material science where the investigation of polycrystalline materials is of a great importance. In particular, the properties of materials are strongly related to their microstructure. Crystalline matter is anisotropic. This means that the instantaneous and time-dependent deformation of crystalline aggregates depends on the direction of the mechanical loads and geometrical constraints imposed. An essential consequence of the crystalline anisotropy of material is that its mechanical properties are orientation dependent.

We are interested in modelling and investigating large deformations of advanced materials, that outperform conventional materials with superior mechanical properties such as toughness, hardness, accompanied by relatively good ductility, and durability. Moreover, advanced materials may have also novel properties including the ability to memorize shape or respond to environmental changes, this is however beyond the scope of this dissertation.

The mechanical properties of crystalline materials are determined by several factors, the average grain size of the material plays a significant, and often a dominant, role. A new advanced materials can be developed by further grain refinement. In general, the smaller the grain size, the bigger the strength of a material. This behaviour is described through the empirical Hall–Petch relation $\sigma_y = \sigma_0 + k_y d^{-\frac{1}{2}}$, where σ_y stands for yield stress, σ_0 is friction stress, k_y is a constant of yielding, and d is grain size [1, 2]. Expected mechanical properties are exhibited by ultra fine grain (UFG) materials, namely polycrystals having very small grains with average grain sizes less than $1\mu\text{m}$.

Experimental studies show that applying severe plastic deformation (SPD) is suitable to obtain small grain size. SPD techniques are characterized by imposing high strains without introducing any change in the overall dimensions of the material. Several metal forming processes achieving severe plastic deformations are now available. Let us list major SPD processes:

- Equal channel angular pressing (ECAP), Segal [3, 4, 5],
- High pressure torsion (HPT), Bridgman [6, 7],
- Accumulative roll bonding (ARB), Saito, Tsuji, Utsunomiya, Sakai [8],
- Cyclic extrusion compression (CRC), Richert, Richert [9],
- Repetitive corrugation and straightening (RCS), Huang, Zhu, Jiang, Lowe [10].

For detailed description of SPD processes that are addressed in this work see Section 0.2. Note that conventional metal processing (extrusion or rolling) cannot impose very high strains because the dimensions of a sample are reduced.

The objective of this Ph.D. thesis is the development of a model able to capture the behaviour of crystalline material processed by severe plastic deformation. We aim to describe very large deformations, that are typical for fluid models, thus the Eulerian formulation is employed. Numerical simulation equipped with necessary mathematical analysis, can predict microstructure evolution, including the material hardening, shear band formation and strain localization.

0.2 Techniques for severe plastic deformation processing

The origin of metal processing goes back to the ancient age. At that time SPD processes were used in blacksmith's production to fabricate quality steel with superior properties, consisted of striking and repetitive folding and forging. We refer to the early metal-working of ancient China, the high-quality Damascus steel in the Middle East, and the Wootz steel in ancient India, see [11, 12].

Contemporary studies were started by Bridgman [6, 7] who introduced High-Pressure Torsion (HPT) process. He studied how the mechanical properties of materials can improve subjected to large deformation under high applied pressures. For his contribution to this field he was awarded the Nobel Prize in Physics in 1946.

The next breakthrough in the field of material science was the introduction of new analytical tools, such as orientation imaging microscopy, transmission electron microscope (TEM), and electron back-scatter diffraction (EBSD). These tools demonstrated that materials processed by SPD contain ultrafine grains.

We chose the equal channel angular extrusion and high pressure torsion because it has proven highly suitable for experimental and theoretical studies. The nature of the imposed deformation is a simple shear.

0.2.1 Equal-channel angular pressing

Since it was first developed by Segal [3, 4, 5], ECAP became a popular topic of investigation. A work piece is extruded several times through a die in the shape of curved channel with a 90° -angle turn. Each pass introduces additional strain, see Figure 1.

The main advantages of using ECAP, also known as equal channel angular extrusion (ECAE), in comparison to alternative experiments are minor changes in the cross-section of the billet and the possibility to look at various amounts of strain in a specimen. This is accomplished by extruding the work piece around a corner. ECAP owes its popularity to the following factors: its relatively simple setting, applicability to materials with different crystal structures, applicability to fairly large billets so that there is the potential for applications.

Moreover, in this work we also focus on multi-pass ECAP (e.g. 2-turn ECAP) as a simple method for imposing a high strain in a single pass of ECAP.

0.2.2 High-pressure torsion

As already mentioned, the studies of HPT originate in the early work of Bridgman [6, 7]. Later in the eighties the topic was extensively studied in Russia [13].

In a modern HPT facility a sample in the form of disk, is placed between two anvils. A plunger, the top anvil, applies compressive pressure (typically several GPa). Simultaneously, a support, the bottom anvil, rotates and imposes a torsional strain.

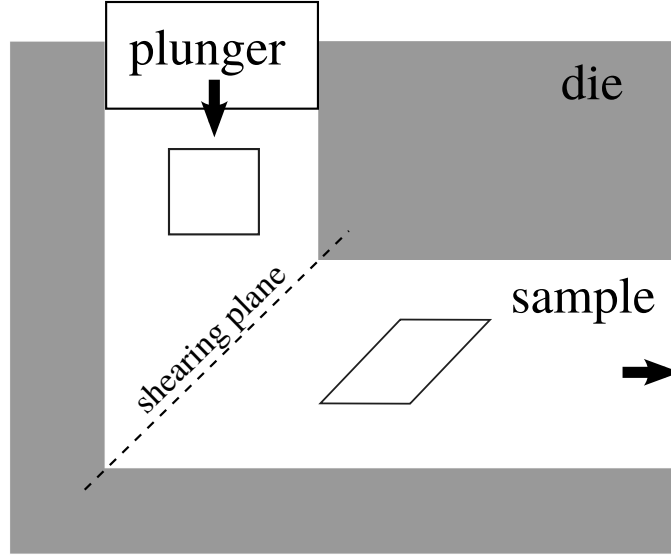


Figure 1: Schematic illustration of a typical ECAP facility, showing the shearing plane within the die.

0.3 Framework and outline of the thesis

The thesis consists of three broad areas: mathematical modelling of responses of elasto-viscoplastic materials, mathematical analysis of newly developed models, and the development of numerical schemes to capture the behaviour of such materials. In the centre of this overall investigation are fully Eulerian models for large deformations of crystal plastic materials.

0.3.1 Modelling of large deformation crystal plasticity

To start with, the approach via continuum mechanics is recalled. After a review of kinematics, balance equations, and the second law of thermodynamics we discuss one-dimensional mechanical analogues of elasto-viscoplastic elements. It provides a motivation for consideration of a rate type material models.

Later in Section 1.3 we address a constitutive theory, focusing on a stress-strain relation. Starting point to the modelling of large deformation plasticity is to employ the multiplicative decomposition of the deformation gradient. We present two approaches to modelling large deformations. Multiplicative decomposition by Kroner [14, 15] and natural configuration by Rajagopal [16, 17], both lead to the additive decomposition of the deformation gradient, but are based on different thermodynamical basis.

Following the paper by [18], we employ the Gibbs potential to derive an equation, which describes the evolution of the Cauchy stress. For detailed discussion on models of a rate type

$$f(\dot{\mathbf{T}}, \mathbf{T}, \mathbf{L}) = 0, \quad (1)$$

where the constitutive relation contains the Cauchy stress \mathbf{T} , the rate of stress $\dot{\mathbf{T}}$, and the velocity gradient \mathbf{L} , we refer to [19, 18]. The comparison between the derivation of the rate type stress-strain relation using the Helmholtz and the Gibbs potential is given. The emphasis is on the

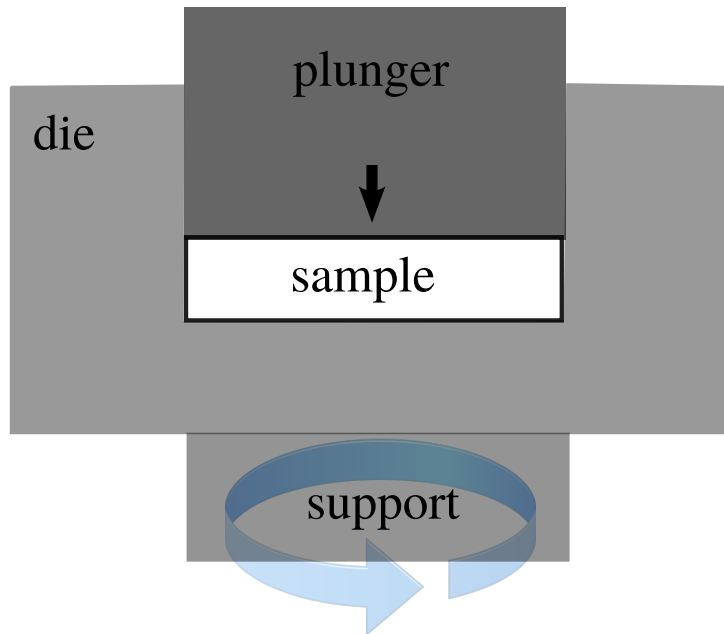


Figure 2: Schematic illustration of a typical HPT facility.

application of the Gibbs potential to obtain a rate-type model, describing flow of crystal plastic material through adjustable lattice.

Next step is to equip the derived model with plastic effects. Section 1.4 covers the description of crystal plastic behaviour and introduces all necessary variables and constitutive assumptions. For formulation of rate dependent flow rule and hardening law, we refer to early references such as Asaro et al.[20, 21, 22] and Hill et al. [23].

Later in Section 1.4.5 we discuss possible extension of the rate dependent flow rule by a rate independent implicit constitutive relation, see [24, 25].

Finally we employ a maximization of the rate of entropy production principle [16, 17] to derive governing equations for crystal plasticity on a different thermodynamic basis. The goal is to replace the single crystal hypothesis, by postulating proper rate of dissipation function, see Section 1.5.

The obtained model is fully Eulerian. What is important is the Eulerian description of the evolution of the crystal lattice. The classical derivation is compared to a new way of deriving crystal plasticity equations. In particular we aim to focus on underlying assumptions, advantages and drawbacks.

0.3.2 Mathematical analysis of a rate-type fluid model arising from crystal plasticity

Chapter 2 addresses mathematical properties of the incompressible version of considered model. We make several simplifying assumptions and analyse a model that captures essential mathematical difficulties. Despite our effort we were unable to show the existence of the solution to the derived system, see Appendix B. Therefore, attention is focused on particular regularization that enables us to prove the global in time existence of a weak solution. Note that in comparison with standard Maxwell type fluid model considered system lacks viscous contribution to the momentum balance. The proposed regularisation helps us to improve a priori estimates that are then shown to be sufficient to establish the large data existence of a weak solution.

0.3.3 Numerical methods and simulations

Numerical analysis of the derived models is based on the Finite Element Method. In Chapter 3 we give a thorough description of the numerical methods used in the dissertation. To start with we provide a brief overview of Crystal Plasticity Finite Element Methods as well as Finite Element Methods dedicated to visco-elastic problems.

Later in Sections (3.1)-(3.4.1) we recall necessary tools in order to discretize the fluid in model of crystal plasticity both in space and time, such that: triangulation of a domain, proper finite dimensional spaces and time discretization schemes. The discrete system resulting from the weak formulation of the considered system is solved by means of the Newton's method. Also the discussion on the choice of finite elements focuses on velocity-pressure-stress triples, that satisfy the stability condition is provided, see Section 3.5.

Section 3.6 covers an Arbitrary Lagrangian Eulerian (ALE) method to study free boundary problem. The crystal plasticity equation are reformulated in ALE coordinates, which enables us to compute the problems in time-varying domains.

Finally, in Chapter 4 the results of performed numerical simulations are discussed in detail. We present three numerical examples: channel-die compression, micropillar compression, and 2-turn equal channel angular extrusion. The first two settings refer to experimental studies and are dedicated to comparison of the results, see [26, 27]. We propose a finite element discretization scheme for a numerical solution in an Arbitrary Lagrangian Eulerian coordinates. Our numerical predictions are in a good agreement with experiments. The third one is a novel computational example, motivated by papers of Rosochowski and Olejnik, [28, 29]. We show that elastic stretches are important part of the model, because they allow us to reduce high values of stress in the vicinity of inner turns of the 2-turn channel.

All numerical computations are performed for system describing crystal plasticity in Eulerian coordinates and we solve fully coupled problems. We show the ability of our model to capture high strains, in particular in the case of compression we are able to cover nominal strain up to 0.4.

We conclude with a short overview of achieved results.

Some of the results presented in this thesis are published in the peer-reviewed journals:

- P. Minakowski, J. Hron, J. Kratochvíl, M. Kružík, J. Málek, *Plastic deformation treated as material adjustable crystal lattice flow through crystal lattice*, Materials Science and Engineering, IOP Conference Series, Vol. 63, 012130
<http://doi:10.1088/1757-899X/63/1/012130>
- P. Minakowski, *Fluid Model of Crystal Plasticity: Numerical Simulations of 2-turn Equal Channel Angular Extrusion*, Technische Mechanik, 2014, 34, 213-221,
http://www.ovgu.de/ifme/zeitschrift_tm/2014_Heft3_4/07_Minakowski_color.pdf

Additional results in the theory of anisotropic Orlicz spaces and its applications in continuum mechanics are published here:

- P. Gwiazda, P. Minakowski and A. Wróblewska-Kamińska, *Elliptic problem in generalized Orlicz-Musielak spaces*, Central European Journal of Mathematics, December 2012, Volume 10, Issue 6, 2019-2032, <http://link.springer.com/article/10.2478/s11533-012-0126-3>
- P. Gwiazda, P. Minakowski and A. Świerczewska-Gwiazda, *On the anisotropic Orlicz spaces applied in the problems of continuum mechanics*, Discrete and Continuous Dynamical Systems. Series S., (Vol. 6, No. 5) October 2013
<http://www.aims sciences.org/journals/displayArticlesnew.jsp?paperID=8337>

0.4 Potential applications

The development of advanced materials leads to the design and introduction of new products in a wide range of commercial sectors. Among SPD procedures ECAP, HPT, are already well-established methods for commercial production of UFG materials. Examples include the fabrication of titanium dental implants to support crowns. Due to significant improvement of mechanical properties of CP Grade 1 Titanium processed by ECAP, one can reduce a diameter of an implant. Moreover, currently fabrication of bulk nanostructured materials is of a great interest.

0.5 List of Notations

We indicate here after repeated patters in the notations used in the thesis.

a	scalars
$\mathbf{a} = a_i \mathbf{e}_i$	vectors
\mathbf{a}_i	lattice vectors
\mathbf{a}^i	reciprocal dual lattice vectors
$\mathbf{A} = A_{ij} \mathbf{e}_i \otimes \mathbf{e}_j$	second-order tensors
$\mathbf{A} = A_{ijkl} \mathbf{e}_i \otimes \mathbf{e}_j \otimes \mathbf{e}_k \otimes \mathbf{e}_l$	fourth-order tensors in the current configuration
$\mathbb{A} = A_{IJKLEI} \mathbf{e}_I \otimes \mathbf{e}_J \otimes \mathbf{e}_K \otimes \mathbf{e}_L$	fourth-order tensors in the reference configuration
\mathbb{A}_h	finite element space
\mathbf{a}	acceleration
$\overset{\nabla}{\mathbf{A}} = \frac{\partial \mathbf{A}}{\partial t} + \mathbf{v} \cdot \nabla \mathbf{A} - \nabla \mathbf{v} \mathbf{A} - \mathbf{A} \nabla \mathbf{v}^T$	upper convected Oldroyd material time derivative
\mathbf{A}^d	$\mathbf{A} - \frac{1}{d}(\text{tr } \mathbf{A})\mathbf{I}$, deviatoric part of tensor
$\mathbf{a} \otimes \mathbf{b} = a_i b_j$	outer product of two vectors
$\mathbf{A} : \mathbf{B} = A_{ij} B_{ij}$	scalar product of two second-order tensors
$\mathbf{A} : \mathbf{B} = A_{ijkl} B_{kl}$	scalar product of forth-order and second-order tensors
\mathbf{b}	volume force
$\mathbf{E} = \frac{1}{2}(\mathbf{F}\mathbf{F}^T - \mathbf{I})$	left Cauchy-Green tensor
E	Young's modulus
d	space dimension
$\mathbf{D} = \frac{1}{2}(\nabla \mathbf{v} + \nabla \mathbf{v}^T)$	symmetric part of the velocity gradient, strain rate
Div	divergence w.r.t the reference configuration
div	divergence w.r.t the current configuration
$\{e_i\}_{i=1}^d$	Cartesian basis in the current configuration
$\{e_I\}_{I=1}^d$	Cartesian basis in the reference configuration
η	specific entropy
ε	specific internal energy, one dimensional strain
ε_e	one dimensional elastic strain
ε_p	one dimensional plastic strain
\mathbf{F}	deformation gradient
\mathbf{F}_e	elastic part of the deformation gradient
\mathbf{F}_p	plastic part of the deformation gradient
Grad	gradient w.r.t the reference configuration
G	Gibbs potential
∇	gradient w.r.t the current configuration
$\dot{\gamma}$	shear rate
\mathbf{I}	identity matrix

J	$\det \mathbf{F}$ Jacobian
κ_R	reference configuration
$\kappa_{p(t)}$	natural/relaxed configuration
κ_t	current configuration
ξ	rate of entropy production
$\mathbf{m}^{(\alpha)}$	α -th normal to slip direction
μ, μ_ν	viscosity
μ_e, λ_e	Lame coefficients
\mathbf{n}	normal vector
$\nu, \nu^{(\alpha)}$	slip rate
ν_0	reference slip rate
ν_{acc}	accumulated slip
ν_{pois}	Poisson's ratio
p	pressure
\mathbf{P}	first Piola-Kirchhoff stress tensor
Ψ	Helmholtz free energy
r	density of energy sources
Re	Reynolds number
ϱ	density
\mathbf{S}	Kirchhoff stress tensor
$\mathbf{s}^{(\alpha)}$	α -th slip direction
Σ	second Piola-Kirchhoff stress tensor
σ	one dimensional stress
σ_Y	yield stress
\mathbf{q}	heat flux
\mathbf{v}	velocity
t	time
\mathbf{T}	Cauchy stress tensor
$\tau^{(\alpha)}$	resolved shear stress
$\tau_c^{(\alpha)}$	critical resolved shear stress
τ_0	reference stress
\mathcal{T}_h	triangulation
θ	temperature
\mathbf{u}	displacement
$[uvw] (uvw)$	crystallographic direction family
$\mathbf{W} = \frac{1}{2} (\nabla \mathbf{v} - \nabla \mathbf{v}^T)$	antisymmetric part of velocity gradient, spin
Wi	Weissenberg number
x	point in the current configuration
X	point in the reference configuration

Chapter 1

Mathematical modelling

1.1 Continuum Mechanics

In this thesis we employ the continuum description of matter at length scales that are large compared to the molecular scale. Continuum physics aims to describe materials with variables such as velocity, density, stress, etc., under an assumption that a given number of molecules is large enough to warrant the use of a smooth continuum description. We briefly recall basic concepts of solid and fluid mechanics, introduce necessary quantities, and derive balance laws, see [30]. All the details are included in the corresponding appendixes.

1.1.1 Kinematics

Let Ω_0 denote the reference configuration of a body at a given time t_0 and let Ω_t denote the current configuration at time t . The material point, which was at the position $X \in \Omega_0$ in the reference configuration, is in the current configuration at time t in the position

$$x = \chi(X, t) \text{ for } X \in \Omega_0, x \in \Omega_t. \quad (1.1)$$

The mapping $\chi(X, t)$ is one-to-one from Ω_0 onto Ω_t , continuously differentiable with respect to the position and time, see Figure 1.1. For a fixed time t , the mapping $\chi(X, t)$ considered as a function of X is called the deformation at time t .

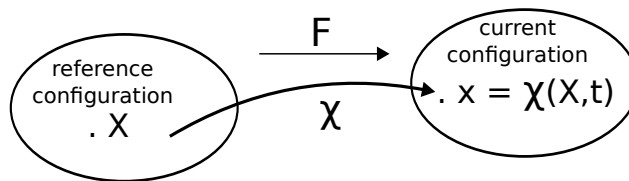


Figure 1.1: Reference and current configuration

In this chapter we will assume that all introduced functions are as regular as needed for all the mathematical operations performed to be justified.

The tensor field

$$\mathbf{F} = \frac{\partial \chi(X, t)}{\partial X} \quad (1.2)$$

is referred to as the deformation gradient. We denote the determinant of \mathbf{F} by J and assume its non-negativity

$$J = \det \mathbf{F} > 0. \quad (1.3)$$

The displacement, the velocity, and the acceleration are defined through

$$\mathbf{u}(X, t) = \chi(X, t) - X, \quad (1.4)$$

$$\mathbf{v}(X, t) = \frac{\partial \chi(X, t)}{\partial t}, \quad (1.5)$$

$$\mathbf{a}(X, t) = \frac{\partial^2 \chi(X, t)}{\partial t^2}. \quad (1.6)$$

Notice that vectors \mathbf{v} and \mathbf{a} are independent of reference time t_0 .

1.1.2 Lagrangian and Eulerian description

We distinguish between the Lagrangian description of the motion, where we track the trajectory of individual fluid parcel as it moves from the initial position and the Eulerian description, for which a velocity field \mathbf{v} at position x at time t is given.

Any field quantity φ can be expressed in the Lagrangian coordinates as a function of the reference position. This is called material description

$$\varphi = \bar{\varphi}(X, t) : \Omega_0 \times [0, \infty) \mapsto \mathbb{R}^d.$$

In the Eulerian framework a quantity φ is defined in the current configuration. This is called the spatial description and is given by

$$\varphi = \tilde{\varphi}(x, t) : \Omega_t \times [0, \infty) \mapsto \mathbb{R}^d.$$

Since the mapping $\chi(X, t)$ is invertible in X for fixed t , it has an inverse

$$X = \chi^{-1}(x, t).$$

Eulerian and Lagrangian descriptions are related through

$$\bar{\varphi}(X, t) = \tilde{\varphi}(\chi(X, t), t), \quad \tilde{\varphi}(x, t) = \bar{\varphi}(\chi^{-1}(x, t), t). \quad (1.7)$$

We introduce the following notation for derivatives in the Lagrangian coordinates

$$\dot{\varphi} = \frac{d}{dt} \bar{\varphi}(X, t), \quad \text{Grad} \varphi = \frac{\partial \bar{\varphi}(X, t)}{\partial X}, \quad \text{Div} \varphi = \text{tr Grad} \varphi. \quad (1.8)$$

In the Eulerian coordinates, corresponding derivatives, read as follows

$$\frac{\partial \tilde{\varphi}(x, t)}{\partial t}, \quad \nabla \varphi = \frac{\partial \tilde{\varphi}(x, t)}{\partial x}, \quad \text{div} \varphi = \text{tr} \nabla \varphi. \quad (1.9)$$

Notice, that we distinguish between gradients and time derivatives with respect to the reference ($\text{Grad} \varphi$, $\dot{\varphi}$) and the current ($\nabla \varphi$, $\frac{\partial \varphi}{\partial t}$) configurations. For the sake of brevity, where there is no confusion we omit superposed notation ($\varphi = \bar{\varphi} = \tilde{\varphi}$).

In what follows the correspondence between the reference (Lagrangian) and the current (Eulerian) configuration is frequently mentioned and we take advantage of following relations, for details we refer to Appendix C. By the chain-rule, for φ (a scalar field) and $\boldsymbol{\varphi}$ (a vector field) it holds

$$\text{Grad} \varphi = \mathbf{F}^T \nabla \varphi, \quad \text{Grad} \boldsymbol{\varphi} = \nabla \boldsymbol{\varphi} \mathbf{F}. \quad (1.10)$$

Moreover, Eulerian and Lagrangian time derivatives read

$$\dot{\varphi}(x, t) = \frac{\partial \varphi(x, t)}{\partial t} + \mathbf{v}(x, t) \cdot \nabla(\varphi(x, t)), \quad (1.11)$$

$$\dot{\boldsymbol{\varphi}}(x, t) = \frac{\partial \boldsymbol{\varphi}(x, t)}{\partial t} + \nabla(\boldsymbol{\varphi}(x, t)) \mathbf{v}(x, t). \quad (1.12)$$

The spatial gradient of the velocity and the deformation gradient are related through

$$\nabla \mathbf{v} = \dot{\mathbf{F}} \mathbf{F}^{-1}. \quad (1.13)$$

1.1.3 Balance equations

The evolution of the state of a body is subject to the balance of mass, momentum, angular momentum, total energy per unit mass and the second law of thermodynamics. We briefly derive balance equations. To this aim we recall the Reynold's transport theorem

$$\begin{aligned}
 \frac{d}{dt} \int_{\Omega_t} \varphi \, dx &= \frac{d}{dt} \int_{\Omega_0} \varphi J \, dX = \int_{\Omega_0} \left(\frac{d}{dt} \varphi J + \varphi \frac{d}{dt} J \right) dX \\
 &= \int_{\Omega_0} \left(\left(\frac{\partial}{\partial t} \varphi + \mathbf{v} \nabla \varphi \right) J + \varphi J \operatorname{div} \mathbf{v} \right) dX \\
 &= \int_{\Omega_t} \frac{\partial \varphi}{\partial t} + \operatorname{div}(\varphi \mathbf{v}) \, dx = \int_{\Omega_t} \frac{\partial \varphi}{\partial t} \, dx + \int_{\partial \Omega_t} \varphi \mathbf{v} \cdot \mathbf{n} \, dS.
 \end{aligned} \tag{1.14}$$

Mass conservation

In a closed region Ω_t , the mass M of a body is conserved, namely

$$M = \int_{\Omega_t} \varrho(x, t) \, dx, \quad \frac{d}{dt} M = 0, \tag{1.15}$$

where $\varrho(x, t)$ stands for the density. From (1.15) and (1.14) we obtain

$$\frac{d}{dt} \int_{\Omega_t} \varrho(x, t) \, dx = \int_{\Omega_t} \frac{\partial \varrho(x, t)}{\partial t} + \operatorname{div}(\varrho(x, t) \mathbf{v}(x, t)) \, dx = 0. \tag{1.16}$$

Let us consider a fixed domain B such that $B \subset \Omega_t$. Then the mass of the fluid contained in B is conserved

$$\int_B \frac{\partial \varrho(x, t)}{\partial t} + \operatorname{div}(\varrho(x, t) \mathbf{v}(x, t)) \, dx = 0. \tag{1.17}$$

Since B is arbitrary and all quantities are smooth enough we multiply (1.17) by $\frac{1}{|B|}$ and pass to the limit with $|B| \rightarrow 0^+$, we get mass balance in the Eulerian coordinates

$$\frac{\partial \varrho(x, t)}{\partial t} + \operatorname{div}(\varrho(x, t) \mathbf{v}(x, t)) = 0. \tag{1.18}$$

Analogous procedure will be conducted to obtain other balance laws in a differential form.

In the Lagrangian coordinates condition (1.15) yields

$$\frac{d}{dt} \int_{\Omega_t} \varrho(x, t) \, dx = \frac{d}{dt} \int_{\Omega_0} \varrho(X, t) \det F(X, t) \, dX = 0, \tag{1.19}$$

what implies that

$$\varrho(X, t) \det \mathbf{F}(X, t) = \varrho(X, 0) = \text{Const}. \tag{1.20}$$

In the case of an incompressible material (1.18) and (1.20) reduce to

$$\operatorname{div} \mathbf{v}(x, t) = 0 \text{ and } \det \mathbf{F}(X, t) = 1. \tag{1.21}$$

Balance of linear momentum

The derivation of the balance of linear momentum, $\int_{\Omega_t} \rho(x, t) \mathbf{v}(x, t) \, dx$, is based on two principles. The change of the linear momentum equals the sum of volume forces \mathbf{b} acting on a body Ω_t and the Cauchy traction \mathbf{t} acting on a surface $\partial\Omega_t$,

$$\frac{d}{dt} \int_{\Omega_t} \rho(x, t) \mathbf{v}(x, t) \, dx = \int_{\Omega_t} \mathbf{b}(x, t) \, dx + \int_{\partial\Omega_t} \mathbf{t}(x, t, \mathbf{n}(x, t)) \, dS. \quad (1.22)$$

The Cauchy's stress theorem states that there exists a second-order tensor field $\mathbf{T}(x, t)$, called the Cauchy stress tensor, independent of the normal vector $\mathbf{n}(x, t)$, such that $\mathbf{t}(x, t, \mathbf{n})$ is a linear function of $\mathbf{n} = \mathbf{n}(x, t)$,

$$\mathbf{t}(x, t, \mathbf{n}) = \mathbf{T}(x, t) \mathbf{n}. \quad (1.23)$$

Formulae (1.22), (1.23), together with the Reynold's theorem (1.14), the mass balance (1.18) and the divergence theorem imply

$$\begin{aligned} \frac{d}{dt} \int_{\Omega_t} \rho(x, t) \mathbf{v}(x, t) \, dx &= \int_{\Omega_t} \mathbf{b}(x, t) \, dx + \int_{\partial\Omega_t} \mathbf{T}(x, t) \mathbf{n} \, dS \\ \int_{\Omega_t} \rho \frac{\partial \mathbf{v}}{\partial t} + \rho \mathbf{v} \nabla \mathbf{v} + v \underbrace{\left(\frac{\partial \rho}{\partial t} + \operatorname{div}(\rho \mathbf{v}) \right)}_{=0} \, dx &= \int_{\Omega_t} \mathbf{b} \, dx + \int_{\Omega_t} \operatorname{div} \mathbf{T} \, dx \end{aligned}$$

The local balance of linear momentum in Eulerian framework has the form

$$\rho(x, t) \dot{\mathbf{v}}(x, t) - \operatorname{div} \mathbf{T}(x, t) = \rho(x, t) \mathbf{b}(x, t). \quad (1.24)$$

Transforming (1.24) to Lagrangian coordinates yields

$$\rho(X, 0) \frac{d}{dt} \mathbf{v}(X, t) - \operatorname{Div} \mathbf{P}(X, t) = \mathbf{b}(X, t), \quad (1.25)$$

where $\mathbf{P}(X, t)$ stands for the first Piola-Kirchhoff stress

$$\mathbf{P} = (\det \mathbf{F}) \mathbf{T} \mathbf{F}^{-T}. \quad (1.26)$$

Moreover, we define two auxiliary stress measures the Kirchhoff stress \mathbf{S} and the second Piola-Kirchhoff stress $\mathbf{\Sigma}$. The Kirchhoff stress is related to the Cauchy stress by the determinant of the deformation gradient, therefore it is sometimes called the weighted Cauchy stress

$$\mathbf{S} = \frac{\mathbf{T}}{\rho} \text{ or } \mathbf{S} = \mathbf{T} \det \mathbf{F}. \quad (1.27)$$

To motivate (1.27) we refer to the mass balance in Lagrangian coordinates (1.20), remembering that the determinant of the deformation gradient represents the ratio of the current volume to the reference volume. Thus, for isochoric deformation the Kirchhoff stress equals the Cauchy stress.

The second Piola-Kirchhoff stress reads

$$\mathbf{\Sigma} = \mathbf{F}^{-1} \mathbf{P}. \quad (1.28)$$

Introduced stress measures are related through

$$\begin{aligned} \mathbf{T} &= J^{-1} \mathbf{F} \mathbf{\Sigma} \mathbf{F}^T, \\ \mathbf{S} &= \mathbf{F} \mathbf{\Sigma} \mathbf{F}^T. \end{aligned}$$

Balance of angular momentum

Together with the linear momentum we require that the change of the angular momentum, $\int_{\Omega_t} x \times \varrho(x, t) \mathbf{v}(x, t) dx$, equals the sum of the moments of all forces acting on Ω_t , therefore

$$\frac{d}{dt} \int_{\Omega_t} x \times \varrho(x, t) \mathbf{v}(x, t) dx = \int_{\Omega_t} x \times \mathbf{b}(x, t) dx + \int_{\partial\Omega_t} x \times \mathbf{t}(x, t, \mathbf{n}) dS. \quad (1.29)$$

The local balance of the angular momentum in the Eulerian coordinates states the symmetry of the Cauchy stress tensor,

$$\mathbf{T}(x, t) = \mathbf{T}(x, t)^T. \quad (1.30)$$

Notice that the symmetry condition for the first Piola-Kirchhoff stress, reads

$$\mathbf{P}(X, t) \mathbf{F}^T = \mathbf{F} \mathbf{P}(X, t)^T. \quad (1.31)$$

Balance of energy

We introduce the balance of energy as equilibrium between temporal change of the sum of the kinetic energy \mathcal{K} and the internal energy \mathcal{E} and the sum of the mechanical \mathcal{W} and the thermal \mathcal{Q} power,

$$\frac{d}{dt} (\mathcal{K}(\Omega_t) + \mathcal{E}(\Omega_t)) = \mathcal{W}(\Omega_t) + \mathcal{Q}(\Omega_t). \quad (1.32)$$

Contributions to the energy balance reads as follows

$$\mathcal{K}(\Omega_t) = \int_{\Omega_t} \frac{1}{2} \varrho |\mathbf{v}|^2 dx, \quad (1.33)$$

$$\mathcal{E}(\Omega_t) = \int_{\Omega_t} \varrho \varepsilon dx, \quad (1.34)$$

$$\mathcal{W}(\Omega_t) = \int_{\partial\Omega_t} \mathbf{T} \mathbf{v} \cdot \mathbf{n} dS + \int_{\Omega_t} \mathbf{b} \cdot \mathbf{v} dx, \quad (1.35)$$

$$\mathcal{Q}(\Omega_t) = - \int_{\partial\Omega_t} \mathbf{q} \cdot \mathbf{n} dS + \int_{\Omega_t} \varrho r dx, \quad (1.36)$$

where ε is the specific internal energy, \mathbf{q} is the heat flux vector, and r is the specific heat source.

Substituting the explicit forms for \mathcal{K} , \mathcal{E} , \mathcal{W} , and \mathcal{Q} into (1.32) yields

$$\frac{d}{dt} \int_{\Omega_t} \varrho \left(\varepsilon + \frac{1}{2} |\mathbf{v}|^2 \right) dx = \int_{\partial\Omega_t} \mathbf{T} \mathbf{v} \cdot \mathbf{n} dS + \int_{\Omega_t} \mathbf{b} \cdot \mathbf{v} dx - \int_{\partial\Omega_t} \mathbf{q} \cdot \mathbf{n} dS + \int_{\Omega_t} \varrho r dx \quad (1.37)$$

We transform the first term on the right hand side according to the chain rule

$$\int_{\partial\Omega_t} \mathbf{T} \mathbf{v} \cdot \mathbf{n} dS = \int_{\Omega_t} \mathbf{v} \operatorname{div} \mathbf{T} + \int_{\Omega_t} \mathbf{T} : \nabla \mathbf{v}. \quad (1.38)$$

From the divergence theorem, (1.24), (1.38) and the mass balance we get

$$\int_{\Omega_t} \varrho \dot{\varepsilon} dx = \int_{\Omega_t} \mathbf{T} : \mathbf{D} dx + - \int_{\Omega_t} \operatorname{div} \mathbf{q} dx + \int_{\Omega_t} \varrho r dx. \quad (1.39)$$

Therefore, the local form of the energy conservation reads

$$\varrho(x, t) \dot{\varepsilon}(x, t) = \varrho(x, t) r(x, t) - \operatorname{div} \mathbf{q}(x, t) + \mathbf{T}(x, t) : \mathbf{D}(x, t), \quad (1.40)$$

where \mathbf{D} stands for the symmetric part of the velocity gradient.

Lagrangian form of (1.40) reads

$$\varrho(X, 0)\dot{\varepsilon}(X, t) = \varrho(X, 0)r(X, t) - \text{Div } \mathbf{q}(X, t) + \mathbf{P}(X, t) : \dot{\mathbf{F}}(X, t). \quad (1.41)$$

The second law of thermodynamics

We require that the second law is fulfilled, namely the production of the entropy is non-negative

$$\mathcal{H}(\mathcal{P}_t) = \frac{d}{dt}\mathcal{S}(\Omega_t) - \mathcal{J}(\Omega_t) \geq 0, \quad (1.42)$$

where \mathcal{S} and \mathcal{J} stand for the internal entropy and the entropy flow (the rate at which the entropy is transferred to Ω_t), respectively.

$$\mathcal{S}(\Omega_t) = \int_{\Omega_t} \varrho\eta \, dx, \quad (1.43)$$

$$\mathcal{J}(\Omega_t) = - \int_{\partial\Omega_t} \mathbf{j} \cdot \mathbf{n} \, dS + \int_{\Omega_t} j \, dx, \quad (1.44)$$

where η is the specific entropy, \mathbf{j} the entropy flux, and j the entropy supply.

Moreover, we assume that there exists scalar temperature field θ , such that

$$\theta > 0, \quad \mathbf{j} = \frac{\mathbf{q}}{\theta}, \quad j = \frac{\varrho r}{\theta}. \quad (1.45)$$

Note that the entropy and the heat flow are in the same direction, and neither can vanish without the other.

Combining explicit forms of \mathcal{S} and \mathcal{J} with (1.42) and (1.45) yields Clausius-Duhem inequality

$$\frac{d}{dt} \int_{\Omega_t} \varrho\eta \, dx \geq - \int_{\partial\Omega_t} \frac{\mathbf{q}}{\theta} \cdot \mathbf{n} \, dS + \int_{\Omega_t} \frac{\varrho r}{\theta} \, dx. \quad (1.46)$$

As a consequence of (1.14), the divergence theorem, and (1.46) we find out that

$$\int_{\Omega_t} \left(\varrho\dot{\eta} + \text{div} \left(\frac{\mathbf{q}}{\theta} \right) - \frac{\varrho r}{\theta} \right) dx \geq 0, \quad (1.47)$$

and

$$\varrho\dot{\eta} + \text{div} \left(\frac{\mathbf{q}}{\theta} \right) - \frac{\varrho r}{\theta} \geq 0. \quad (1.48)$$

We introduce one more state variable the Helmholtz free energy Ψ , also referred to as the specific free energy. The relation between thermodynamic variables reads as follows

$$\Psi := \varepsilon - \theta\eta. \quad (1.49)$$

We restrict attention to the isothermal case, $\theta = \text{Const.}$, that implies

$$\text{div} \left(\frac{\mathbf{q}}{\theta} \right) = \frac{1}{\theta} \text{div } \mathbf{q} - \frac{1}{\theta^2} \mathbf{q} \cdot \nabla \theta \underset{\theta=\text{Const.}}{\equiv} \frac{1}{\theta} \text{div } \mathbf{q}. \quad (1.50)$$

The inequality (1.48) together with total energy balance (1.40), (1.50), and equation (1.49) yields

$$\mathbf{T} : \mathbf{D} - \varrho\dot{\Psi} \geq 0.$$

We introduce the specific rate of dissipation ξ as

$$\rho\xi := \mathbf{T} : \mathbf{D} - \rho\dot{\Psi} \geq 0. \quad (1.51)$$

It is convenient to divide (1.51) by density and reformulate that equality in terms of the Kirchhoff stress

$$\xi = \mathbf{S} : \mathbf{D} - \dot{\Psi} \geq 0. \quad (1.52)$$

We conclude this section stressing that in this thesis the evolution of the state of the body is subject to the balance of mass, momentum, angular momentum, energy, and the second law of thermodynamics which in the Eulerian coordinates takes the form

$$\dot{\rho} + \rho \operatorname{div} \mathbf{v} = 0, \quad (1.53a)$$

$$\rho \dot{\mathbf{v}} - \operatorname{div} \mathbf{T} = \mathbf{b}, \quad \mathbf{T} = \mathbf{T}^T, \quad (1.53b)$$

$$\rho \dot{\varepsilon} = \rho r - \operatorname{div} \mathbf{q} + \mathbf{T} : \mathbf{D}, \quad (1.53c)$$

$$\mathbf{T} : \mathbf{D} - \rho \dot{\Psi} \geq 0. \quad (1.53d)$$

Moreover, since we distinguish between the Cauchy stress and the Kirchhoff stress

$$\dot{\rho} + \rho \operatorname{div} \mathbf{v} = 0, \quad (1.54a)$$

$$\rho \dot{\mathbf{v}} - \operatorname{div} (\rho \mathbf{S}) = \rho \mathbf{b}', \quad \mathbf{S} = \mathbf{S}^T, \quad (1.54b)$$

$$\dot{\varepsilon} = r - \frac{1}{\rho} \operatorname{div} \mathbf{q} + \mathbf{S} : \mathbf{D}, \quad (1.54c)$$

$$\mathbf{S} : \mathbf{D} - \dot{\Psi} \geq 0. \quad (1.54d)$$

where \mathbf{b}' is a specific external force.

Both formulations are often used in the thesis, but we particularly focus on the Kirchhoff stress. It is worth to recall that in the case of isochoric deformations \mathbf{T} and \mathbf{S} are equal.

The system (1.53) applies to a body without specifying its kind. Thus, to indicate what kind of a material we are modelling, we need to add a proper constitutive relation which describes the response of a material to external stimuli. Another reason why we need extra equations comes from the fact that from (1.53) one is not able to determine deformation.

1.2 Elasto-Visco-Plasticity

This section is devoted to comparison of different classes of material responses. We aim to give a motivation and show that it is necessary to consider rate-type models. To this aim we provide a discussion of one dimensional elastic, viscous and plastic constitutive responses, namely we investigate its stress-strain behaviour under a uni-axial loading. Note that usually in the literature visco-elastic and plastic models are discussed separately.

Within this section we use notation σ and ε for the one dimensional stress and strain, respectively (in contrary to Section 1.1 where ε stands for the specific internal energy).

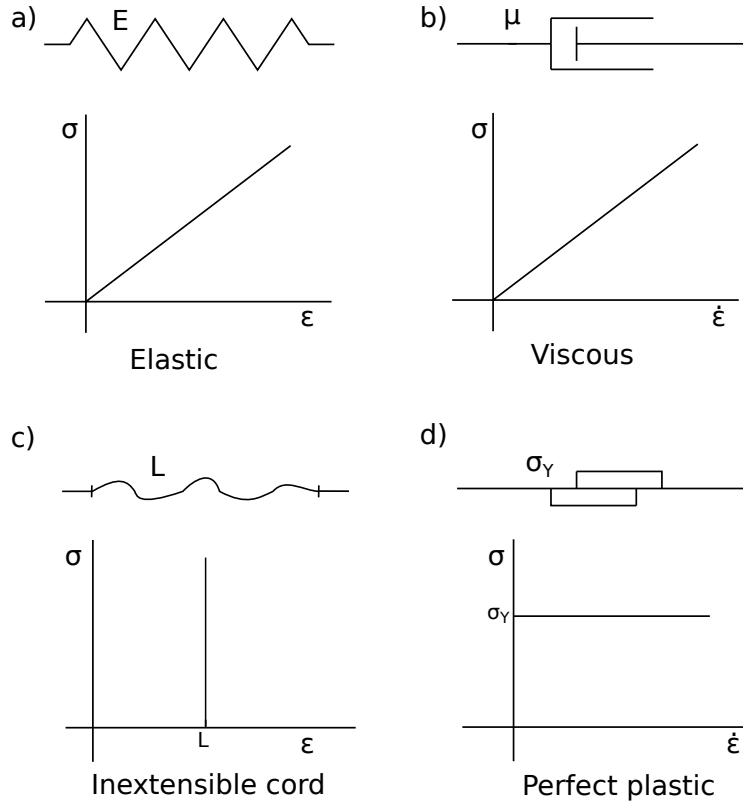


Figure 1.2: Elementary rheological models

1.2.1 One-dimensional mechanical analogues

We use simple one-dimensional rheological elements, shown in Figure 1.2, to amplify different classes of constitutive responses.

An elastic element (Figure 1.2a) represents a fully recoverable behaviour. A spring element, is an analogue of a linear elastic material. The stress-strain relation, referred to as Hooke's law, can be written as

$$\sigma = E\epsilon, \quad (1.55)$$

where proportionality constant E is called the Young's modulus.

A viscous element (Figure 1.2b) represents response where the stress is a function of a rate of strain. The dash-pot is a cylinder filled with viscous fluid, which resists motion via viscous friction. The response of a linear dash-pot, reads

$$\sigma = \mu\dot{\epsilon}, \quad (1.56)$$

where μ is the viscosity of a fluid.

An inextensible cord (Figure 1.2c) exhibits strain limiting behaviour. Unlike the implications of the Hooke's law (1.55) the strains remain small, $\epsilon \leq L$, when the stress blows up. We mention inextensible cord because similarly to frictional device it posses threshold and can be modelled in a class of implicit constitutive models, which are referred to as limiting strain models. For details we refer to [25, 31].

A plastic element (Figure 1.2d) is one where the strain remains zero until the stress exceeds a certain value (yield stress σ_Y). Detailed description of a frictional device is covered in Section 1.2.3.

1.2.2 Viscoelasticity

Viscoelastic material exhibits both elastic and viscous behaviours. We can join linear spring and linear dash-pot in parallel and get well known visco-elastic Kelvin-Voigt element. On the other these elements connected in series give the Maxwell element, see Figure 1.3. By combining (1.55) and (1.56) with the geometry of considered elements, one can derive stress-strain relation for those models

$$\text{Maxwell model} \quad \frac{\mu}{E} \dot{\sigma} + \sigma = \mu \dot{\varepsilon}, \quad (1.57)$$

$$\text{Kelvin-Voigt model} \quad \sigma = E\varepsilon + \mu \dot{\varepsilon}. \quad (1.58)$$

Visco-elastic models are capable of describing non-linear response exhibited by most of the materials during creep and stress relaxation tests. For more details on visco-elastic behaviour we refer to [32].

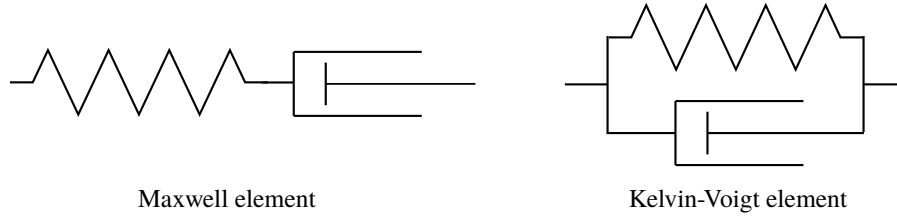


Figure 1.3: Visco-elastic models

1.2.3 One dimensional plastic element

The response of a frictional device, see Figure 1.4, is characterized as follows. The stress in the frictional device cannot be greater in absolute value than the yield stress σ_Y . This is called the yield condition and is given by

$$|\sigma| \leq \sigma_Y. \quad (1.59)$$

Change in the configuration of frictional device is possible only if $\dot{\varepsilon}_p \neq 0$. If the absolute value of the applied stress is less than the yield stress, no change in ε_p takes place, i.e., $\dot{\varepsilon}_p = 0$. If stress equals to yield stress, the frictional device experiences slip in the direction of the applied stress, with slip rate $\nu \geq 0$, namely

$$\begin{cases} \dot{\varepsilon}_p = \nu & \text{for } \sigma = \sigma_Y \\ \dot{\varepsilon}_p = -\nu & \text{for } \sigma = -\sigma_Y \end{cases}. \quad (1.60)$$

Note that the evolution of plastic strain, for any admissible stress (1.60) can be rewritten as a single equation

$$\dot{\varepsilon}_p = \nu \text{sign}(\sigma), \quad (1.61)$$

which is referred to as a flow rule. It is important to specify proper constitutive law for the slip rate ν . Notice that the point $(0,0)$ belongs to the response graph, see Figure 1.4 (right).

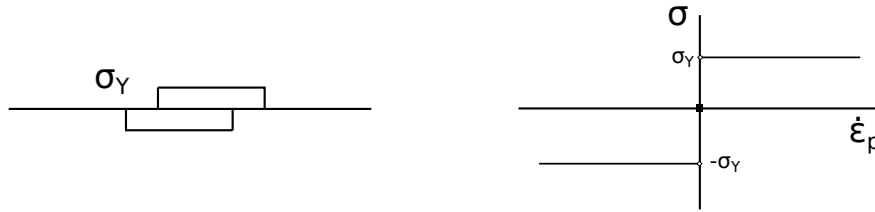


Figure 1.4: One-dimensional frictional element

1.2.4 Elasto/visco-plasticity

At first we focus on a parallel connection of viscous and plastic elements, see Figure 1.5. The total stress is a sum of viscous and plastic contributions

$$\sigma = \sigma_v + \sigma_p, \quad \varepsilon = \varepsilon_e = \varepsilon_p.$$

Stress-strain relation reads as follows

$$\sigma = \mu \dot{\varepsilon} + \sigma_Y \text{sign}(\dot{\varepsilon}) \quad (1.62)$$

and is referred to as the Bingham model.

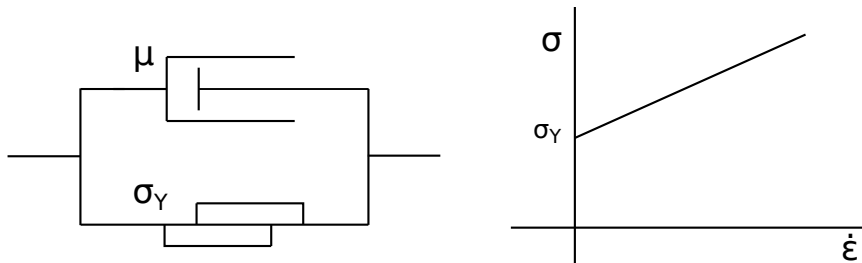


Figure 1.5: One-dimensional mechanical analogue of the Bingham model

Now let consider a device consisting of elastic and plastic element connected in series, see Figure 1.6

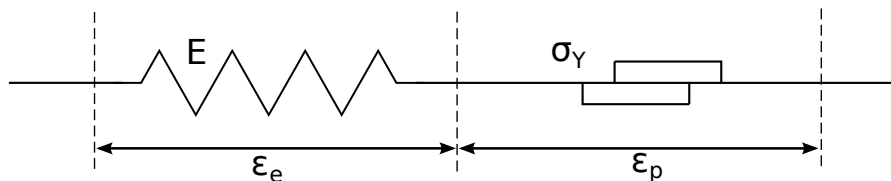


Figure 1.6: One-dimensional mechanical analogue

The total strain ε splits into elastic and plastic contributions

$$\varepsilon = \varepsilon_e + \varepsilon_p, \quad \sigma = \sigma_e = \sigma_p.$$

The stress in the spring with Young's modulus E is σ

$$\sigma = E\varepsilon_e = E(\varepsilon - \varepsilon_p). \quad (1.63)$$

Equations (1.61) and (1.63) give us the set of stress-strain constitutive relation. We can either couple (1.63) with the evolution of the plastic strain (1.61)

$$\begin{cases} \sigma = E\varepsilon_e = E(\varepsilon - \varepsilon_p) \\ \dot{\varepsilon}_p = \nu \operatorname{sign}(\sigma) \end{cases}, \quad (1.64)$$

or consider the stress-strain relation in a rate form

$$\begin{cases} \dot{\sigma} = E\dot{\varepsilon}_e = E(\dot{\varepsilon} - \dot{\varepsilon}_p) \\ \dot{\varepsilon}_p = \nu \operatorname{sign}(\sigma) \end{cases}. \quad (1.65)$$

System (1.64) together with the proper definition of the slip rate ν is a one-dimensional version of a wide class of models. For instance, putting $\nu = \nu(\sigma) = |\sigma|^N$ leads to the Norton-Hoff model.

In the thesis we focus on a class of a rate type models, thus the considered stress-strain constitutive equation is in the form (1.65). Having one-dimensional case as a toy example we proceed to general rate type materials.

1.2.5 Generalization of one-dimensional models

In the previous section we presented one-dimensional analogues of basic mechanical responses and combined it into couple of well known models. We aim to provide the description of material behaviour in higher space dimensions. In the view of models (1.57), (1.58), (1.62), and (1.65), we generalise the stress σ as the Cauchy stress \mathbf{T} and the strain rate $\dot{\varepsilon}$ as the symmetric part of the velocity gradient \mathbf{D} . The skew-symmetric part of the velocity gradient is denoted by \mathbf{W} . Notice that this approach is purely phenomenological. In Section 1.3 we give thermodynamic derivation of a rate-type fluid model.

Since we are interested in models that contain the rate of stress (1.65), among several principles and assumptions which one have to take into account when formulating a constitutive equation, material objectivity is crucial. The principle of material objectivity says that the form of the constitutive equation does not depend on a motion of an observer. For details on frame indifference and objective stress tensors, see Appendix E, where we explain consequences of the material objectivity principle such as, that the material time derivative $\frac{\partial \mathbf{T}}{\partial t} + \mathbf{v} \nabla \mathbf{T} := \frac{\partial \mathbf{T}}{\partial t} + v_k \frac{\partial \mathbf{T}}{\partial x^k}$ is not objective.

The objective form of the time derivative of a tensor can be written in the form

$$\overset{\nabla a}{\mathbf{T}} = \frac{\partial \mathbf{T}}{\partial t} + \mathbf{v} \nabla \mathbf{T} - (\mathbf{W} \mathbf{T} - \mathbf{T} \mathbf{W}) + a(\mathbf{D} \mathbf{T} + \mathbf{T} \mathbf{D}), \quad a \in [-1, 1]. \quad (1.66)$$

For $a = 1$, derivative (1.66) is referred to as the lower convected Oldroyd derivative

$$\overset{\nabla l}{\mathbf{T}} = \frac{\partial \mathbf{T}}{\partial t} + \mathbf{v} \nabla \mathbf{T} + \mathbf{T} \nabla \mathbf{v} + (\nabla \mathbf{v})^T \mathbf{T}, \quad (1.67)$$

for $a = -1$, as the upper convected Oldroyd derivative

$$\overset{\nabla u}{\mathbf{T}} = \frac{\partial \mathbf{T}}{\partial t} + \mathbf{v} \nabla \mathbf{T} - \mathbf{T} (\nabla \mathbf{v})^T - \nabla \mathbf{v} \mathbf{T}, \quad (1.68)$$

and for $\bar{a} = 0$, as the Jaumann derivative

$$\overset{\nabla J}{\mathbf{T}} = \frac{\partial \mathbf{T}}{\partial t} + \mathbf{v} \nabla \mathbf{T} - \mathbf{W} \mathbf{T} + \mathbf{T} \mathbf{W}. \quad (1.69)$$

Moreover, there exist some widely used visco-elastic models without objective time derivative, as the Maxwell model

$$\frac{\partial \mathbf{T}}{\partial t} + \gamma \mathbf{T} = \mathbf{D}$$

or the transport model

$$\frac{\partial \mathbf{T}}{\partial t} + \mathbf{v} \cdot \nabla \mathbf{T} + \gamma \mathbf{T} = \mathbf{D}.$$

A parallel combination of the Maxwell element and a viscous element with viscosity ν is referred to as the Oldroyd model. Then the stress is splitted into the Newtonian part and the elastic part

$$\mathbf{T} = \mathbf{T}_{\text{Newtonian}} + \mathbf{T}_{\text{elastic}},$$

where

$$\mathbf{T}_{\text{Newtonian}} = 2\nu \mathbf{D},$$

and

$$\frac{\partial}{\partial t} \mathbf{T}_{\text{elastic}} + \mathbf{v} \cdot \nabla \mathbf{T}_{\text{elastic}} - \nabla \mathbf{v} \mathbf{T}_{\text{elastic}} - (\nabla \mathbf{v})^T \mathbf{T}_{\text{elastic}} + \gamma \mathbf{T}_{\text{elastic}} = 2\mu \mathbf{D}. \quad (1.70)$$

From the modelling point of view this approach is well suited for polymeric material. The Newtonian law corresponds to solvent and (1.70) describes the behaviour of a polymer.

When there is no confusion or there is no need to specify objective time derivative, superscript is omitted. We conclude by stating the generalised stress strain constitutive relation (1.65)

$$\overset{\nabla}{\mathbf{T}} = \mathbf{C} \mathbf{D}, \quad (1.71)$$

where \mathbf{C} stands for elastic compliance tensor, see Section 1.3.5.

1.3 Constitutive theory

Starting point to the constitutive theory is a multiplicative decomposition of the deformation gradient. We present and compare two approaches, by Kröner [14, 15]) and Rajagopal, Srinivasa [16, 17]. Later we show how to obtain rate type model through the Gibbs potential [18] and the Helmholtz potential [20, 21, 22], see Appendix D.

1.3.1 Multiplicative decomposition of the deformation gradient

In order to model large deformations, namely elastic-plastic deformations at finite strains we assume the multiplicative decomposition of the deformation gradient \mathbf{F} (Kröner [14], Lee and Liu [15]). The decomposition is based on the introduction of intermediate configuration, also known as relaxed or lattice configuration, corresponding to the unloaded state of a material, which is deformed only plastically, see Figure 1.7.

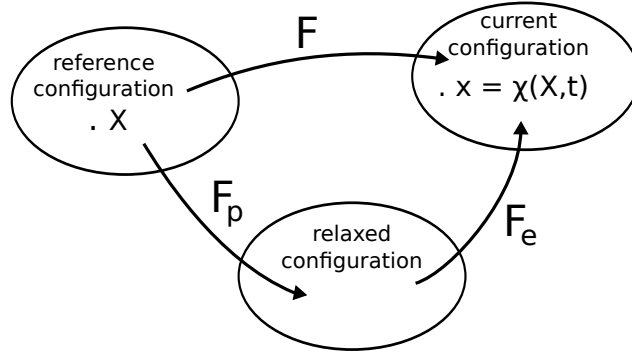


Figure 1.7: Schematic of the Kröner decomposition

The multiplicative decomposition reads

$$\mathbf{F} = \mathbf{F}_e \mathbf{F}_p, \quad (1.72)$$

where \mathbf{F}_e stands for elastic distortion (stretch and rotation of the lattice) and \mathbf{F}_p for plastic distortion (distortion of the lattice due to formation of dislocations). All the volumetric changes are assumed to result from the elastic stretches in the lattice,

$$\det \mathbf{F}_p = 1, \quad \det \mathbf{F} = \det \mathbf{F}_e > 0. \quad (1.73)$$

The multiplicative decomposition of the deformation gradient finds a solid and consistent physical justification in the slip theory of crystals, see also Section 1.4 below.

Following Rajagopal and Srinivasa [16, 17, 33], the deformation from the natural configuration to the current configuration represents the elastic deformation of the body. By natural configuration of a material we understand the configuration which is attained when all external stimuli are removed [33]. In order to quantify this, we introduce \mathbf{F}_{κ_p} as the gradient of the deformation from $\kappa_p(t)$ to κ_t . In order to quantify the local structural changes in the material, we introduce the tensor $\mathbf{G} := \mathbf{F}_{\kappa_r \rightarrow \kappa_p(t)}$, which is the gradient of the mapping from κ_r to $\kappa_p(t)$, see Figure 1.8.

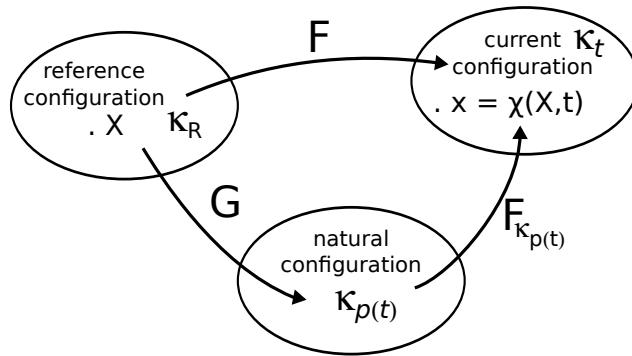


Figure 1.8: Schematic of the current natural configuration of the body

Thus changes in \mathbf{G} represent microstructural changes. They are related through

$$\mathbf{F}_{\kappa_p} = \mathbf{F}_{\kappa_r} \mathbf{G}^{-1}, \quad (J = \det(\mathbf{F}_{\kappa_p}) \det(\mathbf{G})). \quad (1.74)$$

These approaches vary through the thermodynamical underpinnings to the traditional plasticity, but leads to the same result, namely the additive decomposition of the velocity gradient.

As pointed out by Rajagopal and Srinivasa [16] within classical plasticity literature it is usual to specify some evolution equation for the plastic strain and then to define the rate of dissipation as the inner product of the stress with the rate of plastic strain, see e.g. [34, 35]. This approach is reflected in Section 1.4.2 where single crystal hypothesis is discussed.

On the other hand, one can choose different set of assumptions, namely make constitutive assumptions on the nature of the work done, the Helmholtz potential and the rate of dissipation. By postulating that the rate of dissipation per unit volume is the maximum possible, we arrive at the form of the evolution equation for \mathbf{G} , see Section 1.5.

For the detailed comparison of classical plasticity with the presented approach, see [16, Section VI. Comparison with traditional approaches to plasticity] and [17, I.1. Dissipation and inelasticity].

1.3.2 The additive decomposition of the velocity gradient

The multiplicative decomposition (1.72) leads to the additive decomposition of the velocity gradient.

Equation (1.72) together with (1.13) yields

$$\begin{aligned}\nabla \mathbf{v} &= \dot{\mathbf{F}} \mathbf{F}^{-1} = (\dot{\mathbf{F}}_e \mathbf{F}_p + \mathbf{F}_e \dot{\mathbf{F}}_p) (\mathbf{F}_e \mathbf{F}_p)^{-1}, \\ \nabla \mathbf{v} &= \dot{\mathbf{F}}_e (\mathbf{F}_e)^{-1} + \mathbf{F}_e (\dot{\mathbf{F}}_p (\mathbf{F}_p)^{-1}) (\mathbf{F}_e)^{-1}.\end{aligned}\tag{1.75}$$

Let us denote by \mathbf{L}_e and \mathbf{L}_p elastic and plastic parts of the velocity gradient (also called distortion-rate tensors) through

$$\mathbf{L}_e = \dot{\mathbf{F}}_e \mathbf{F}_e^{-1}, \quad \mathbf{L}_p = \dot{\mathbf{F}}_p (\mathbf{F}_p)^{-1}.\tag{1.76}$$

We conclude with decomposition

$$\nabla \mathbf{v} = \mathbf{L}_e + \mathbf{F}_e \mathbf{L}_p \mathbf{F}_e^{-1}.\tag{1.77}$$

On the other hand, the second approach (1.74), gives us analogous result. We apply the material time derivative to \mathbf{F}_{κ_p}

$$\dot{\mathbf{F}}_{\kappa_p} = \dot{\mathbf{F}}_{\kappa_p} |_{\mathbf{G} \text{ fixed}} + \dot{\mathbf{F}}_{\kappa_p} |_{\mathbf{F}_{\kappa_p} \text{ fixed}} = \nabla \mathbf{v} \mathbf{F}_{\kappa_p} + (-\mathbf{F}_{\kappa_p} \dot{\mathbf{G}} \mathbf{G}^{-1}).\tag{1.78}$$

and rewrite (1.78) into

$$\nabla \mathbf{v} = \dot{\mathbf{F}}_{\kappa_p} (\mathbf{F}_{\kappa_p})^{-1} + \mathbf{F}_{\kappa_p} \dot{\mathbf{G}} \mathbf{G}^{-1} (\mathbf{F}_{\kappa_p})^{-1}.\tag{1.79}$$

In what follows we use the classical notation, set $\mathbf{F}_e := \mathbf{F}_{\kappa_p}$ and $\mathbf{F}_p := \mathbf{G}$

$$\begin{aligned}\mathbf{L}_e &= \dot{\mathbf{F}}_{\kappa_p} (\mathbf{F}_{\kappa_p})^{-1} = \dot{\mathbf{F}}_e \mathbf{F}_e^{-1}, \\ \mathbf{L}_p &= \dot{\mathbf{G}} \mathbf{G}^{-1} = \dot{\mathbf{F}}_p (\mathbf{F}_p)^{-1}.\end{aligned}$$

Moreover, we introduce additional notation. The elastic stretching \mathbf{D}_e , the elastic spin \mathbf{W}_e , the plastic stretching \mathbf{D}_p , and the plastic spin \mathbf{W}_p

$$\mathbf{D}_e = \frac{1}{2} (\mathbf{L}_e + \mathbf{L}_e^T), \quad \mathbf{W}_e = \frac{1}{2} (\mathbf{L}_e - \mathbf{L}_e^T)\tag{1.80}$$

$$\mathbf{D}_p = \frac{1}{2} (\mathbf{F}_e \mathbf{L}_p \mathbf{F}_e^{-1} + (\mathbf{F}_e \mathbf{L}_p \mathbf{F}_e^{-1})^T), \quad \mathbf{W}_p = \frac{1}{2} (\mathbf{F}_e \mathbf{L}_p \mathbf{F}_e^{-1} - (\mathbf{F}_e \mathbf{L}_p \mathbf{F}_e^{-1})^T).\tag{1.81}$$

We can relate the above tensors with the elastic Green strain \mathbf{E}_e ,

$$\mathbf{E}_e = \frac{1}{2} (\mathbf{F}_e^T \mathbf{F}_e - \mathbf{I}), \quad (1.82)$$

by

$$\mathbf{D}_e = \frac{1}{2} (\mathbf{L}_e + \mathbf{L}_e^T) = \frac{1}{2} (\dot{\mathbf{F}}_e \mathbf{F}_e^{-1} + \mathbf{F}_e^{-T} \dot{\mathbf{F}}_e^T), \quad (1.83)$$

$$\mathbf{W}_e = \frac{1}{2} (\mathbf{L}_e - \mathbf{L}_e^T) = \frac{1}{2} (\dot{\mathbf{F}}_e \mathbf{F}_e^{-1} - \mathbf{F}_e^{-T} \dot{\mathbf{F}}_e^T), \quad (1.84)$$

$$\dot{\mathbf{E}}_e = \frac{1}{2} (\mathbf{F}_e^T \dot{\mathbf{F}}_e + \dot{\mathbf{F}}_e^T \mathbf{F}_e) = \frac{1}{2} \mathbf{F}_e^T (\dot{\mathbf{F}}_e \mathbf{F}_e^{-1} + \mathbf{F}_e^{-T} \dot{\mathbf{F}}_e^T) \mathbf{F}_e = \mathbf{F}_e^T \mathbf{D}_e \mathbf{F}_e. \quad (1.85)$$

Notice that the relation between $\dot{\mathbf{E}}_e$ and \mathbf{D} reads

$$\dot{\mathbf{E}}_e = \mathbf{F}_e^T \mathbf{D}_e \mathbf{F}_e = \mathbf{F}_e^T (\mathbf{D} - \mathbf{D}_p) \mathbf{F}_e. \quad (1.86)$$

1.3.3 Stress-strain dependence

In early references, such as [23, 20, 21, 22], the authors postulate that the Jaumann rate of the Kirchhoff stress is related to the elastic rate of stretching by usual elastic moduli tensor. In this approach the constitutive equation is obtained as a rate of stress which is derived from a Helmholtz potential.

To the author's knowledge the description of this phenomena, which is thermodynamically admissible and uses a Helmholtz potential does not lead to the Jaumann rate type model, see [36]. The detailed derivation of the evolution equation for the Cauchy stress based on the Helmholtz potential is provided in Appendix D.

In the following sections we present the approach of using the Gibbs potential to derive a rate-type model, see [18].

1.3.4 Gibbs potential approach - stress dependence

In the case of the Helmholtz potential, the stress is defined as the derivative of the Helmholtz potential with respect to the elastic Green tensor (D.2). We would like to avoid dependency on the strain. As pointed out for example in Málek et al. [37], from the casual point of view, it is more natural to consider deformation as effect and force as cause and not otherwise. To this aim we transform the Helmholtz potential into the Gibbs potential $G(\mathbf{S}, \theta)$. The relation is given by the Legendre transformation

$$\Psi(\mathbf{S}, \theta) = G(\mathbf{S}, \theta) - \frac{\partial G(\mathbf{S}, \theta)}{\partial \mathbf{S}} : \mathbf{S}. \quad (1.87)$$

We recall the thermodynamic variables, and assume that they depend on the temperature θ and the Kirchhoff stress \mathbf{S} :

$$\begin{aligned} \varepsilon(\mathbf{S}, \theta) &- \text{specific internal energy,} \\ \Psi(\mathbf{S}, \theta) &- \text{specific Helmholtz potential,} \\ \eta(\mathbf{S}, \theta) &- \text{specific entropy.} \end{aligned}$$

Following [18] we stipulate that for the given Gibbs potential the specific internal energy and the specific entropy read

$$\varepsilon(\mathbf{S}, \theta) = G(\mathbf{S}, \theta) - \frac{\partial G(\mathbf{S}, \theta)}{\partial \mathbf{S}} : \mathbf{S} - \frac{\partial G(\mathbf{S}, \theta)}{\partial \theta}, \quad (1.88)$$

$$\eta(\mathbf{S}, \theta) = -\frac{\partial G(\mathbf{S}, \theta)}{\partial \theta}. \quad (1.89)$$

Since thermodynamic variables are related through (1.49) we substitute (1.87) into (1.40),

$$\begin{aligned} \varrho \left(\overline{G - \frac{\partial G}{\partial \mathbf{S}} : \mathbf{S} - \frac{\partial G}{\partial \theta} \theta} \right) &= \varrho r - \operatorname{div} \mathbf{q} + \varrho \mathbf{S} : \mathbf{D}, \\ -\varrho \theta \frac{\dot{\partial G}}{\partial \theta} + \varrho \left(\frac{\partial G}{\partial \mathbf{S}} : \dot{\mathbf{S}} - \frac{\partial G}{\partial \mathbf{S}} : \dot{\mathbf{S}} - \frac{\dot{\partial G}}{\partial \mathbf{S}} : \mathbf{S} \right) &= \varrho r - \operatorname{div} \mathbf{q} + \varrho \mathbf{S} : \mathbf{D}, \\ \varrho \theta \dot{\eta} - \varrho \left(\frac{\partial^2 G}{\partial \mathbf{S}^2} \dot{\mathbf{S}} + \frac{\partial^2 G}{\partial \mathbf{S} \partial \theta} \dot{\theta} \right) : \mathbf{S} &= \varrho r - \operatorname{div} \mathbf{q} + \varrho \mathbf{S} : \mathbf{D}. \end{aligned}$$

For isothermal processes we get

$$\varrho \theta \dot{\eta} = \varrho r - \operatorname{div} \mathbf{q} + \varrho \left(\mathbf{S} : \left(\mathbf{D} + \frac{\partial^2 G}{\partial \mathbf{S}^2} \dot{\mathbf{S}} \right) \right).$$

Further we identify the rate of dissipation (the rate of entropy production per unit mass) as

$$\xi = \mathbf{S} : \left(\mathbf{D} + \frac{\partial^2 G}{\partial \mathbf{S}^2} \dot{\mathbf{S}} \right) = \mathbf{S} : \left(\mathbf{D} - \mathcal{A} \dot{\mathbf{S}} \right), \quad (1.90)$$

where $\mathcal{A} = -\frac{\partial^2 G}{\partial \mathbf{S}^2}$. Note that if the Gibbs potential is in the form

$$G = -\frac{\mathbf{S} : \mathcal{A} \mathbf{S}}{2} \text{ then } -\frac{\partial^2 G}{\partial \mathbf{S}^2} = \mathcal{A}.$$

We refer to fourth order symmetric tensor \mathcal{A} as elastic compliance tensor.

Objective rate of stress

The relation (1.90) contains the material derivative of the Kirchhoff stress, $\dot{\mathbf{S}} = \frac{\partial}{\partial t} \mathbf{S} + \mathbf{v} \nabla \mathbf{S}$, which is not objective. We require a rate of stress to satisfy frame-indifference principle, for more details see Appendix E.

We can avoid this obstacle in two ways. For the isotropic material we use an "objectivity trick", namely show that necessary corotational terms do not contribute to the dissipation. In the anisotropic case, we slightly modify the above procedure and the objective time derivative of \mathbf{S} appears in a natural way. For both approaches we provide the details next.

Isotropic material

In order to obtain the objective stress-strain constitutive relation we follow [18]. The right hand side of (1.90) contains \mathbf{D} and \mathcal{A} , that are both objective tensors, and $\dot{\mathbf{S}}$, which itself is not objective (however $\mathbf{S} : \mathcal{A} \mathbf{S}$ is objective). To overcome this difficulty we notice that, $\mathcal{A} \mathbf{S}$ is isotropic function of \mathbf{S} and take the form

$$\mathcal{A} \mathbf{S} = \alpha_1 \mathbf{I} + \alpha_2 \mathbf{S} + \alpha_3 \mathbf{S}^2,$$

where α_i ($i = 1, 2, 3$) are scalar functions of the invariants of \mathbf{S} . From the representation of $\mathcal{A} \mathbf{S}$ we can observe that

$$(\mathcal{A} \mathbf{S}) \mathbf{S} = \mathbf{S} (\mathcal{A} \mathbf{S}).$$

Now let us consider an arbitrary tensor \mathbf{B} and the expression

$$\mathbf{S} : \mathcal{A}(\mathbf{B}\mathbf{S} - \mathbf{S}\mathbf{B}).$$

From the symmetry of \mathcal{A} and \mathbf{S} ($\mathbf{S} = \mathbf{S}^T$) together with the above observation we obtain

$$\mathbf{S} : \mathcal{A}(\mathbf{B}\mathbf{S} - \mathbf{S}\mathbf{B}) = \mathcal{A}\mathbf{S} : (\mathbf{B}\mathbf{S} - \mathbf{S}\mathbf{B}) = \mathbf{B} : ((\mathcal{A}\mathbf{S})\mathbf{S} - \mathbf{S}(\mathcal{A}\mathbf{S})) = 0. \quad (1.91)$$

Next we specify $\mathbf{B} := \mathbf{W}$, where \mathbf{W} is a skew-symmetric part of the velocity gradient.

By adding (1.91) to (1.90) we get

$$\xi = \mathbf{S} : \left(\mathbf{D} - \mathcal{A}(\dot{\mathbf{S}} + \mathbf{W}\mathbf{S} - \mathbf{S}\mathbf{W}) \right) = \mathbf{S} : \mathbf{D}_*, \quad (1.92)$$

where

$$\mathbf{D}_* = \mathbf{D} - \mathcal{A}(\dot{\mathbf{S}} + \mathbf{W}\mathbf{S} - \mathbf{S}\mathbf{W}). \quad (1.93)$$

Since \mathcal{A} is invertible, we put $\mathcal{C} = \mathcal{A}^{-1}$ and from (1.93) we obtain relation

$$\dot{\mathbf{S}} + \mathbf{W}\mathbf{S} - \mathbf{S}\mathbf{W} = \mathcal{C}(\mathbf{D} - \mathbf{D}_*). \quad (1.94)$$

To reformulate (1.93) in terms of the Cauchy stress we substitute $\mathbf{S} = \mathbf{T}/\varrho$ and deduce

$$\dot{\mathbf{T}} + \mathbf{T}\operatorname{div} \mathbf{v} + \mathbf{W}\mathbf{T} - \mathbf{T}\mathbf{W} = \varrho\mathcal{C}(\mathbf{D} - \mathbf{D}_*). \quad (1.95)$$

Anisotropic material

By anisotropy of a material we indicate dependence of the Gibbs potential on a rotated stress

$$G = G(\bar{\mathbf{S}}, \theta) = G(\mathbf{R}^T \mathbf{S} \mathbf{R}, \theta), \quad (1.96)$$

where \mathbf{R} is a rotation tensor that is objective, see Appendix E. Examples of such objective rotation tensors are given below.

Repeating the procedure above leading to (1.90) we obtain

$$\xi = \mathbf{S} : \mathbf{D} + \frac{\partial^2 G}{\partial \bar{\mathbf{S}}^2} \dot{\bar{\mathbf{S}}} : \bar{\mathbf{S}} = \mathbf{S} : \mathbf{D} - \bar{\mathcal{A}} \dot{\bar{\mathbf{S}}} : \bar{\mathbf{S}}, \quad (1.97)$$

where $\bar{\mathcal{A}} = -\frac{\partial^2 G}{\partial \bar{\mathbf{S}}^2}$ and $G(\bar{\mathbf{S}}) = -\frac{\bar{\mathbf{S}} : \bar{\mathcal{A}} \bar{\mathbf{S}}}{2}$.

Substituting $\bar{\mathbf{S}} = \mathbf{R}^T \mathbf{S} \mathbf{R}$ yield

$$\begin{aligned} \xi &= \mathbf{S} : \mathbf{D} - \bar{\mathcal{A}} \dot{\bar{\mathbf{S}}} : \mathbf{R}^T \mathbf{S} \mathbf{R} = \mathbf{S} : \left(\mathbf{D} - \overline{\mathbf{R} \bar{\mathcal{A}} \mathbf{R}^T \dot{\mathbf{S}} \mathbf{R} \mathbf{R}^T} \right) \\ &= \mathbf{S} : \left(\mathbf{D} - \mathbf{R} \bar{\mathcal{A}} (\dot{\mathbf{R}}^T \mathbf{S} \mathbf{R} + \mathbf{R}^T \dot{\mathbf{S}} \mathbf{R} + \mathbf{R}^T \mathbf{S} \dot{\mathbf{R}}) \mathbf{R}^T \right) \\ &= \mathbf{S} : \left(\mathbf{D} - \mathbf{R} \bar{\mathcal{A}} \mathbf{R}^T (\mathbf{R} \dot{\mathbf{R}}^T \mathbf{S} + \dot{\mathbf{S}} + \mathbf{S} \dot{\mathbf{R}} \mathbf{R}^T) \mathbf{R} \mathbf{R}^T \right) \\ &= \mathbf{S} : \left(\mathbf{D} - \mathcal{A}(\dot{\mathbf{S}} + \mathbf{\Omega}^T \mathbf{S} + \mathbf{S} \mathbf{\Omega}) \right), \end{aligned} \quad (1.98)$$

where $\mathcal{A} = \mathbf{R} \bar{\mathcal{A}} \mathbf{R}^T$ and $\mathbf{\Omega} = \dot{\mathbf{R}} \mathbf{R}^T$. Notice that in this case the objective time derivative appears automatically without any need to add extra terms.

By choosing different rotated stress tensors, we end up with different objective time derivatives. For example, by choosing \mathbf{R} as the spatial rotation whose rate is related to the skew-symmetric part of the velocity gradient \mathbf{W} , we get the Jaumann derivative of the stress. This derivative is extensively used in the crystal plasticity literature, see e.g. [21]. On the other hand, if we choose \mathbf{R} to be the body rotation, then we will get the Green-McInnis-Naghdi derivative.

1.3.5 Elasticity

It remains to specify an elastic response. We employ the framework of finite elasticity. A number of models has been proposed to describe a material response undergo finite deformations.

A material is said to be Cauchy elastic if the Cauchy stress tensor is a function of the deformation gradient

$$\mathbf{T} = \mathcal{G}(\mathbf{F}). \quad (1.99)$$

Elastic stress-strain relation in which the stress can be obtained from the strain energy (potential) function, are referred to as Green elasticity also known as hyperelasticity

$$\mathbf{T} = \frac{\partial \mathcal{W}(\mathbf{E})}{\partial \mathbf{E}}, \quad (1.100)$$

where \mathbf{E} stands for a strain measure.

Hypoelastic materials are described by a relation between the rate of stress and the rate of strain

$$\dot{\mathbf{T}} = \mathbb{C} \dot{\mathbf{E}}. \quad (1.101)$$

In Section 1.3 we introduced the elasticity tensors \mathbb{C} and \mathcal{C} . We restrict attention to linear isotropic elasticity and quadratic strain energy function

$$\Psi(\mathbf{E}) = \frac{1}{2} \mathbf{E} : \mathbb{C} \mathbf{E}. \quad (1.102)$$

Therefore recalling (D.2) and (D.3) yields

$$\mathbf{T} = \frac{\partial \Psi(\mathbf{E})}{\partial \mathbf{E}} \Rightarrow \mathbf{T} = \mathbb{C} \mathbf{E} = \lambda_e (\text{tr } \mathbf{E}) \mathbf{I} + 2\mu_e \mathbf{E}, \quad (1.103)$$

where λ_e and μ_e are the Lamé coefficients. Fourth order elasticity tensor \mathbb{C} is given by

$$\begin{aligned} \mathbb{C} &= \lambda_e \mathbf{I} \otimes \mathbf{I} + 2\mu_e \mathbb{I}, \\ \mathbb{C}_{IJKL} &= \lambda_e \delta_{IJ} \delta_{KL} + \mu_e (\delta_{IK} \delta_{JL} + \delta_{JK} \delta_{IL}). \end{aligned}$$

In a crystal with cubic symmetry (such as face-centered cubic FCC or body-centered cubic BCC), with the Cartesian axes oriented along the cube edges, the nonzero elements of \mathbb{C} are the same ones as for the isotropic solid, but the three values C_{11} , C_{12} and C_{44} are independent. So, for FCC crystals the elasticity matrix takes the following form

$$\mathbb{C} = \begin{pmatrix} C_{11} & C_{12} & C_{12} & 0 & 0 & 0 \\ C_{12} & C_{11} & C_{12} & 0 & 0 & 0 \\ C_{12} & C_{12} & C_{11} & 0 & 0 & 0 \\ 0 & 0 & 0 & C_{44} & 0 & 0 \\ 0 & 0 & 0 & 0 & C_{44} & 0 \\ 0 & 0 & 0 & 0 & 0 & C_{44} \end{pmatrix}, \quad (1.104)$$

where we used Voigt single index notation for the components of \mathbf{T} and \mathbf{E}

$$\begin{aligned} (T_1, T_2, T_3, T_4, T_5, T_6)^T &= (T_{11}, T_{22}, T_{33}, T_{23}, T_{13}, T_{12})^T \\ (E_1, E_2, E_3, E_4, E_5, E_6)^T &= (E_{11}, E_{22}, E_{33}, 2E_{23}, 2E_{13}, 2E_{12})^T \end{aligned}$$

and rewrite constitutive relation (1.103) in the form

$$\begin{pmatrix} T_1 \\ T_2 \\ T_3 \\ T_4 \\ T_5 \\ T_6 \end{pmatrix} = \begin{pmatrix} C_{11} & C_{12} & C_{12} & 0 & 0 & 0 \\ C_{12} & C_{11} & C_{12} & 0 & 0 & 0 \\ C_{12} & C_{12} & C_{11} & 0 & 0 & 0 \\ 0 & 0 & 0 & C_{44} & 0 & 0 \\ 0 & 0 & 0 & 0 & C_{44} & 0 \\ 0 & 0 & 0 & 0 & 0 & C_{44} \end{pmatrix} \begin{pmatrix} E_1 \\ E_2 \\ E_3 \\ E_4 \\ E_5 \\ E_6 \end{pmatrix}.$$

Moreover, the rate form (1.71) and equivalently (1.101) reads

$$\overset{\nabla}{\mathbf{T}} = \mathbb{C} \dot{\mathbf{E}} = \lambda_e (\text{tr } \dot{\mathbf{E}}) \mathbf{I} + 2\mu_e \dot{\mathbf{E}}. \quad (1.105)$$

1.4 Crystal Plasticity

In crystal plasticity theory, the material plastic deformation is modelled using the slip system activity concept. Dislocations are assumed to move across the crystal lattice along specific slip systems, which are characterized by specific crystallographic planes and directions. When the material is subjected to loading, the applied stress resolved along the slip direction on the slip plane initiates and controls the extent of dislocation glide. This latter has the effect of shearing the material whereas the material volume remains unchanged and the crystal lattice remains constant. Moreover, the crystal lattice can deform elastically. However, elastic strains are small compared to plastic strains and are sometimes neglected in crystal plasticity models.

A summary of the modelling concepts underlying the plastic deformation of crystallographic structures is presented in this section.

The total deformation \mathbf{F} of a crystal structure is assumed to be composed of two separable deformations \mathbf{F}_e and \mathbf{F}_p , see (1.72). The elastic contribution represents the lattice rotation and distortion. The plastic deformation is associated with sliding between crystal blocks. The motion of dislocations occurs in a certain slip directions on certain slip plane, see Figure 1.9. We assume that plastic deformation does not change the structure of the lattice.



Figure 1.9: Rearrangement of atoms in elastic and plastic (slip) deformations

We introduce the concept of lattice vectors also known as a Bravais lattice, where \mathbf{a}_1 , \mathbf{a}_2 , \mathbf{a}_3 are primitive which form a basis in \mathbb{R}^3 and span the lattice, see Figure 1.10. Moreover, together with lattice vectors we define reciprocal dual lattice vectors by

$$\mathbf{a}^1 = \frac{\mathbf{a}_2 \times \mathbf{a}_3}{\mathbf{a}_1 \cdot (\mathbf{a}_2 \times \mathbf{a}_3)}, \quad (1.106)$$

with \mathbf{a}^2 and \mathbf{a}^3 defined by cyclically permuting 1, 2, and 3. Note that $\mathbf{a}_i \cdot \mathbf{a}^j = \delta_{ij}$ even if basis $\{\mathbf{a}_i\}$ is not orthogonal.

The slip directions ($\mathbf{s}^{(\alpha)}$) and normal vectors to the slip planes ($\mathbf{m}^{(\alpha)}$) can be specified once and for all times in terms of lattice vectors.

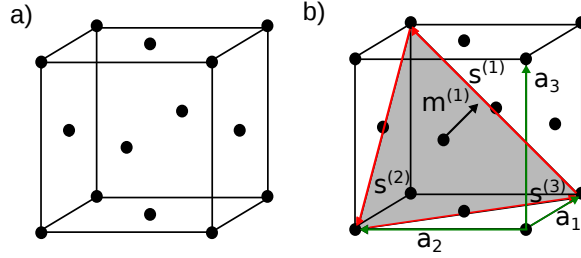


Figure 1.10: Face center cubic FCC crystal structure (a) and some example slip system, the plane along which the crystal will slide is shown in grey (b).

These vectors for α -th ($\alpha = 1, 2, \dots, N$) slip direction are given by the crystallographic structure and are represented as

$$\mathbf{s}_0^{(\alpha)} = s_i^{(\alpha)} \mathbf{a}_i(x, 0), \quad (1.107)$$

$$\mathbf{m}_0^{(\alpha)} = m_i^{(\alpha)} \mathbf{a}^i(x, 0), \quad (1.108)$$

where $s_i^{(\alpha)}$ and $m_i^{(\alpha)}$ are constant coefficients. For example, the slip direction $\mathbf{s}^{(1)} = \mathbf{a}_1 + \mathbf{a}_2$ is called (110) direction.

Stated precisely, our description contains slip directions

$$\mathbf{s}^{(\alpha)}, \quad \alpha = 1, 2, \dots, N, \quad (1.109)$$

and slip planes are identified by their normals

$$\mathbf{m}^{(\alpha)}, \quad \alpha = 1, 2, \dots, N. \quad (1.110)$$

A slip plane with a slip direction is referred to as slip system.

The slip systems are labelled by a superscript α , with $\alpha = 1, 2, \dots, N$ where N is the total number of slip systems. The vectors $\mathbf{s}_0^{(\alpha)}$ and $\mathbf{m}_0^{(\alpha)}$ denote the slip directions and the slip plane normal in the reference and intermediate configurations. In the current state they are represented by (1.109) and (1.110), respectively.

The slip plane is mostly a crystallographic plane which has the highest density of atoms, and slip directions in these planes are directions in which the atoms are most closely packed, see Figure 1.11 (c). Most common crystal structures in metals are

- face-centered cubic (FCC), e.g. Al, Cu, Ni, Ag;
- body-centered cubic (BCC), e.g. Ta, V, Mo, Cr.

Schematics of corresponding structures are shown in Figure 1.11 (a) and (b).

The substantial work on the subject may be traced to papers by Taylor [38], Hill [39], Rice [40], Asaro [41], and Asaro and Needleman [22].

1.4.1 The evolution of the lattice

Let us recall the multiplicative decomposition $\mathbf{F} = \mathbf{F}_e \mathbf{F}_p$ (1.72). The tensor \mathbf{F}_p defines the stress-free intermediate configuration. In this configuration resulting from plastic shearing along well-defined slip planes of the crystal lattice, the orientation of the crystal lattice is identical to

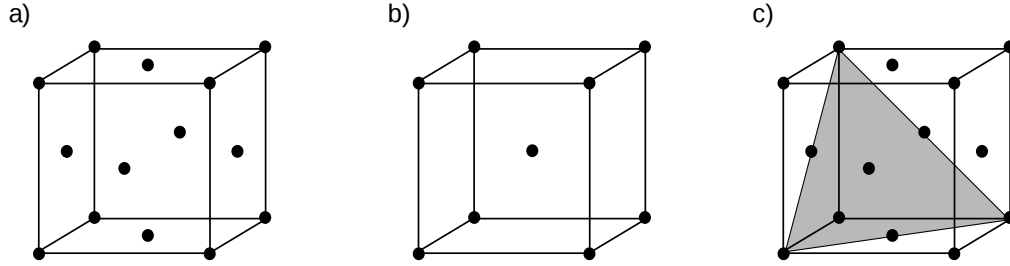


Figure 1.11: Unit cell of FCC crystal (a); unit cell of BCC crystal (b); a triangular portion of the slip plane (corresponding slip directions are parallel to the sides of the triangle).

the orientation in the reference state. The tensor \mathbf{F}_e reflects the lattice deformation and local rigid body rotations.

We assume that the lattice vectors can distort elastically together with \mathbf{F}_e

$$\mathbf{a}_i(x, t) = \mathbf{F}_e(x, t)\mathbf{a}_i(x, 0) \Rightarrow \mathbf{s}^{(\alpha)}(x, t) = \mathbf{F}_e(x, t)\mathbf{s}^{(\alpha)}(x, 0) \quad (1.111)$$

The rate form of (1.111) reads

$$\dot{\mathbf{a}}_i(x, t) = \mathbf{L}_e\mathbf{a}_i(x, t) \Rightarrow \dot{\mathbf{s}}^{(\alpha)}(x, t) = \mathbf{L}_e\mathbf{s}^{(\alpha)}(x, t). \quad (1.112)$$

Following Srinivasa [36], we connect the evolution of the lattice vectors to the lattice rate \mathbf{L}_e through

$$\mathbf{L}_e = \dot{\mathbf{F}}_e\mathbf{F}_e^{-1} = \sum_{i=1}^d \dot{\mathbf{a}}_i \otimes \mathbf{a}^i \iff \dot{\mathbf{a}}_j = \mathbf{L}_e\mathbf{a}_j. \quad (1.113)$$

To see that (1.113) holds, we first multiply $\sum_{i=1}^d \dot{\mathbf{a}}_i \otimes \mathbf{a}^i$ by \mathbf{a}_j ($\mathbf{a}^i \cdot \mathbf{a}_j = \delta_{ij}$) and observe that

$$\mathbf{L}_e = \sum_{i=1}^d \dot{\mathbf{a}}_i \otimes \mathbf{a}^i \Rightarrow \dot{\mathbf{a}}_j = \mathbf{L}_e\mathbf{a}_j.$$

On the other hand, the opposite implication, i.e.

$$\mathbf{L}_e = \sum_{i=1}^d \dot{\mathbf{a}}_i \otimes \mathbf{a}^i \Leftarrow \dot{\mathbf{a}}_j = \mathbf{L}_e\mathbf{a}_j$$

follows from the definition of the reciprocal basis (1.106).

1.4.2 Single Crystal Hypothesis

Plastic effects are modelled as the deformations of a material due to the flow of material dislocations through the lattice. The single-crystal hypothesis is based on the assumption that the motion of dislocations in crystalline materials takes place in preferred slip directions on preferred slip planes. The plastic part of the velocity gradient \mathbf{L}_p is assumed to be given by [40]

$$\begin{aligned} \mathbf{L}_p &= \sum_{\alpha=1}^N \nu^{(\alpha)} \mathbf{s}_0^{(\alpha)} \otimes \mathbf{m}_0^{(\alpha)}, \\ \mathbf{D}_p &= \sum_{\alpha=1}^N \nu^{(\alpha)} \text{sym} \left(\mathbf{s}_0^{(\alpha)} \otimes \mathbf{m}_0^{(\alpha)} \right), \end{aligned} \quad (1.114)$$

where $\nu^{(\alpha)}(x, t)$ stands for the slip rates, which are the functions that oppose the slip on individual slip system and are given by a flow rule (1.120) below. The initial slip directions $\mathbf{s}_0^{(\alpha)}$ refer to the reference configuration, we introduce the current slip directions and those normal to the current slip directions, which depend on the deformation gradient through the relation

$$\mathbf{s}^{(\alpha)} = \mathbf{F}_e \mathbf{s}_0^{(\alpha)}, \quad \mathbf{m}^{(\alpha)} = \mathbf{F}_e^{-T} \mathbf{m}_0^{(\alpha)}.$$

From (1.77) we again obtain the additive decomposition of $\nabla \mathbf{v}$,

$$\nabla \mathbf{v} = \mathbf{L}_e + \sum_{\alpha=1}^N \nu^{(\alpha)} \mathbf{F}_e \mathbf{s}_0^{(\alpha)} \otimes \mathbf{m}_0^{(\alpha)} (\mathbf{F}_e)^{-1} = \mathbf{L}_e + \sum_{\alpha=1}^N \nu^{(\alpha)} \mathbf{s}^{(\alpha)} \otimes \mathbf{m}^{(\alpha)}. \quad (1.115)$$

As pointed out in Section 1.3.1 we aim to avoid the single crystal hypothesis by choosing different type of constitutive assumptions. The procedure is described in Section 1.5.

Decomposition of the velocity gradient

To conclude we express the velocity gradient in terms of the lattice basis vectors. Substituting the elastic and the plastic parts from (1.113) and (1.115) into (1.77) yields

$$\nabla \mathbf{v} = \sum_{i=1}^d \dot{\mathbf{a}}_i \otimes \mathbf{a}^i + \sum_{\alpha=1}^N \nu^{(\alpha)} \mathbf{s}^{(\alpha)} \otimes \mathbf{m}^{(\alpha)}. \quad (1.116)$$

Resolved shear stress

Resolved shear stress is the shear component of an applied stress resolved along a slip plane that is other than perpendicular or parallel to the stress axis.

We define the resolved shear stress as

$$\tau^{(\alpha)} = \mathbf{s}^{(\alpha)} : \mathbf{S} \mathbf{m}^{(\alpha)} \text{ for } \alpha = 1, \dots, N. \quad (1.117)$$

1.4.3 The flow rule and hardening

The slip rates are then formulated as a function of the resolved shear stress $\tau^{(\alpha)}$ and the critical resolved shear stress $\tau_c^{(\alpha)}$

$$\nu^{(\alpha)} = \mathcal{F} \left(\tau^{(\alpha)}, \tau_c^{(\alpha)} \right) \quad (1.118)$$

and the evolution of material state as a function of the slip rates

$$\tau_c^{(\alpha)} = \mathcal{G} \left(\nu^{(\alpha)} \right). \quad (1.119)$$

In its simplest form (1.118), the viscoplastic behaviour is described by a power law, as first introduced by Hutchinson [42] and used in computations by Peirce, Asaro and Needleman [21]

$$\nu^{(\alpha)} = \nu_0 \operatorname{sgn} \left(\tau^{(\alpha)} \right) \left(\frac{|\tau^{(\alpha)}|}{\tau_c^{(\alpha)}} \right)^{1/m}, \quad (1.120)$$

where m is a rate sensitivity parameter, and ν_0 is a reference slip rate.

The hardening rule (1.119) represents the strain-induced evolution of the material resistance to plastic deformation. This strain-induced evolution is a consequence of the increased number of dislocations present in the material during plastic deformation. The critical stresses $\tau_c^{(i)}$ representing dissipative internal forces that oppose the slip are assumed to be governed by the evolution equation

$$\dot{\tau}_c^{(\alpha)} = \sum_j H_{\alpha\beta} |\nu^{(\beta)}|, \quad (1.121a)$$

$$\tau_c^{(\alpha)}|_{t=0} = \tau_0, \quad (1.121b)$$

where the hardening coefficients H_{ij} are functions of accumulated slip rate.

One of the possible forms of the hardening matrix components, proposed by Asaro et al. [21] reads

$$H_{\alpha\beta} = H_0 \operatorname{sech}^2 \left(\frac{H_0 \nu_{acc}}{\tau_s - \tau_0} \right) \quad (1.122)$$

with the initial hardening rate $H_0 = 8.9\tau_0$, the saturation strength $\tau_s = 1.8\tau_0$ and the accumulated slip

$$\nu_{acc}(t) = \sum_{\alpha} \int_0^t |\nu^{(\alpha)}| dt. \quad (1.123)$$

1.4.4 The second law of thermodynamics

Let us notice that under the above assumptions the second law of thermodynamics is satisfied

$$\xi = \mathbf{T} : \mathbf{D}_p = \sum_{\alpha=1}^N \nu^{(\alpha)} \mathbf{T} : \left(\mathbf{s}^{(\alpha)} \otimes \mathbf{m}^{(\alpha)} \right) = \sum_{\alpha=1}^N \nu^{(\alpha)} \tau^{(\alpha)} = \sum_{\alpha=1}^N \nu_0 |\tau^{(\alpha)}| \left(\frac{|\tau^{(\alpha)}|}{\tau_c^{(\alpha)}} \right)^{\frac{1}{m}} \geq 0. \quad (1.124)$$

A rate sensitive formulation is used here in order to avoid the non-uniqueness problem associated with a perfect plastic case. On the other hand, one wish to pass to the rate independent limit in (1.120). In Section 1.4.5 we present an approach, where the limiting case is described by an implicit function relating the slip rates, the resolved shear stresses and the critical resolved shear stresses

$$\mathcal{H} \left(\nu^{(\alpha)}, \tau^{(\alpha)}, \tau_c^{(\alpha)} \right) = 0. \quad (1.125)$$

1.4.5 Implicit constitutive relation

Implicit constitutive theory plays an important role in the modelling of material response. Unified thermodynamic framework for implicitly constituted materials has been introduced by Rajagopal

[24, 25], and Rajagopal and Srinivasa [43]. Instead of demanding an explicit relation, e.g. (1.120) we admit discontinuities, in particular to model threshold condition (1.125).

Gwiazda, Málek et al. have recently developed a mathematical theory for models involving implicit constitutive relations [44, 45].

In the constitutive relation (1.120) exponent $\frac{1}{m}$ is responsible for material rate sensitivity. Formula (1.120) is an approximation of the rate independent limit $m \rightarrow 0$, see Figure 1.12.

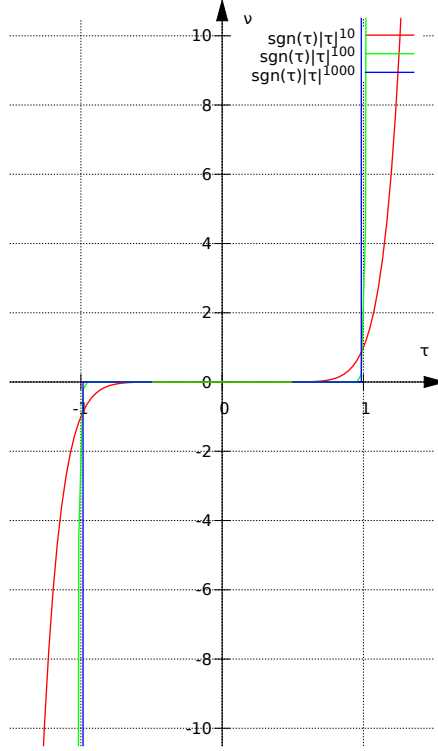


Figure 1.12: Plot of three approximations of the rate independent case.

In the limiting case material response is given by the yield condition:

$$\begin{cases} \nu^{(\alpha)} = 0 & \implies |\tau^{(\alpha)}| < \tau_c^{(\alpha)} \\ |\nu^{(\alpha)}| > 0 & \implies \tau^{(\alpha)} = \tau_c^{(\alpha)} \frac{\nu^{(\alpha)}}{|\nu^{(\alpha)}|} \end{cases} \quad (1.126)$$

The conditions (1.126) are equivalent to the implicit relation

$$f\left(|\tau^{(\alpha)}|\nu^{(\alpha)} - \nu^{(\alpha)}\tau_c^{(\alpha)}\right) + \left(|\tau^{(\alpha)}| - \tau_c^{(\alpha)}\right)_+ = 0, \quad (1.127)$$

where $(x)_+ = \max\{x, 0\}$ and function f satisfies following conditions

- The only root of f is zero

$$f(X) = 0 \iff X = 0.$$

- If $|\tau^{(\alpha)}| > \tau_c^{(\alpha)}$ then $\left(|\tau^{(\alpha)}| - \tau_c^{(\alpha)}\right)_+ = \left(|\tau^{(\alpha)}| - \tau_c^{(\alpha)}\right) \geq 0$ and we require both summands of (1.127) to be zero separately, thus

$$f(X) \neq -\left(|\tau^{(\alpha)}| - \tau_c^{(\alpha)}\right).$$

In the proceeding sections we investigate following admissible functions f

$$\begin{aligned} f(X) &= |X|, \\ f(X) &= X^2, \\ f(X) &= \exp(X) - 1, \\ f(X) &= \frac{1}{2} \arctan(X), \\ f(X) &= \frac{1}{1 + \exp(-X)} - \frac{1}{2}. \end{aligned}$$

The convergence of the finite element approximations of implicit power-law-like models for viscous incompressible fluids have been investigated by Dienes et al. in [46].

We performed the preliminary numerical studies of two dimensional compression and compared the implicit formulation with explicit approximations. The results indicate that the formation of shear bands is faster in the perfect plastic case. The main numerical difficulty encountered is the divergence of the Newton's solver due to the non-differentiable functions in implicit formulation (1.127). Solver is very sensitive with respect to the initial conditions and its parameters.

1.5 Maximization of the rate of entropy production

In Section 1.4.2 we stated the single crystal hypothesis by identifying the plastic part of the velocity gradient with a sum of contributions of individual slip system

$$\mathbf{L}_p = \sum_{\alpha=1}^N \nu^{(\alpha)} \mathbf{s}_0^{(\alpha)} \otimes \mathbf{m}_0^{(\alpha)}.$$

Instead of making the above assumption, we can employ the procedure of maximization of the rate of dissipation, see [33]. The form of \mathbf{D}_p have to be identified. To this aim we make an assumption on one scalar function, the rate of dissipation. The general procedure in the case of rate type model is described in [18, Section 7. The maximum rate of dissipation hypothesis and its consequences]. For details we refer to [16, 17].

We describe the procedure in the case of crystal plasticity. Let us assume that dissipation rate is proportional to the resolved shear stress

$$\begin{aligned} \hat{\xi} &= \sum_{\alpha} \nu_0 |\tau^{(\alpha)}|^{\beta+1} \\ &= \sum_{\alpha} \nu_0 |\mathbf{S} : \mathbf{s}^{(\alpha)} \otimes \mathbf{m}^{(\alpha)}|^{\beta+1} = \sum_{\alpha} \nu_0 |\mathbf{S} : \mathbf{F}_e (\mathbf{s}_0^{(\alpha)} \otimes \mathbf{m}_0^{(\alpha)}) \mathbf{F}_e^{-1}|^{\beta+1} \\ &= \sum_{\alpha} \nu_0 |\mathbf{F}_e^T \mathbf{S} \mathbf{F}_e^{-T} : (\mathbf{s}_0^{(\alpha)} \otimes \mathbf{m}_0^{(\alpha)})|^{\beta+1}, \quad \beta \geq 1, \nu_0 > 0. \end{aligned} \tag{1.128}$$

Our goal is to maximize $\hat{\xi} = \sum_i \nu_0 |\mathbf{S} : (\mathbf{s}^{(\alpha)} \otimes \mathbf{m}^{(\alpha)})|^{\beta+1}$, w.r.t \mathbf{S} under the constraint

$$\xi = \mathbf{S} : \mathbf{D}_p = \mathbf{S} : (\mathbf{F}_e \mathbf{L}_p \mathbf{F}_e^{-1}) = \mathbf{F}_e^T \mathbf{S} \mathbf{F}_e^{-T} : \mathbf{L}_p. \tag{1.129}$$

The maximization is done using the method of Lagrange multipliers. For the auxiliary Lagrange function

$$L = \hat{\xi} + \lambda (\hat{\xi} - \mathbf{F}_e^T \mathbf{S} \mathbf{F}_e^{-T} : \mathbf{L}_p),$$

the necessary condition for finding extremes of L

$$\frac{\partial L}{\partial \mathbf{S}} = 0,$$

leads to

$$\begin{aligned} \frac{1 + \lambda}{\lambda} \frac{\partial \hat{\xi}}{\partial \mathbf{S}} &= \mathbf{F}_e \mathbf{L}_p \mathbf{F}_e^{-1}, \\ \frac{1 + \lambda}{\lambda} \frac{\partial \hat{\xi}}{\partial \mathbf{S}} : \mathbf{S} &= \mathbf{F}_e \mathbf{L}_p \mathbf{F}_e^{-1} : \mathbf{S}, \\ \frac{1 + \lambda}{\lambda} &= \frac{\hat{\xi}}{\frac{\partial \hat{\xi}}{\partial \mathbf{S}} : \mathbf{S}} = \frac{\sum_{\alpha} \nu_0 |\mathbf{F}_e^T \mathbf{S} \mathbf{F}_e^{-T} : (\mathbf{s}_0^{(\alpha)} \otimes \mathbf{m}_0^{(\alpha)})|^{\beta+1}}{(\beta + 1) \left(\sum_{\alpha} \nu_0 |\mathbf{F}_e^T \mathbf{S} \mathbf{F}_e^{-T} : (\mathbf{s}_0^{(\alpha)} \otimes \mathbf{m}_0^{(\alpha)})|^{\beta} \right) \mathbf{F}_e (\mathbf{s}_0^{(\alpha)} \otimes \mathbf{m}_0^{(\alpha)}) \mathbf{F}_e^{-1} : \mathbf{S}}, \\ \frac{1 + \lambda}{\lambda} &= \frac{1}{\beta + 1}. \end{aligned}$$

We obtain

$$\mathbf{L}_p = \sum_{\alpha} \nu_0 \operatorname{sgn}(\tau^{(\alpha)}) |\tau^{(\alpha)}|^{\beta} \left(\mathbf{s}^{(\alpha)} \otimes \mathbf{m}^{(\alpha)} \right).$$

Let us now introduce the flow rule which connects slip rates and resolved shear stresses

$$\nu^{(\alpha)} := \nu_0 \operatorname{sgn}(\tau^{(\alpha)}) |\tau^{(\alpha)}|^{\beta}.$$

We can rewrite \mathbf{D}_p as

$$\mathbf{D}_p = \sum_{\alpha} \nu^{(\alpha)} \operatorname{sym} \left(\mathbf{s}^{(\alpha)} \otimes \mathbf{m}^{(\alpha)} \right).$$

In general we derive a system of governing constitutive equations in dependence on a specific form of dissipation. The unknowns are: the density ϱ , the velocity \mathbf{v} , and the Kirchhoff stress \mathbf{S}

$$\begin{aligned} \dot{\varrho} + \varrho \operatorname{div} \mathbf{v} &= 0, \\ \varrho \dot{\mathbf{v}} - \operatorname{div} \varrho \mathbf{S} &= 0, \\ \mathcal{A} \overset{\nabla}{\mathbf{S}} &= \mathbf{D} - \mathbf{D}_*, \end{aligned}$$

where tensor \mathcal{A} is given through the Gibbs potential G as

$$\mathcal{A} = -\frac{\partial^2 G(\mathbf{S})}{\partial \mathbf{S}^2} \iff G(\mathbf{S}) = -\frac{1}{2} \mathbf{S} : \mathcal{A} \mathbf{S}$$

and \mathbf{D}_* is specified accordingly to chosen dissipation.

It is interesting to investigate other forms of the rate of dissipation. Some examples and resulting models are given in Appendix F.

1.5.1 Incompressibility

Commonly used crystal plasticity assumption is incompressibility. In that case we restrict ourself to the materials with zero divergence, $\operatorname{tr} \mathbf{D} = 0$, and for which the Gibbs potential depends on deviatoric part of the Kirchhoff stress $G = G(\mathbf{S}^d)$, where $\mathbf{S}^d = \mathbf{S} - \frac{1}{d} \operatorname{tr} \mathbf{S}$ and d is the space dimension.

Dissipation in an incompressible case became (since $\text{tr } \mathbf{D} = 0$)

$$\xi = \mathbf{S} : \mathbf{D} - \dot{\Psi} = \mathbf{S}^d : \mathbf{D} - \dot{\Psi}.$$

Mass conservation and balance equations

$$\text{div } \mathbf{v} = 0, \quad (1.130a)$$

$$\dot{\mathbf{v}} - \text{div } \mathbf{S}^d + \nabla p = 0, \quad (1.130b)$$

$$p = -\frac{1}{d} \text{tr } \mathbf{S}, \quad (1.130c)$$

$$\mathcal{A} \overset{\nabla}{\mathbf{S}}^d = \mathbf{D} - \mathbf{D}_*. \quad (1.130d)$$

1.6 Non-dimensional scaling

The aim this section is to perform non-dimensional scaling of the considered model and present typical scales of the problem. We start with a more general set of equations to show how our model ranks among elasto-visco-plastic models. Special emphasis is placed on the similarities and differences with well known models and dimensionless quantities as Reynolds and Weissenberg numbers. Let us consider the following system

$$\dot{\rho} + \rho \text{div } \mathbf{v} = 0, \quad (1.131a)$$

$$\rho \dot{\mathbf{v}} - \mu_\nu \Delta \mathbf{v} - \text{div } \mathbf{T} = 0, \quad (1.131b)$$

$$\overset{\nabla}{\mathbf{T}} + \frac{1}{\lambda} \mathbf{T} = 2\mu_e (\mathbf{D} - \mathbf{D}_p) + \lambda_e \text{tr} (\mathbf{D} - \mathbf{D}_p) \mathbf{I}, \quad (1.131c)$$

where μ_ν is the viscosity, λ is the relaxation time (known from visco-elastic models), λ_e and μ_e are the Lamé coefficients, the objective Jaumann derivative of a stress tensor can be written in the form

$$\overset{\nabla}{\mathbf{T}} = \frac{\partial \mathbf{T}}{\partial t} + \mathbf{v} \nabla \mathbf{T} - \mathbf{W} \mathbf{T} + \mathbf{T} \mathbf{W}, \quad (1.132)$$

and \mathbf{D}_p stands for the plastic part of \mathbf{D}

$$\mathbf{D}_p = \sum_{\alpha} \nu^{(\alpha)} \text{sym} \left(\mathbf{s}^{(\alpha)} \otimes \mathbf{m}^{(\alpha)} \right).$$

Notice that for relaxation time $\lambda = 0$ with $\mu_\nu > 0$ we recover classical compressible Navier-Stokes system. The model with $\lambda \neq 0$, $\mu_\nu > 0$ is referred to as the Johnson-Segalman model with parameter $a = 0$, see (1.66).

We are interested in a system where $\mu_\nu = 0$ and $\lambda = \infty$. In the spirit of visco-elastic models we can say that there is no viscous solvent, i.e. model of caoutchouc-rubber.

Let us now make the system (1.131) non-dimensional. We introduce characteristic values l_0 ,

v_0, t_0, ϱ_0, T_0 , namely quantities intrinsic to the system:

$$\begin{aligned} \text{length} \quad x^* &= \frac{x}{l_0}, \\ \text{velocity} \quad \mathbf{v}^* &= \frac{\mathbf{v}}{v_0}, \\ \text{time} \quad t^* &= \frac{t}{t_0}, \\ \text{density} \quad \varrho^* &= \frac{\varrho}{\varrho_0}, \\ \text{Cauchy stress} \quad \mathbf{T}^* &= \frac{\mathbf{T}}{T_0}. \end{aligned}$$

Derivatives w.r.t. time and space are scaled according to the above equalities,

$$\frac{\partial}{\partial x} = \frac{1}{l_0} \frac{\partial}{\partial x^*}, \quad \frac{\partial}{\partial t} = \frac{1}{t_0} \frac{\partial}{\partial t^*}.$$

Since we deal with material time derivative (denoted by superposed dot) it is convenient to choose reference time as $t_0 = \frac{l_0}{v_0}$,

$$\frac{d}{dt} = \frac{\partial}{\partial t} + (\mathbf{v} \cdot \nabla), \quad \frac{d}{dt^*} = \frac{1}{t_0} \frac{\partial}{\partial t^*} + \frac{v_0}{l_0} (\mathbf{v}^* \cdot \nabla^*).$$

At first we scale the momentum balance (1.131b). Dimensional quantities are replaced by nondimensionalized multiplied by corresponding scales. For the sake of brevity asterisks are omitted

$$\begin{aligned} \frac{\varrho_0 v_0^2}{l_0} \left(\varrho \frac{\partial}{\partial t} \mathbf{v} + \varrho \mathbf{v} \nabla \mathbf{v} \right) - \mu_\nu \frac{v_0}{l_0^2} \Delta \mathbf{v} - \frac{T_0}{l_0} \operatorname{div} \mathbf{T} &= 0, \\ \varrho_0 v_0 l_0 \left(\varrho \frac{\partial}{\partial t} \mathbf{v} + \varrho \mathbf{v} \nabla \mathbf{v} \right) - \mu_\nu \Delta \mathbf{v} - \underbrace{\frac{T_0 l_0}{v_0}}_{=\mu} \operatorname{div} \mathbf{T} &= 0. \end{aligned}$$

Let us define the viscosity in our system $\mu = \frac{T_0 l_0}{v_0}$ and divide by it

$$\frac{\varrho_0 v_0 l_0}{\mu} \left(\varrho \frac{\partial}{\partial t} \mathbf{v} + \varrho \mathbf{v} \nabla \mathbf{v} \right) - \frac{\mu_\nu}{\mu} \Delta \mathbf{v} - \operatorname{div} \mathbf{T} = 0.$$

We introduce the Reynolds number

$$\operatorname{Re} = \frac{\varrho_0 v_0 l_0}{\mu},$$

$$\operatorname{Re} \left(\varrho \frac{\partial}{\partial t} \mathbf{v} + \varrho \mathbf{v} \nabla \mathbf{v} \right) - \frac{\mu_\nu}{\mu} \Delta \mathbf{v} - \operatorname{div} \mathbf{T} = 0.$$

The stress evolution equation (1.131c) reads as follows

$$\frac{v_0 T_0}{l_0} \overset{\nabla}{\mathbf{T}} + \frac{T_0}{\lambda} \mathbf{T} = 2\mu_e \frac{v_0}{l_0} (\mathbf{D} - \mathbf{D}_p) + \lambda_e \frac{v_0}{l_0} \operatorname{tr}(\mathbf{D} - \mathbf{D}_p) \mathbf{I}. \quad (1.133)$$

Due to the plastic effects additional time scale appear. Since $\mathbf{D}_p = \sum_{\alpha} \nu^{(\alpha)} \text{sym}(\mathbf{s}^{(\alpha)} \otimes \mathbf{m}^{(\alpha)})$ we introduce the reference slip rate ν_0 of dimension [1/s] and require that

$$\nu_0 = \frac{v_0}{l_0}. \quad (1.134)$$

Let us replace the Lamé coefficient in terms of the Young modulus E [Pa] and the Poisson ratio ν_{pois} [nondimensional]

$$\mu_e = \frac{E}{2(1 + \nu_{pois})}, \quad \lambda_e = \frac{E\nu_{pois}}{(1 + \nu_{pois})(1 - 2\nu_{pois})}.$$

We multiply (1.133) by $\frac{l_0}{v_0 E}$.

$$\frac{T_0}{E} \overset{\nabla}{\mathbf{T}} + \frac{T_0}{E} \frac{l_0}{v_0 \lambda} \mathbf{T} = \frac{1}{1 + \nu_{pois}} (\mathbf{D} - \mathbf{D}_p) + \frac{\nu_{pois}}{(1 + \nu_{pois})(1 - 2\nu_{pois})} \text{tr}(\mathbf{D} - \mathbf{D}_p) \mathbf{I}$$

and introduce the Weissenberg number

$$\text{Wi} = \frac{\lambda v_0}{l_0},$$

$$\frac{T_0}{E} \overset{\nabla}{\mathbf{T}} + \frac{T_0}{E} \frac{1}{\text{Wi}} \mathbf{T} = \frac{1}{1 + \nu_{pois}} (\mathbf{D} - \mathbf{D}_p) + \frac{\nu_{pois}}{(1 + \nu_{pois})(1 - 2\nu_{pois})} \text{tr}(\mathbf{D} - \mathbf{D}_p) \mathbf{I}.$$

Note that in contrary to the scaling of visco-elastic models, the dimension of the terms of (1.133) is [Pa/s]. The term $\frac{T_0}{E} \frac{1}{\text{Wi}} \mathbf{T}$ in our case is artificial. The units in the mass balance (1.131a) reduce and the equation remains without any dimensionless number

$$\dot{\varrho} + \varrho \text{div} \mathbf{v} = 0.$$

It remains to express T_0 in therns of the Young's modulus

$$T_0 = cE.$$

The the general nondimensionalized system reads

$$\dot{\varrho} + \varrho \text{div} \mathbf{v} = 0,$$

$$\text{Re} \left(\varrho \frac{\partial}{\partial t} \mathbf{v} + \varrho \mathbf{v} \nabla \mathbf{v} \right) - \frac{\mu_\nu}{\mu} \Delta \mathbf{v} - \text{div} \mathbf{T} = 0,$$

$$c \overset{\nabla}{\mathbf{T}} + \frac{c}{\text{Wi}} \mathbf{T} = \frac{1}{1 + \nu_{pois}} (\mathbf{D} - \mathbf{D}_p) + \frac{\nu_{pois}}{(1 + \nu_{pois})(1 - 2\nu_{pois})} \text{tr}(\mathbf{D} - \mathbf{D}_p) \mathbf{I}.$$

In the center of our attention is the system without the viscous contribution $\mu_\nu = 0$ and with the time scale $\lambda = \infty$

$$\dot{\varrho} + \varrho \text{div} \mathbf{v} = 0, \quad (1.135a)$$

$$\text{Re} \left(\varrho \frac{\partial}{\partial t} \mathbf{v} + \varrho \mathbf{v} \nabla \mathbf{v} \right) - \text{div} \mathbf{T} = 0, \quad (1.135b)$$

$$c \overset{\nabla}{\mathbf{T}} = \frac{1}{1 + \nu_{pois}} (\mathbf{D} - \mathbf{D}_p) + \frac{\nu_{pois}}{(1 + \nu_{pois})(1 - 2\nu_{pois})} \text{tr}(\mathbf{D} - \mathbf{D}_p) \mathbf{I}, \quad (1.135c)$$

$$\mathbf{D}_p = \frac{v_0}{l_0 \nu_0} \sum_{\alpha} \nu^{(\alpha)} \text{sym}(\mathbf{s}^{(\alpha)} \otimes \mathbf{m}^{(\alpha)}). \quad (1.135d)$$

1.6.1 Typical scales of the problem

Having the nondimensionalized system (1.135) we present the typical values for our problem:

$$\begin{aligned}v_0 &= 10^{-5}\text{m/s} = 10\mu\text{m/s}, \\l_0 &= 10^{-2}\text{m}, \\ \nu_0 &= \frac{v_0}{l_0} = 10^{-3}\text{1/s}, \\T_0 &= 10^8\text{Pa} = 100\text{MPa}, \\ \varrho_0 &= 3000\text{kg/m}^3, \\E &= 1000T_0.\end{aligned}$$

The characteristic values imply very high viscosity

$$\mu = 10^3\text{s } 100\text{ MPa} = 10^{11}\text{Pa s},$$

and in consequence very low Reynolds number

$$\text{Re} = \frac{3000\text{ kg/m}^3 10^{-5}\text{m/s } 10^{-2}\text{m}}{10^{11}\text{Pa s}} \approx 10^{-15}.$$

The results considered material is highly viscous for comparison typical viscosity of viscoelastic pitch is of order 10^8 Pa s. Due to the smallness of the Reynolds number the quasi-static assumption would be justified. Although we keep this term for computational purposes.

1.7 Formulation of the problem

To sum up we present the system of equations we aim to solve. At first we formulate the system which is an outcome of the modelling. Later we show the simplification that is made for the sake of mathematical analysis.

Let $T > 0$, $\Omega \subset \mathbb{R}^d$ open, $\varrho_0 : \Omega \rightarrow \mathbb{R}$, $\mathbf{v}_0 : \Omega \rightarrow \mathbb{R}^d$, $\mathbf{S}_0 : \Omega \rightarrow \mathbb{R}^{d \times d}$, $\mathbf{a}_{i0} : \Omega \rightarrow \mathbb{R}^d$, $i = 1, 2, \dots, d$, $\mathbf{v}_D : \Gamma_D \rightarrow \mathbb{R}^d$, $\mathbf{t} : \Gamma_N \rightarrow \mathbb{R}^d$. The system is satisfied inside the domain $\Omega \subset \mathbb{R}^d$, the boundary $\partial\Omega$ consists of two non-intersecting parts Γ_D and Γ_N corresponding to the Dirichlet and the Neumann boundary conditions, respectively. We look for the density ϱ , the velocity \mathbf{v} , the Kirchhoff stress \mathbf{S} , and the lattice vectors $\mathbf{a}_1, \mathbf{a}_2, \dots, \mathbf{a}_d$ ($\mathbf{s}^{(\alpha)}$ and $\mathbf{m}^{(\alpha)}$ are given through lattice vectors) satisfying

$$\dot{\varrho} + \varrho \operatorname{div} \mathbf{v} = 0 \quad \text{in } \Omega \times (0, T), \quad (1.136a)$$

$$\varrho \dot{\mathbf{v}} = \operatorname{div} (\varrho \mathbf{S}) \quad \text{in } \Omega \times (0, T), \quad (1.136b)$$

$$\mathcal{A} \overset{\nabla}{\mathbf{S}} = \mathbf{D} - \sum_{\alpha=1}^N \nu^{(\alpha)} \operatorname{sym} \left(\mathbf{s}^{(\alpha)} \otimes \mathbf{m}^{(\alpha)} \right) \quad \text{in } \Omega \times (0, T), \quad (1.136c)$$

$$\sum_{i=1}^d \dot{\mathbf{a}}_i \otimes \mathbf{a}^i = \nabla \mathbf{v} - \sum_{\alpha=1}^N \nu^{(\alpha)} \left(\mathbf{s}^{(\alpha)} \otimes \mathbf{m}^{(\alpha)} \right) \quad \text{in } \Omega \times (0, T), \quad (1.136d)$$

$$\varrho(x, 0) = \varrho_0(x) \quad \forall x \in \Omega, \quad (1.136e)$$

$$\mathbf{v}(x, 0) = \mathbf{v}_0(x) \quad \forall x \in \Omega, \quad (1.136f)$$

$$\mathbf{S}(x, 0) = \mathbf{S}_0(x) \quad \forall x \in \Omega, \quad (1.136g)$$

$$\mathbf{a}_i(x, 0) = \mathbf{a}_{i0}(x) \quad \forall x \in \Omega, \quad (1.136h)$$

$$\mathbf{v} = \mathbf{v}_D \quad \text{on } \Gamma_D \times (0, T), \quad (1.136i)$$

$$\mathbf{S} \mathbf{n} = \mathbf{t} \quad \text{on } \Gamma_N \times (0, T). \quad (1.136j)$$

Chapter 2 is devoted to the mathematical analysis of the simplified problem. We assume incompressibility, namely the mass balance (1.136a) is equivalent to the divergence free condition (1.21). This incompressible case has been discussed in Section 1.5.1, we put $\varrho = 1$, $p = -\frac{1}{2} \operatorname{tr} \mathbf{S}$ and for the sake of brevity denote the deviatoric part of stress as \mathbf{S} . Moreover, plastic effects are neglected, thus equation (1.136d) and corresponding unknowns are not taken into account.

Let $T > 0$, $\Omega \subset \mathbb{R}^2$ periodic, $\mathbf{v}_0 : \Omega \rightarrow \mathbb{R}^2$, $\mathbf{S}_0 : \Omega \rightarrow \mathbb{R}^{2 \times 2}$. Find the velocity \mathbf{v} , the pressure p , and the Kirchhoff stress \mathbf{S} such that

$$\begin{aligned} \operatorname{div} \mathbf{v} &= 0, & \text{in } \Omega \times (0, T), \\ \frac{\partial \mathbf{v}}{\partial t} + \mathbf{v} \nabla \mathbf{v} + \nabla p &= \operatorname{div} \mathbf{S}, & \text{in } \Omega \times (0, T), \\ \frac{\partial \mathbf{S}}{\partial t} + \mathbf{v} \nabla \mathbf{S} + \mathbf{W} \mathbf{S} - \mathbf{S} \mathbf{W} &= \mathbf{D} & \text{in } \Omega \times (0, T), \\ \mathbf{v}(x, 0) &= \mathbf{v}_0(x) & \forall x \in \Omega, \\ \mathbf{S}(x, 0) &= \mathbf{S}_0(x) & \forall x \in \Omega. \end{aligned}$$

In Chapter 4 we provide a numerical solutions to the system (1.136), however it can reformulated according to the specific experimental setting.

Chapter 2

Mathematical analysis of a rate-type fluid model arising from crystal plasticity

The mathematical theory of initial and boundary value problems involving visco-elastic fluids gained attention during the last three decades. For the incompressible model Oldroyd-B model, there is a vast amount of results in the literature, see Section 2.2. We aim to provide the analytical result for a rate-type fluid model originated in crystal plasticity. In comparison with Oldroyd-B model our system lacks viscous contribution to the momentum balance, thus the momentum equation is similar to the Euler equation. This makes the analysis of the complete problem (1.136) difficult. We propose a regularisation of the rate type equation for the extra (elastic) stress \mathbf{S} . This regularization helps us to improve a priori estimates that are then shown to be sufficient to establish the large data existence of a weak solution. There exists studies of stress diffusive Oldroyd-type models, but to the author's knowledge the system investigated in this chapter have not been studied so far.

2.1 Problem formulation

The system (1.136) derived in Chapter 1 describes behaviour of crystal plastic material. For the sake of mathematical analysis of the system we make the following simplifications: consider the incompressible case and neglect plastic effects. The following problem captures essential mathematical difficulties, find $(\mathbf{v}, \mathbf{S}, p)$ spatially periodic in $[0, L]^d \times (0, T)$ such that

$$\operatorname{div} \mathbf{v} = 0, \tag{2.1a}$$

$$\frac{\partial \mathbf{v}}{\partial t} + \mathbf{v} \nabla \mathbf{v} + \nabla p = \operatorname{div} \mathbf{S}, \tag{2.1b}$$

$$\frac{\partial \mathbf{S}}{\partial t} + \mathbf{v} \nabla \mathbf{S} + \mathbf{W} \mathbf{S} - \mathbf{S} \mathbf{W} = \mathbf{D}. \tag{2.1c}$$

Despite our effort we were unable to show the existence of the solution to the system (2.1). Detail description of the structure of standard a priori estimates to system (2.1) in two dimensions are given in Appendix B. Therefore we propose two different regularizations, namely adding a regularization term $-\Delta \mathbf{S}$ or $-\Delta \frac{\partial}{\partial t} \mathbf{S}$.

Here we will not give the physical justification for proposed regularizing term. In the literature one can find visco-elastic models with a diffusive term appearing in the evolution equation for the

visco-elastic stress tensor that are an outcome of modelling, see e.g. diffusive Peterlin model [47] or [48, 49]. Moreover, numerical stability of the effect of stress diffusive term into the classical Oldroyd-B constitutive equation has been studied in [50].

2.2 Overview of the known results

2.2.1 Visco-elastic fluids

Let us recall that the evolution of visco-elastic fluids is governed by the system of equations

$$\begin{aligned} \operatorname{div} \mathbf{v} &= 0, \\ \rho \left(\frac{\partial \mathbf{v}}{\partial t} + [\nabla \mathbf{v}] \mathbf{v} \right) &= \operatorname{div} \mathbf{T}, \\ \mathbf{T} &= -p \mathbf{I} + \mathbf{S}_\nu + \mathbf{S}_e, \\ \mathbf{S}_\nu &= 2\mu_\nu \mathbf{D}, \\ \overset{\nabla}{\mathbf{S}}_e + \mathbf{S}_e &= 2\mu_e \mathbf{D}, \end{aligned}$$

where explicitly splitted the stress tensor into the Newtonian part \mathbf{S}_ν and visco-elastic part \mathbf{S}_e . We present the overview of various mathematical results dealing with the questions of the existence of solutions to the viscoelastic flows and in particular with the Oldroyd-B model.

To the author's knowledge, the first result on incompressible Oldroyd-B fluids was obtained by Guillopé and Saut [51]. The result concerns local existence of regular strong solutions and existence of global solutions for small initial data in an Hilbert framework. The main obstacle was the fact that, in general, there is no appropriate energy estimate for such non-Newtonian fluid. For the review paper we refer to Fernández-Cara, Guillén and Ortega [52].

The existence of global weak solutions for a model with corotational time derivative was established by Lions and Masmoudi [53]. This seems to be one of the most significant results in this area. Due to the similarity of considered system of equations to system (2.1) we would like to recall the result. Main theorem of [53] in two dimensional, periodic case, reads as follows

Theorem 1.

$$\begin{aligned} \operatorname{div} \mathbf{v} &= 0 \\ \frac{\partial \mathbf{v}}{\partial t} + \mathbf{v} \nabla \mathbf{v} - \mu_\nu \Delta \mathbf{v} + \nabla p &= \operatorname{div} \mathbf{T} \\ \frac{\partial \mathbf{T}}{\partial t} + \mathbf{v} \nabla \mathbf{T} + \mathbf{T} \mathbf{W} - \mathbf{W} \mathbf{T} + a \mathbf{T} &= b \mathbf{D} \\ \mathbf{v}|_{t=0} = \mathbf{v}_0 \in L^2(\Omega), \quad \mathbf{T}|_{t=0} = \mathbf{T}_0 \in L^2(\Omega) \end{aligned} \quad (2.2)$$

Moreover, $\operatorname{div} \mathbf{v}_0 = 0$ in \mathcal{D}' , $\mathbf{T} = \mathbf{T}^T$, and all functions are assumed to be periodic.

Then there exists a global weak solution $(\mathbf{v}, \mathbf{T}, p)$ to the system (2.2) such that, for all $T \in (0, \infty)$

$$\mathbf{v} \in L^2(0, T; H^1), \quad \mathbf{T} \in C([0, \infty); L^2),$$

$$p \in L^1(0, T; W^{2,1}) \cap L^2(0, T; W^{1,1}) \cap L^q(0, T; L^r),$$

where $\mu_\nu > 0$, $a, b \geq 0$, $1 \leq q < \infty$, $r = \frac{q}{q-1}$ and $\int_\Omega p \, dx = 0$.

The authors use an essential feature of the Jaumann objective time derivative (and only for them), namely that the energy estimates are available. The above theorem was generalised by Bejaoui and Majdoub in [54] where the authors replaced the Laplacian term by $\operatorname{div}(f(\mathbf{D}))$ with tensorial function f , which is C^1 , monotone, coercive with p -growth.

For the well-posedness results in scaling invariant Besov spaces, we refer to the work of Chemin and Masmoudi [55], where they also give some blow-up criterions both for two and three dimensions. Further interesting results concerning the local well posedness of the initial boundary value problem for the Oldroyd type fluids have been done in several other studies, see [56, 57].

On the other hand, there are relatively few results for the compressible model. Lei [58] proved the local and global existence of classical solutions for a compressible Oldroyd-B system in a torus with small initial data. He also studied the incompressible limit problem and showed that the compressible flows with well-prepared initial data converge to incompressible ones when the Mach number converges to zero. For recent studies on strong solutions of 3D compressible Oldroyd-B fluids we refer to Fung and Zi [59].

All the results mentioned above take advantage of the presence of the Newtonian stress tensor and in consequence of the boundedness of the velocity gradient. Our model lacks the viscous term and we must deal with mathematical disadvantages. The system (2.1) has its origin in the modelling of crystal plastic materials. In the context of visco-elastic models, one can think of a model of a material where there is no solvent e.g. caoutchouc rubber.

2.2.2 Euler equation

Due to the similar structure, we dedicate the second part of this overview to the incompressible Euler equations

$$\begin{aligned} \operatorname{div} \mathbf{v} &= 0, \\ \frac{\partial \mathbf{v}}{\partial t} + \mathbf{v} \nabla \mathbf{v} + \nabla p &= \mathbf{f} (= \operatorname{div} \mathbf{S}), \\ \mathbf{v}(x, 0) &= \mathbf{v}_0, \end{aligned} \tag{2.3}$$

where we can think that the divergence of stress $\operatorname{div} \mathbf{S}$ plays a role of a driving force. We consider as solvability of the Euler equation important in the context of the system (2.3).

The Euler equation can be viewed as a limit of the Navier-Stokes equations when passing with the Reynold's number to infinity.

The vorticity $\boldsymbol{\omega} = \operatorname{curl} \mathbf{v}$ is a key quantity in an analysis of the motion of an incompressible inviscid fluid. Applying vorticity to equation (2.3) yields

$$\begin{aligned} \operatorname{div} \mathbf{v} &= 0, \\ \frac{\partial \boldsymbol{\omega}}{\partial t} + \mathbf{v} \nabla \boldsymbol{\omega} - \boldsymbol{\omega} \nabla \mathbf{v} &= \operatorname{curl} \mathbf{f}, \\ \boldsymbol{\omega} &= \operatorname{curl} \mathbf{v}. \end{aligned} \tag{2.4}$$

In the presence of physical boundaries, the above system is supplemented with the perfect slip boundary condition

$$\mathbf{v} \cdot \mathbf{n} = 0.$$

In two dimensions the vorticity is a scalar quantity

$$\omega = \operatorname{curl} \mathbf{v} = \partial_1 v_2 - \partial_2 v_1,$$

further due to the incompressibility

$$\operatorname{curl}(\mathbf{v}\nabla\mathbf{v}) = \partial_1(v_i\partial_i v_2) - \partial_2(v_i\partial_i v_1) = v_i\partial_i(\partial_1 v_2 - \partial_2 v_1) = \mathbf{v}\nabla\omega.$$

Finally we obtain

$$\frac{\partial\omega}{\partial t} + \mathbf{v}\nabla\omega = \operatorname{curl}\mathbf{f}. \quad (2.5)$$

In what follows we confine to two dimensions.

This is important that the equations

$$\operatorname{div}\mathbf{v} = 0, \quad \boldsymbol{\omega} = \operatorname{curl}\mathbf{v}, \quad \mathbf{v} \cdot \mathbf{n} = 0$$

completely determine the velocity in terms of the vorticity. More precisely, the operator

$$\mathbf{v}(x) = K(\omega(x)) = \nabla \frac{1}{2\pi} \int_{\Omega} \omega(y) \log|x-y|dy + \nabla\Phi(x),$$

where $\nabla = (-\partial_2, \partial_1)$ and Φ is a harmonic function on Ω with a Neumann boundary condition so that $K\omega \cdot \mathbf{n} = 0$ on $\partial\Omega$. $K : \omega \mapsto \mathbf{v}$ is a continuous linear map from $C^\alpha(\Omega)$ to $C^{\alpha+1}(\Omega)$ (with $\alpha > 0$), and also from $H^s(\Omega)$ to $H^{s+1}(\Omega)$.

The first theorems on the local in time existence and uniqueness of solutions were obtained by Lichtenstein [60] and Günther [61]. The global solvability in two space dimensions was proved by Wolibner [62]. Concerning classical solutions we present more modern result by Kato [63] that includes an external force

Theorem 2. *Let $\mathbf{v}_0 \in C^{1+\delta}(\bar{\Omega})$, $\operatorname{div}\mathbf{v}_0 = 0$, $\mathbf{v}_0 \cdot \mathbf{n} = 0$, and $\mathbf{f} \in C^{1+\delta,0}(\bar{\Omega} \times (0,T))$, where $0 < \delta < 1$. Then there exists a solution (\mathbf{v}, p) of (2.3) such that \mathbf{v}, p , and all their derivatives that appear in (2.3) belong to $C(\bar{\Omega} \times (0,T))$. Such a solution is unique up to an arbitrary function of time which may be added to pressure.*

The global-in-time existence of a unique weak solution to (2.3) in two dimensions was established by Yudovich in [64]. The result hold true for initial vorticity

$$\omega_0 \in L^\infty(\Omega). \quad (2.6)$$

Later in [65] Yudovich extended his results and released assumption (2.6).

Following [65], let us define an admissible class and a Yudovich space.

Definition 1. *Admissible class. A function $\theta : [p_0, \infty) \rightarrow (0, \infty)$ is said to be admissible if the auxiliary function ψ defined for $a > 0$ by*

$$\psi_\theta(a) = \inf \left\{ \frac{a^\varepsilon}{\varepsilon} \theta \left(\frac{1}{\varepsilon} \right), 0 < \varepsilon \leq \frac{1}{p_0} \right\}$$

satisfies

$$\int_1^\infty \frac{da}{a\psi_\theta(a)} = \infty.$$

Definition 2. *Space \mathbb{Y}_θ . Given an admissible class θ , with $p_0 > 1$, we denote \mathbb{Y}_θ the space of the divergence free vector fields $\mathbf{f} \in L^2(\Omega)$ tangent to the boundary, such that $\operatorname{curl}\mathbf{f} \in \bigcap_{p \geq p_0} L^p(\Omega)$, and such that there exists $c_f > 0$ such that*

$$\|\mathbf{f}\|_{L^p} \leq c_f \theta(p) \text{ for } p \geq p_0. \quad (2.7)$$

Note that it is a Banach space endowed with the following norm:

$$\|\mathbf{f}\|_{\mathbb{Y}_\theta} = \|\mathbf{f}\|_{L^2} + \sup_{p \geq p_0} \frac{\|\operatorname{curl}\mathbf{f}\|_{L^p}}{\theta(p)}.$$

Theorem 3. *(Yudovich [65]). Assume that the boundary $\partial\Omega$ of the domain is C^2 . Given \mathbf{v}_0 in \mathbb{Y}_θ , there exists a unique weak solution \mathbf{v} to (2.3) in $L^\infty(0, \infty; \mathbb{Y}_\theta)$.*

Logarithmic Sobolev inequality

Here we recall a logarithmic Sobolev inequality that plays a crucial role in a priori estimates. That kind of critical Sobolev inequalities have been extensively studied in the context of the Euler equations, see e.g. Kozono [66, 67].

Proposition 1. *Let $f \in W^{s,p}$ for $n < sp$, then*

$$\|f\|_{L^\infty} \leq C \left(1 + \|\nabla|f|^{\frac{n}{p}}\|_{L^p} (1 + \ln(e + \|f\|_{W^{s,p}}))^{1-\frac{1}{p}}\right).$$

For $n = p = s = 2$ we obtain Brezis–Gallouet inequality, see [68]

$$\|f\|_{L^\infty} \leq C \left(1 + \|\nabla f\|_{L^2} (\ln^+(\|f\|_{W^{2,2}}))^{1/2}\right), \quad (2.8)$$

$$\text{where } \ln^+ = \begin{cases} 1 & \text{for } x < e \\ \ln x & \text{for } x \geq e \end{cases}.$$

Before we prove Proposition 1 we recall basic properties of the Fourier transform.

For a bounded domain $\Omega \subset \mathbb{R}^2$ is well known that an $H^2(\Omega)$ function can be extended by an $H^2(\mathbb{R}^2)$ function. More precisely one can construct an extension P such that:

- operator P is a bounded operator from $H^1(\Omega)$ into $H^1(\mathbb{R}^2)$
- operator P is a bounded operator from $H^2(\Omega)$ into $H^2(\mathbb{R}^2)$
- $P\mathbf{f}|_\Omega = \mathbf{f}$ for every $\mathbf{f} \in H^1(\Omega)$

Let $\mathbf{f} \in H^2(\Omega)$. Let $\mathbf{g} = P\mathbf{f}$ and we denote by $\hat{\mathbf{g}}$ the Fourier transform of \mathbf{g} . We have

$$\|(1 + |\xi|)\hat{\mathbf{g}}\|_{L^2(\mathbb{R}^2)} \leq C\|\mathbf{f}\|_{H^1(\Omega)}, \quad (2.9)$$

$$\|(1 + |\xi|^2)\hat{\mathbf{g}}\|_{L^2(\mathbb{R}^2)} \leq C\|\mathbf{f}\|_{H^2(\Omega)}, \quad (2.10)$$

$$\|\mathbf{f}\|_{L^\infty(\Omega)} \leq \|\mathbf{g}\|_{L^\infty(\mathbb{R}^2)} \leq C\|\hat{\mathbf{g}}\|_{L^1(\mathbb{R}^2)}. \quad (2.11)$$

Proof. (Proposition 1)

$$\begin{aligned} \|\hat{\mathbf{g}}\|_{L^1(\mathbb{R}^2)} &= \int_{|\xi| < R} |\hat{\mathbf{g}}| d\xi + \int_{|\xi| \geq R} |\hat{\mathbf{g}}| d\xi \\ &= \int_{|\xi| < R} (1 + |\xi|)|\hat{\mathbf{g}}| \frac{1}{1 + |\xi|} d\xi + \int_{|\xi| \geq R} (1 + |\xi|^2)|\hat{\mathbf{g}}| \frac{1}{1 + |\xi|^2} d\xi \\ &\leq \left(\int_{|\xi| < R} (1 + |\xi|)^2 |\hat{\mathbf{g}}|^2 d\xi \right)^{1/2} \left(\int_{|\xi| < R} \frac{1}{(1 + |\xi|)^2} d\xi \right)^{1/2} \\ &\quad + \left(\int_{|\xi| \geq R} (1 + |\xi|^2)^2 |\hat{\mathbf{g}}|^2 d\xi \right)^{1/2} \left(\int_{|\xi| \geq R} \frac{1}{(1 + |\xi|^2)^2} d\xi \right)^{1/2} \\ &\leq C\|\mathbf{f}\|_{H^1} (\ln(e + R))^{1/2} + C\|\mathbf{f}\|_{H^2} \frac{1}{1 + R}. \end{aligned} \quad (2.12)$$

Inequality (2.12) holds for every $R \geq 0$. We put $R = \|\mathbf{f}\|_{H^2}$ and by (2.11) we get (2.8)

$$\|\mathbf{f}\|_{L^\infty(\Omega)} \leq C \left(1 + \|\mathbf{f}\|_{H^1} (\ln^+(\|\mathbf{f}\|_{H^2}))^{1/2}\right).$$

□

2.3 Existence of a global weak solution to the regularised problem

We consider the model 2.1 regularized by $-\Delta \frac{\partial}{\partial t} S$. It describes a flow of crystal plastic material in a two dimensional periodic domain. Note that one can multiply the regularization term by an arbitrary small constant $-\varepsilon \Delta \frac{\partial}{\partial t} S$, however we are unable to pass to the limit with $\varepsilon \rightarrow 0$ so for the sake of brevity we put $\varepsilon = 1$.

The system of governing equations reads. Find $\mathbf{v}(x, t) : \Omega \times [0, T] \mapsto \mathbb{R}^2$, $p(x, t) : \Omega \times [0, T] \mapsto \mathbb{R}$, and $\mathbf{S}(x, t) : \Omega \times [0, T] \mapsto \mathbb{R}_{\text{sym}}^{2 \times 2}$ such that

$$\operatorname{div} \mathbf{v} = 0, \quad (2.13a)$$

$$\frac{\partial \mathbf{v}}{\partial t} + \mathbf{v} \nabla \mathbf{v} + \nabla p = \operatorname{div} \mathbf{S}, \quad (2.13b)$$

$$\frac{\partial \mathbf{S}}{\partial t} + \mathbf{v} \nabla \mathbf{S} + \mathbf{W} \mathbf{S} - \mathbf{S} \mathbf{W} - \varepsilon \Delta \frac{\partial}{\partial t} \mathbf{S} = \mathbf{D}, \quad (2.13c)$$

$$\mathbf{v}(x, 0) = \mathbf{v}_0, \quad (2.13d)$$

$$\mathbf{S}(x, 0) = \mathbf{S}_0. \quad (2.13e)$$

Let us now define a weak solution and state the main result.

Definition 3. Let $\Omega \subset \mathbb{R}^2$ open. Let $\mathbf{v}_0 \in L^2_{0,\operatorname{div}}(\Omega)$ and $\mathbf{S}_0 \in L^2(\Omega)$. Then the couple

$$(\mathbf{v}, \mathbf{S}) \in L^\infty(0, T; W^{1,2}_{0,\operatorname{div}}(\Omega)) \times L^\infty(0, T; W^{1,2}(\Omega)) \cap L^2(0, T; W^{2,2}(\Omega))$$

with $\frac{\partial \mathbf{v}}{\partial t} \in L^1(0, T; (W^{1,2}_{0,\operatorname{div}}(\Omega))^*)$ is called a global weak solution to the system (2.13) corresponding to data \mathbf{v}_0 and \mathbf{S}_0 , if

$$\int_{\Omega} \frac{\partial \mathbf{v}}{\partial t} \boldsymbol{\varphi} \, dx + \int_{\Omega} (\mathbf{v} \cdot \nabla \mathbf{v}) \boldsymbol{\varphi} \, dx = - \int_{\Omega} \mathbf{S} : \mathbf{D}(\boldsymbol{\varphi}) \, dx \quad \forall \boldsymbol{\varphi} \in \{C_0^\infty(\Omega \times (-\infty, T))^2, \operatorname{div} \boldsymbol{\varphi} = 0\}, \quad (2.14a)$$

$$\begin{aligned} \int_{\Omega} \frac{\partial \mathbf{S}}{\partial t} \boldsymbol{\Sigma} \, dx + \int_{\Omega} \mathbf{v} \nabla \mathbf{S} : \boldsymbol{\Sigma} \, dx + \int_{\Omega} \mathbf{S} \mathbf{W} : \boldsymbol{\Sigma} - \mathbf{W} \mathbf{S} : \boldsymbol{\Sigma} \, dx \\ + \varepsilon \int_{\Omega} \nabla \frac{\partial \mathbf{S}}{\partial t} : \nabla \boldsymbol{\Sigma} \, dx = \int_{\Omega} \mathbf{D} : \boldsymbol{\Sigma} \, dx \quad \forall \boldsymbol{\Sigma} \in \{C_0^\infty(\Omega \times (-\infty, T))^{2 \times 2}\}, \end{aligned} \quad (2.14b)$$

Theorem 4. *Existence of Weak Solution.* There exists a global weak solution to the problem (2.13) such that (2.14) is satisfied.

2.3.1 A priori estimates

We present formal a priori estimates for system (2.13) on a two dimensional periodic domain Ω .

First a priori estimate

We multiply (2.13b) by the velocity \mathbf{v} and integrate

$$\int_0^T \int_{\Omega} \frac{\partial \mathbf{v}}{\partial t} \cdot \mathbf{v} \, dx \, dt + \int_0^T \int_{\Omega} \mathbf{v} \nabla \mathbf{v} \cdot \mathbf{v} \, dx \, dt + \int_0^T \int_{\Omega} \nabla p \cdot \mathbf{v} \, dx \, dt = \int_0^T \int_{\Omega} \operatorname{div} \mathbf{S} \cdot \mathbf{v} \, dx \, dt,$$

$$\begin{aligned}
& \frac{1}{2} \int_0^T \frac{d}{dt} \int_{\Omega} |\mathbf{v}|^2 dx dt - \underbrace{\frac{1}{2} \int_0^T \int_{\Omega} |\mathbf{v}|^2 \operatorname{div} \mathbf{v} dx dt}_{=0} + \underbrace{\frac{1}{2} \int_0^T \int_{\partial\Omega} (\mathbf{v} \cdot \mathbf{n}) |\mathbf{v}|^2 dS dt}_{=0} \\
&= \underbrace{\int_0^T \int_{\Omega} p \operatorname{div} \mathbf{v} dx dt}_{=0} - \underbrace{\int_0^T \int_{\partial\Omega} (\mathbf{v} \cdot \mathbf{n}) p dS dt}_{=0} + \int_0^T \int_{\Omega} \mathbf{S} : \nabla \mathbf{v} dx dt.
\end{aligned}$$

The underbraced terms above are equal to zero due to the divergence free condition (2.13a) and the boundary conditions

$$\begin{aligned}
& \int_{\Omega} \nabla p \mathbf{v} = - \int_{\Omega} p \operatorname{div} \mathbf{v} = 0, \\
& \int_{\Omega} \mathbf{v} \nabla \mathbf{v} \cdot \mathbf{v} = \frac{1}{2} \int_{\Omega} \mathbf{v} \cdot \nabla |\mathbf{v}|^2 = -\frac{1}{2} \int_{\Omega} |\mathbf{v}|^2 \operatorname{div} \mathbf{v} = 0.
\end{aligned}$$

Finally we obtain

$$\frac{1}{2} \int_0^T \frac{d}{dt} \|\mathbf{v}\|_{L^2}^2 dt = - \int_0^T \int_{\Omega} \mathbf{S} : \nabla \mathbf{v} dx dt = - \int_0^T \int_{\Omega} \mathbf{S} : \mathbf{D} dx dt. \quad (2.15)$$

Now, we multiply (2.13c) by the stress \mathbf{S} and integrate

$$\begin{aligned}
& \int_0^T \int_{\Omega} \frac{\partial \mathbf{S}}{\partial t} : \mathbf{S} dx dt + \int_0^T \int_{\Omega} \mathbf{v} \nabla \mathbf{S} : \mathbf{S} dx dt + \int_0^T \int_{\Omega} (\mathbf{S} \mathbf{W} - \mathbf{W} \mathbf{S}) : \mathbf{S} dx dt \\
& \quad - \int_0^T \int_{\Omega} \Delta \frac{\partial}{\partial t} \mathbf{S} : \mathbf{S} dx dt = \int_0^T \int_{\Omega} \mathbf{D} : \mathbf{S} dx dt, \\
& \frac{1}{2} \int_0^T \frac{d}{dt} \int_{\Omega} |\mathbf{S}|^2 dx dt - \frac{1}{2} \int_0^T \int_{\Omega} \operatorname{div} \mathbf{v} |\mathbf{S}|^2 dx dt + \frac{1}{2} \int_0^T \int_{\partial\Omega} (\mathbf{v} \cdot \mathbf{n}) |\mathbf{S}|^2 dS dt \\
& \quad + \underbrace{\int_0^T \int_{\Omega} (\mathbf{S} \mathbf{W} - \mathbf{W} \mathbf{S}) : \mathbf{S} dx dt}_{=0} + \int_0^T \frac{d}{dt} \int_{\Omega} |\nabla \mathbf{S}|^2 dx dt \\
& \quad - \int_0^T \int_{\partial\Omega} (\mathbf{S} \cdot \mathbf{n}) \nabla \mathbf{S} dS dt = \int_0^T \int_{\Omega} \mathbf{D} : \mathbf{S} dx dt.
\end{aligned}$$

Again, the inertia term equals zero due to relation

$$\int_{\Omega} \mathbf{v} \nabla \mathbf{S} : \mathbf{S} dx = \frac{1}{2} \int_{\Omega} \mathbf{v} \cdot \nabla |\mathbf{S}|^2 dx = -\frac{1}{2} \int_{\Omega} |\mathbf{S}|^2 \operatorname{div} \mathbf{v} dx = 0.$$

Moreover, notice that the co-rotational term disappears when multiplied by \mathbf{S}

$$\begin{aligned}
& -\mathbf{W} \mathbf{S} : \mathbf{S} + \mathbf{S} \mathbf{W} : \mathbf{S} = S_{ij} W_{jk} S_{ik} - W_{ij} S_{jk} S_{ik} = S_{ij} W_{jk} S_{ki} - W_{ij} S_{jk} S_{ki} \\
& = \operatorname{tr}(\mathbf{S} \mathbf{W} \mathbf{S}) - \operatorname{tr}(\mathbf{W} \mathbf{S} \mathbf{S}) = \operatorname{tr}(\mathbf{S} \mathbf{W} \mathbf{S}) - \operatorname{tr}(\mathbf{S}^T \mathbf{W} \mathbf{S}) = 0.
\end{aligned} \quad (2.16)$$

Finally

$$\frac{1}{2} \int_0^T \frac{d}{dt} \|\mathbf{S}\|_{L^2}^2 dt + \frac{1}{2} \int_0^T \frac{d}{dt} \|\nabla \mathbf{S}\|_{L^2}^2 dt = \int_0^T \int_{\Omega} \mathbf{D} : \mathbf{S} dx dt. \quad (2.17)$$

We sum up (2.15) and (2.17), the integration over time yields

$$\|\mathbf{v}(t)\|_{L^2}^2 + \|\mathbf{S}(t)\|_{L^2}^2 + \|\nabla \mathbf{S}(t)\|_{L^2}^2 = \|\mathbf{v}(0)\|_{L^2}^2 + \|\mathbf{S}(0)\|_{L^2}^2 + \|\nabla \mathbf{S}(0)\|_{L^2}^2 \text{ a.e. } t \in (0, T). \quad (2.18)$$

Equation (2.18) indicates

$$\mathbf{v} \in L^\infty(0, T; L^2(\Omega)), \quad \mathbf{S} \in L^\infty(0, T; W^{1,2}(\Omega)).$$

Second a priori estimate

We multiply (2.13b) by $-\Delta \mathbf{v}$ and integrate

$$\begin{aligned} & -\int_0^T \int_\Omega \left(\frac{\partial \mathbf{v}}{\partial t} \right) : \Delta \mathbf{v} \, dx \, dt - \int_0^T \int_\Omega (\mathbf{v} \nabla \mathbf{v}) : \Delta \mathbf{v} \, dx \, dt - \int_0^T \int_\Omega (\nabla p) : \Delta \mathbf{v} \, dx \, dt \\ & \qquad \qquad \qquad = -\int_0^T \int_\Omega (\operatorname{div} \mathbf{S}) : \Delta \mathbf{v} \, dx \, dt, \\ & \int_0^T \int_\Omega \nabla \left(\frac{\partial \mathbf{v}}{\partial t} \right) : \nabla \mathbf{v} \, dx \, dt + \int_0^T \int_\Omega \nabla (\mathbf{v} \nabla \mathbf{v}) : \nabla \mathbf{v} \, dx \, dt + \int_0^T \int_\Omega \nabla (\nabla p) : \nabla \mathbf{v} \, dx \, dt \\ & \qquad \qquad \qquad = \int_0^T \int_\Omega \nabla (\operatorname{div} \mathbf{S}) : \nabla \mathbf{v} \, dx \, dt, \\ & \frac{1}{2} \int_0^T \frac{d}{dt} \|\nabla \mathbf{v}\|_{L^2}^2 + \underbrace{\int_0^T \int_\Omega \nabla (\mathbf{v} \nabla \mathbf{v}) : \nabla \mathbf{v} \, dx \, dt}_{=0} - \underbrace{\int_0^T \int_\Omega (\nabla p) : \nabla (\operatorname{div} \mathbf{v}) \, dx \, dt}_{=0} \\ & \qquad \qquad \qquad = \int_0^T \int_\Omega \nabla (\operatorname{div} \mathbf{S}) : \nabla \mathbf{v} \, dx \, dt. \end{aligned}$$

Note that the inertia term vanishes, i.e.

$$\int_\Omega \nabla (\mathbf{v} \nabla \mathbf{v}) : \nabla \mathbf{v} \, dx = \int_\Omega \partial_k (v_j \partial_j v_i) \partial_k v_i \, dx = 0$$

due to the two dimensional divergence free condition

$$\frac{\partial v_1}{\partial x_1} = -\frac{\partial v_2}{\partial x_2}$$

and corresponding cancellations.

Thus we obtain

$$\frac{1}{2} \int_0^T \frac{d}{dt} \|\nabla \mathbf{v}\|_{L^2}^2 \, dt = \int_0^T \int_\Omega \nabla (\operatorname{div} \mathbf{S}) : \nabla \mathbf{v} \, dx \, dt. \quad (2.19)$$

Now, we multiply (2.13b) by $-\Delta \mathbf{S}$ and integrate over domain

$$\begin{aligned}
& \int_0^T \int_{\Omega} \frac{\partial \mathbf{S}}{\partial t} : \Delta \mathbf{S} \, dx \, dt + \int_0^T \int_{\Omega} \mathbf{v} \nabla \mathbf{S} : \Delta \mathbf{S} \, dx \, dt + \int_0^T \int_{\Omega} (\mathbf{S} \mathbf{W} - \mathbf{W} \mathbf{S}) : \Delta \mathbf{S} \, dx \, dt \\
& \quad - \int_0^T \int_{\Omega} \Delta \frac{\partial}{\partial t} \mathbf{S} : \Delta \mathbf{S} \, dx \, dt = \int_0^T \int_{\Omega} \mathbf{D} : \Delta \mathbf{S} \, dx \, dt, \\
& \frac{1}{2} \int_0^T \frac{d}{dt} \int_{\Omega} |\nabla \mathbf{S}|^2 \, dx \, dt - \int_0^T \int_{\Omega} ([\nabla \mathbf{v}] \nabla \mathbf{S}) : \nabla \mathbf{S} \, dx \, dt + \int_0^T \int_{\Omega} (\mathbf{S} \mathbf{W} - \mathbf{W} \mathbf{S}) : \Delta \mathbf{S} \, dx \, dt \\
& \quad + \frac{1}{2} \int_0^T \frac{d}{dt} \int_{\Omega} |\Delta \mathbf{S}|^2 \, dx \, dt = - \int_0^T \int_{\Omega} \nabla \mathbf{D} : \nabla \mathbf{S} \, dx \, dt,
\end{aligned}$$

The form of convective is provided by the following equality

$$\int_{\Omega} \nabla(\mathbf{v} \nabla \mathbf{S}) : \nabla \mathbf{S} \, dx = \int_{\Omega} \partial v_k \frac{\partial S_{ij}}{\partial x_k} \frac{\partial S_{ij}}{\partial x_l} + \underbrace{v_k \frac{\partial^2 S_{ij}}{\partial x_l \partial x_k} \frac{\partial S_{ij}}{\partial x_l}}_{=0 \text{ twice by parts}} \, dx = \int_{\Omega} ([\nabla \mathbf{v}] \nabla \mathbf{S}) : \nabla \mathbf{S} \, dx. \quad (2.20)$$

We get

$$\begin{aligned}
\frac{1}{2} \int_0^T \frac{d}{dt} (\|\nabla \mathbf{S}\|_{L^2}^2 + \|\Delta \mathbf{S}\|_{L^2}^2) \, dt &= \underbrace{\int_0^T \int_{\Omega} ([\nabla \mathbf{v}] \nabla \mathbf{S}) : \nabla \mathbf{S} \, dx \, dt}_{\text{A}} \\
&\quad - \underbrace{\int_0^T \int_{\Omega} (\mathbf{W} \mathbf{S} - \mathbf{S} \mathbf{W}) : \Delta \mathbf{S} \, dx \, dt}_{\text{B}} \\
&\quad - \int_0^T \int_{\Omega} \nabla \mathbf{D} : \nabla \mathbf{S} \, dx \, dt.
\end{aligned} \quad (2.21)$$

Moreover, similarly to the first a priori estimate we take advantage of the right hand sides cancellation,

$$\begin{aligned}
\int_{\Omega} \nabla(\mathbf{D}) : \nabla \mathbf{S} \, dx &= \int_{\Omega} \nabla \nabla \mathbf{v} : \nabla \mathbf{S} \, dx = \int_{\Omega} \nabla(\partial_i v_j) : \nabla S_{ij} \, dx \\
&= - \int_{\Omega} \nabla(v_j) : \nabla \partial_i S_{ij} \, dx = - \int_{\Omega} \nabla(\operatorname{div} \mathbf{S}) : \nabla \mathbf{v} \, dx.
\end{aligned}$$

Summing up (2.19) and (2.21) yields

$$\int_0^T \frac{d}{dt} (\|\nabla \mathbf{v}\|_{L^2}^2 + \|\nabla \mathbf{S}\|_{L^2}^2 + \|\Delta \mathbf{S}\|_{L^2}^2) \, dt = 2 \int_0^T \underbrace{\int_{\Omega} ([\nabla \mathbf{v}] \nabla \mathbf{S}) : \nabla \mathbf{S} \, dx}_{\text{A}} - \underbrace{\int_{\Omega} (\mathbf{W} \mathbf{S} - \mathbf{S} \mathbf{W}) : \Delta \mathbf{S} \, dx}_{\text{B}} \, dt \quad (2.22)$$

The next step is the estimation of the right hand side of (2.22). For term A we apply embedding theorem (Proposition 5) and interpolation inequality (Proposition 7)

$$\begin{aligned}
\int_{\Omega} |([\nabla \mathbf{v}] \nabla \mathbf{S}) : \nabla \mathbf{S}| \, dx &\leq \|\nabla \mathbf{v}\|_{L^2} \|\nabla \mathbf{S}\|_{L^4} \|\nabla \mathbf{S}\|_{L^4} \leq \|\nabla \mathbf{v}\|_{L^2} \|\mathbf{S}\|_{W^{1,4}}^2 \stackrel{\text{embedding}}{\leq} \|\nabla \mathbf{v}\|_{L^2} \|\mathbf{S}\|_{W^{\frac{3}{2},2}}^2 \\
\|\nabla \mathbf{v}\|_{L^2} \|\mathbf{S}\|_{W^{\frac{3}{2},2}}^2 &\stackrel{\text{interpolation}}{\leq} C \|\nabla \mathbf{v}\|_{L^2} \|\mathbf{S}\|_{W^{1,2}} \|\mathbf{S}\|_{W^{2,2}} \leq C \|\nabla \mathbf{v}\|_{L^2}^2 \|\nabla \mathbf{S}\|_{L^2}^2 + C \|\Delta \mathbf{S}\|_{L^2}^2.
\end{aligned} \quad (2.23)$$

For the treatment of the second term B we apply the logarithmic Sobolev inequality (Proposition 1) originated with the works of Brezis–Gallouet [68] and Brezis–Wainger [69]

$$\begin{aligned}
\int_{\Omega} (\mathbf{W}\mathbf{S} - \mathbf{S}\mathbf{W}) : \Delta\mathbf{S} \, dx &\leq 2\|\nabla\mathbf{v}\|_{L^2}\|\mathbf{S}\|_{L^\infty}\|\Delta\mathbf{S}\|_{L^2} \\
&\stackrel{\text{B-D ineq.}}{\leq} C\|\nabla\mathbf{v}\|_{L^2} \left(1 + \|\nabla\mathbf{S}\|_{L^2} (\ln^+(\|\mathbf{S}\|_{W^{2,2}}))^{\frac{1}{2}}\right) \|\Delta\mathbf{S}\|_{L^2} \\
&\leq C\|\nabla\mathbf{v}\|_{L^2}\|\Delta\mathbf{S}\|_{L^2} + C\|\nabla\mathbf{v}\|_{L^2}\|\nabla\mathbf{S}\|_{L^2} (\ln^+(\|\Delta\mathbf{S}\|_{L^2}))^{\frac{1}{2}} \|\Delta\mathbf{S}\|_{L^2} \\
&\leq C(\|\nabla\mathbf{v}\|_{L^2}^2 + \|\Delta\mathbf{S}\|_{L^2}^2) + C\|\nabla\mathbf{v}\|_{L^2} (\ln^+(\|\Delta\mathbf{S}\|_{L^2}))^{\frac{1}{2}} \|\Delta\mathbf{S}\|_{L^2} \\
&\leq C(\|\nabla\mathbf{v}\|_{L^2}^2 + \|\Delta\mathbf{S}\|_{L^2}^2) + C\ln^+(\|\Delta\mathbf{S}\|_{L^2})\|\Delta\mathbf{S}\|_{L^2}^2.
\end{aligned} \tag{2.24}$$

Let us now sum up (2.22), (2.23), and (2.24)

$$\frac{d}{dt} (\|\nabla\mathbf{v}\|_{L^2}^2 + \|\nabla\mathbf{S}\|_{L^2}^2 + \|\Delta\mathbf{S}\|_{L^2}^2) \leq C(\|\nabla\mathbf{v}\|_{L^2}^2 + \|\Delta\mathbf{S}\|_{L^2}^2) + C\ln^+(\|\Delta\mathbf{S}\|_{L^2})\|\Delta\mathbf{S}\|_{L^2}^2 \tag{2.25}$$

We increase the right hand side of (2.25) by adding some positive terms and taking advantage of a fact that function $\ln^+(x) \geq 1$,

$$\begin{aligned}
\frac{d}{dt} (\|\nabla\mathbf{v}\|_{L^2}^2 + \|\nabla\mathbf{S}\|_{L^2}^2 + \|\Delta\mathbf{S}\|_{L^2}^2) \\
\leq C(\|\nabla\mathbf{v}\|_{L^2}^2 + \|\nabla\mathbf{S}\|_{L^2}^2 + \|\Delta\mathbf{S}\|_{L^2}^2) (1 + \ln^+(\|\nabla\mathbf{v}\|_{L^2}^2 + \|\nabla\mathbf{S}\|_{L^2}^2 + \|\Delta\mathbf{S}\|_{L^2}^2)).
\end{aligned} \tag{2.26}$$

ODE

Let us denote $Y = \|\nabla\mathbf{v}\|_{L^2}^2 + \|\nabla\mathbf{S}\|_{L^2}^2 + \|\Delta\mathbf{S}\|_{L^2}^2$ and rewrite (2.26) as

$$\begin{aligned}
\frac{d}{dt} Y &\leq Y + Y \ln^+ Y, \\
\int \frac{dY}{2Y(1 + \ln^+ Y)} &\leq \int dt.
\end{aligned} \tag{2.27}$$

We divide the time interval into $[0, e) \cup [e, T)$ and use the definition of the function \ln^+

$$\begin{aligned}
\int_0^e \frac{dY}{2Y} + \int_e^T \frac{dY}{Y(1 + \ln Y)} &\leq \int_0^T dt, \\
\frac{1}{2} \ln \frac{Y(e)}{Y(0)} + \int_e^T \frac{dY}{Y(1 + \ln Y)} &\leq T.
\end{aligned}$$

Let $Z = 1 + \ln Y$

$$\int_e^T \frac{dY}{Y(1 + \ln Y)} = \int_e^T \frac{dZ}{Z} = \ln \frac{Z(T)}{Z(e)} \Rightarrow Y(T) \leq C \exp(C \exp(T)).$$

We conclude that for $\forall T < \infty$

$$\mathbf{v} \in L^\infty(0, T; W^{1,2}(\Omega)), \quad \mathbf{S} \in L^\infty(0, T; W^{2,2}(\Omega)).$$

Note that the existence and uniqueness for the ODE corresponding to (2.27) follows from the Osgood criterion, see Proposition 12.

2.3.2 Galerkin approximation

Let us take $(\omega^i)_{i=1}^\infty$ and $(w^i)_{i=1}^\infty$ the bases of space V^s and \tilde{V}^s , respectively given by Proposition 4. For more details on definitions and construction of basis, see [70].

Definition 4. Let $T > 0$ and $N \geq 1$ be fixed. Functions

$$\mathbf{v}^N(x, t) = \sum_{i=1}^N c_i^N(t) \omega^i(x) \text{ and } \mathbf{S}^N(x, t) = \sum_{i=1}^N d_i^N(t) w^i(x)$$

are called the n -th Galerkin approximation, if

$$\int_{\Omega} \frac{\partial \mathbf{v}^N}{\partial t} \omega^i + \int_{\Omega} (\mathbf{v}^N \cdot \nabla \mathbf{v}^N) \omega^i = - \int_{\Omega} \mathbf{S}^N : \nabla \omega^i \quad \forall i = 1, \dots, N, \quad (2.28a)$$

$$\int_{\Omega} \frac{\partial \mathbf{S}^N}{\partial t} w^j + \int_{\Omega} \mathbf{v}^N \nabla \mathbf{S}^N : w^j + \int_{\Omega} (\mathbf{S}^N \mathbf{W}^N - \mathbf{W}^N \mathbf{S}^N) : w^j \quad (2.28b)$$

$$+ \int_{\Omega} \nabla \frac{\partial \mathbf{S}^N}{\partial t} : \nabla w^j = \int_{\Omega} \mathbf{D}^N : w^j \quad \forall j = 1, \dots, N, \quad (2.28c)$$

$$c_i^N(0) = \int_{\Omega} \mathbf{v}_0 \omega^i, \quad d_j^N(0) = \int_{\Omega} \mathbf{S}_0 w^j, \quad 1 \leq i, j \leq N, \quad (2.28d)$$

with the initial conditions

$$\mathbf{v}^N(x, 0) = P_v^N \mathbf{v}_0(x), \quad \mathbf{S}^N(x, 0) = P_T^N \mathbf{S}_0(x)$$

where P_v^N and P_T^N are the orthogonal continuous projections of H and \tilde{H} respectively onto the linear hulls of the first eigenvectors $\omega^r, r = 1, \dots, N$ and $w^r, r = 1, \dots, N$.

System (2.28) can be rewritten to a system of ordinary differential equations for $(c_1^N, \dots, c_N^N, d_1^N, \dots, d_N^N)$. Let us recall that orthogonality of basis imply $\int_{\Omega} \omega^i \omega^j = \delta_{ij}$ and $\int_{\Omega} w^i w^j = \delta_{ij}$ as

$$\begin{cases} \frac{d}{dt}(c_i^N, d_j^N) = F_{ij}(t, c_1^N, \dots, c_N^N, d_1^N, \dots, d_N^N), \\ c_i^N(0) = \int_{\Omega} \mathbf{v}_0 \omega^i \, dx \quad 1 \leq i \leq N, \\ d_j^N(0) = \int_{\Omega} \mathbf{S}_0 w^j \, dx, \quad 1 \leq j \leq N. \end{cases}$$

We split $F_{ij} = F_{ij}^v + F_{ij}^s$, namely

$$\begin{aligned} \frac{d}{dt} c_i^N &= F_{ij}^v = - \int_{\Omega} \left(\left(\sum_{k=1}^N c_k^N \omega^k \right) \cdot \left(\sum_{k=1}^N c_k^N \nabla \omega^k \right) \right) \omega^i - \int_{\Omega} \left(\sum_{k=1}^N d_k^N w^k \right) : \nabla \omega^i \\ (1 + \lambda_j) \frac{d}{dt} d_j^N &= (1 + \lambda_j) F_{ij}^s = - \int_{\Omega} \left(\sum_{k=1}^N c_k^N \omega^k \right) \left(\sum_{i=1}^N d_k^N \nabla w^k \right) : w^j \\ &\quad - \int_{\Omega} \left(\sum_{i=1}^N d_k^N w^k \right) \left(\sum_{k=1}^N c_k^N \mathbf{W}(\omega^k) \right) : w^j \\ &\quad - \int_{\Omega} \left(\sum_{k=1}^N c_k^N \mathbf{W}(\omega^k) \right) \left(\sum_{i=1}^N d_k^N w^k \right) : w^j \\ &\quad + \int_{\Omega} \left(\sum_{k=1}^N c_k^N \mathbf{D}(\omega^k) \right) : w^j. \end{aligned} \quad (2.29)$$

The standard Caratheodory theory provides the existence of continuous functions $(c_1^N, \dots, c_N^N, d_1^N, \dots, d_N^N)$, which are solutions to (2.28). The uniform estimates, that we will derive in the next subsection, enable us to extend the solution onto the whole time interval $[0, T]$.

2.3.3 Uniform estimates

Following Section 2.3.1 we obtain following uniform estimates

$$\sup_{t \in [0, T]} \|\nabla \mathbf{v}^N\|_{L^2}^2 + \|\nabla \mathbf{S}^N\|_{L^2}^2 + \|\Delta \mathbf{S}^N\|_{L^2}^2 \leq C.$$

What yields

$$\mathbf{v}^N \in L^\infty(0, T; W^{1,2}) \text{ and } \mathbf{S}^N \in L^\infty(0, T; W^{2,2}).$$

Finally, we have shown that there exists a positive constant $C = C(\Omega, T, \mathbf{v}_0, \mathbf{S}_0)$ such that

$$\|\mathbf{v}^N\|_{L^\infty(0, T; W^{1,2})} + \|\mathbf{S}^N\|_{L^\infty(0, T; W^{2,2})} \leq C(\Omega, T, \mathbf{v}_0, \mathbf{S}_0). \quad (2.30)$$

2.3.4 Estimate of the time derivative

Estimate (2.30) is not sufficient for the limit passage. Before we apply a compactness result we need an estimate of time derivatives.

$$\begin{aligned} \left\| \frac{\partial \mathbf{v}^N}{\partial t} \right\|_{L^2(0, T; (W_{0, div}^{1,2})^*)} &= \sup_{\varphi \in L^2(0, T; W_{0, div}^{1,2}), \|\varphi\| \leq 1} \left| \int_0^T \int_\Omega \frac{\partial \mathbf{v}^N}{\partial t} \cdot \varphi \, dx \, dt \right| \\ &= \sup_{\varphi \in L^2(0, T; W_{0, div}^{1,2}), \|\varphi\| \leq 1} \left| \int_0^T \int_\Omega \mathbf{v}^N \nabla \mathbf{v}^N \varphi^N + \mathbf{S}^N \nabla \varphi^N \, dx \, dt \right| \\ &\leq \sup_{\varphi \in L^2(0, T; W_{0, div}^{1,2}), \|\varphi\| \leq 1} \left[\int_0^T \|\mathbf{v}^N\|_4^2 \|\nabla \varphi\|_2 \, dt + \int_0^T \|\mathbf{S}^N\|_2 \|\nabla \varphi\|_2 \, dt \right] \\ &\leq \sup_{\varphi \in L^2(0, T; W_{0, div}^{1,2}), \|\varphi\| \leq 1} C \left[\int_0^T \|\mathbf{v}^N\|_2 \|\nabla \mathbf{v}^N\|_2 \|\nabla \varphi\|_2 \, dt \right. \\ &\quad \left. + \int_0^T \|\mathbf{S}^N\|_2 \|\nabla \varphi\|_2 \, dt \right] \\ &\leq \sup_{\varphi \in L^2(0, T; W_{0, div}^{1,2}), \|\varphi\| \leq 1} C \left[\|\mathbf{v}^N\|_{L^\infty(0, T; L^2)} \|\nabla \mathbf{v}^N\|_{L^2(0, T; L^2)} \|\nabla \varphi\|_{L^2(0, T; L^2)} \right. \\ &\quad \left. + \|\mathbf{S}^N\|_{L^2(0, T; L^2)} \|\nabla \varphi\|_{L^2(0, T; L^2)} \right] \\ &\leq C \|\mathbf{v}^N\|_{L^\infty(0, T; L^2)} \|\nabla \mathbf{v}^N\|_{L^2(0, T; L^2)} + \|\mathbf{S}^N\|_{L^2(0, T; L^2)} \leq C. \end{aligned}$$

For the estimation of $\frac{\partial \mathbf{S}}{\partial t}$, let us first perform an a priori estimate. We multiply (2.13c) by the stress $\frac{\partial \mathbf{S}}{\partial t}$ and integrate

$$\begin{aligned} \int_0^T \int_\Omega \frac{\partial \mathbf{S}}{\partial t} : \frac{\partial \mathbf{S}}{\partial t} \, dx \, dt + \int_0^T \int_\Omega \mathbf{v} \nabla \mathbf{S} : \frac{\partial \mathbf{S}}{\partial t} \, dx \, dt + \int_0^T \int_\Omega (\mathbf{S} \mathbf{W} - \mathbf{W} \mathbf{S}) : \frac{\partial \mathbf{S}}{\partial t} \, dx \, dt \\ - \int_0^T \int_\Omega \Delta \frac{\partial}{\partial t} \mathbf{S} : \frac{\partial \mathbf{S}}{\partial t} \, dx \, dt = \int_0^T \int_\Omega \mathbf{D} : \frac{\partial \mathbf{S}}{\partial t} \, dx \, dt. \end{aligned}$$

Again, that the co-rotational term disappears when multiplied by $\frac{\partial}{\partial t}\mathbf{S}$

$$\begin{aligned} -\mathbf{W}\mathbf{S} : \frac{\partial}{\partial t}\mathbf{S} + \mathbf{S}\mathbf{W} : \frac{\partial}{\partial t}\mathbf{S} &= S_{ij}W_{jk}\frac{\partial}{\partial t}S_{ik} - W_{ij}S_{jk}\frac{\partial}{\partial t}S_{ik} = S_{ij}W_{jk}\frac{\partial}{\partial t}S_{ki} - W_{ij}S_{jk}\frac{\partial}{\partial t}S_{ki} \\ &= \text{tr}\left(\mathbf{S}\mathbf{W}\frac{\partial}{\partial t}\mathbf{S}\right) - \text{tr}\left(\mathbf{W}\mathbf{S}\frac{\partial}{\partial t}\mathbf{S}\right) = \text{tr}\left(\mathbf{S}\mathbf{W}\frac{\partial}{\partial t}\mathbf{S}\right) - \text{tr}\left(\mathbf{S}^T\mathbf{W}\frac{\partial}{\partial t}\mathbf{S}\right) = 0. \end{aligned}$$

We obtain

$$\int_0^T \left\| \frac{\partial \mathbf{S}}{\partial t} \right\|_{L^2}^2 + \left\| \frac{\partial \nabla \mathbf{S}}{\partial t} \right\|_{L^2}^2 dt \leq \left| \int_0^T \int_{\Omega} \mathbf{v} \nabla \mathbf{S} : \frac{\partial \mathbf{S}}{\partial t} + \underbrace{(\mathbf{S}\mathbf{W} - \mathbf{W}\mathbf{S}) : \frac{\partial \mathbf{S}}{\partial t}}_{=0} + \mathbf{D} : \frac{\partial \mathbf{S}}{\partial t} dx dt \right|. \quad (2.31)$$

Further we estimate right hand side of (2.31)

$$\begin{aligned} \left| \int_0^T \int_{\Omega} \mathbf{v} \nabla \mathbf{S} : \frac{\partial \mathbf{S}}{\partial t} dx dt \right| &= \left| - \int_0^T \int_{\Omega} \mathbf{v} \mathbf{S} : \frac{\partial \nabla \mathbf{S}}{\partial t} dx dt \right| \leq \int_0^T \|v\|_{L^2} \|\mathbf{S}\|_{L^\infty} \left\| \frac{\partial \nabla \mathbf{S}}{\partial t} \right\|_{L^2} dt \\ &\leq \int_0^T C \left(\frac{1}{\varepsilon} \right) \|v\|_{L^2}^2 \|\mathbf{S}\|_{L^\infty}^2 + \varepsilon \left\| \frac{\partial \nabla \mathbf{S}}{\partial t} \right\|_{L^2}^2 dt. \end{aligned} \quad (2.32)$$

$$\left| \int_0^T \int_{\Omega} \mathbf{D} : \frac{\partial \mathbf{S}}{\partial t} dx dt \right| \leq \int_0^T \|v\|_{L^2} \left\| \frac{\partial \nabla \mathbf{S}}{\partial t} \right\|_{L^2} dt \leq \int_0^T C \left(\frac{1}{\varepsilon} \right) \|v\|_{L^2}^2 + \varepsilon \left\| \frac{\partial \nabla \mathbf{S}}{\partial t} \right\|_{L^2}^2 dt \quad (2.33)$$

Substituting (2.32) and (2.33) into (2.31) together with previous a priori estimates, yields

$$\int_0^T \left\| \frac{\partial \mathbf{S}}{\partial t} \right\|_{L^2}^2 + \left\| \frac{\partial \nabla \mathbf{S}}{\partial t} \right\|_{L^2}^2 dt \leq C.$$

Finally

$$\frac{\partial \mathbf{S}}{\partial t} \in L^2(0, T; W^{1,2}). \quad (2.34)$$

2.3.5 Limit passage

Let us now pass to the limit in (2.28). Due to the a priori estimates there exists $\mathbf{v} \in L^\infty(W^{1,2})$ with $\frac{\partial \mathbf{v}}{\partial t} \in L^2((W^{1,2})^*)$ and $\mathbf{S} \in L^\infty(W^{2,2})$ with $\frac{\partial \mathbf{S}}{\partial t} \in L^2((W^{1,2}))$. In particular $\frac{\partial}{\partial t}\mathbf{S}^N$ is uniformly bounded in $L^2((W^{1,2})^*)$. The identification of time derivative of a function and a function itself in the limit follows from the distributional formula for time derivative.

We have

$$\mathbf{v}^N \rightharpoonup^* \mathbf{v} \quad \text{in } L^\infty(W^{1,2}), \quad (2.35)$$

$$\frac{\partial \mathbf{v}^N}{\partial t} \rightharpoonup \frac{\partial \mathbf{v}}{\partial t} \quad \text{in } L^2((W^{1,2})^*), \quad (2.36)$$

$$\mathbf{S}^N \rightharpoonup^* \mathbf{S} \quad \text{in } L^\infty(W^{2,2}), \quad (2.37)$$

$$\frac{\partial \mathbf{S}^N}{\partial t} \rightharpoonup \frac{\partial \mathbf{S}}{\partial t} \quad \text{in } L^2((W^{1,2})^*). \quad (2.38)$$

In the linear terms, weak convergence is enough for the limit passage. Moreover, we have

$$W^{1,2}(\Omega) \hookrightarrow L^4(\Omega) \hookrightarrow (W^{1,2}(\Omega))^*.$$

Due to the Aubin-Lions compactness result, see Proposition 10, we get

$$\begin{aligned}\mathbf{S}^N &\longrightarrow \mathbf{S} && \text{in } L^2(L^4), \\ \mathbf{v}^N &\longrightarrow \mathbf{v} && \text{in } L^2(L^4).\end{aligned}$$

This allows us to pass to the limit in nonlinear terms

$$\int_0^T \int_{\Omega} ((\mathbf{S}\mathbf{W} - \mathbf{W}\mathbf{S}) - (\mathbf{S}^N\mathbf{W}^N - \mathbf{W}^N\mathbf{S}^N)) : \boldsymbol{\Sigma} \, dx \, dt. \quad (2.39)$$

We consider one part of (2.39)

$$\begin{aligned}\int_0^T \int_{\Omega} (\mathbf{S}\mathbf{W} - \mathbf{S}^N\mathbf{W}^N) : \boldsymbol{\Sigma} \, dx \, dt &= \int_0^T \int_{\Omega} (\mathbf{S}\mathbf{W}^N - \mathbf{S}^N\mathbf{W}^N - \mathbf{S}\mathbf{W}^N + \mathbf{S}\mathbf{W}) : \boldsymbol{\Sigma} \, dx \, dt \\ &= \int_0^T \int_{\Omega} (\mathbf{S} - \mathbf{S}^N)\mathbf{W}^N : \boldsymbol{\Sigma} \, dx \, dt + \int_0^T \int_{\Omega} \mathbf{S}(\mathbf{W} - \mathbf{W}^N) : \boldsymbol{\Sigma} \, dx \, dt \\ &\leq \int_0^T \|(\mathbf{S} - \mathbf{S}^N)\|_{L^4} \|\mathbf{W}^N\|_{L^2} \|\boldsymbol{\Sigma}\|_{L^4} \, dt + \int_0^T \int_{\Omega} (\mathbf{W}^N - \mathbf{W})\mathbf{S}\boldsymbol{\Sigma} \, dx \, dt \\ &\leq \|(\mathbf{S} - \mathbf{S}^N)\|_{L^2(L^4)} \|\mathbf{W}\|_{L^2(L^2)} \|\boldsymbol{\Sigma}\|_{L^\infty(L^4)} \\ &\quad + \int_0^T \int_{\Omega} (\mathbf{W}^N - \mathbf{W})\mathbf{S}\boldsymbol{\Sigma} \, dx \, dt \longrightarrow 0.\end{aligned}$$

Standard strategy is involved in the limit passage for convective terms.

We have proven the existence of a weak solution to (2.13).

2.3.6 L^p -estimates

This section is dedicated to formal estimates in L^p -spaces for the system that includes vorticity

$$\operatorname{div} \mathbf{v} = 0, \quad (2.40a)$$

$$\boldsymbol{\omega} = \operatorname{curl} \mathbf{v}, \quad (2.40b)$$

$$\frac{\partial \boldsymbol{\omega}}{\partial t} + \mathbf{v}\nabla \boldsymbol{\omega} = \operatorname{curl} \operatorname{div} \mathbf{S}, \quad (2.40c)$$

$$\frac{\partial \mathbf{S}}{\partial t} + \mathbf{v}\nabla \mathbf{S} + \mathbf{W}\mathbf{S} - \mathbf{S}\mathbf{W} - \Delta \frac{\partial \mathbf{S}}{\partial t} = \mathbf{D}. \quad (2.40d)$$

We start with the vorticity equation (2.40c), multiply by $\boldsymbol{\omega}|\boldsymbol{\omega}|^{p-2}$ for $p > 2$,

$$\begin{aligned}\frac{1}{p} \frac{d}{dt} \|\boldsymbol{\omega}(t)\|_{L^p}^p &\leq \int_{\Omega} |\operatorname{curl} \operatorname{div} \mathbf{S}(t)| |\boldsymbol{\omega}(t)|^{p-1} \, dx \leq \|\mathbf{S}(t)\|_{W^{2,p}} \|\boldsymbol{\omega}(t)\|_{L^p}^{p-1} \\ &\leq \varepsilon^p \frac{1}{p} \|\mathbf{S}(t)\|_{W^{2,p}}^p + \left(\frac{1}{\varepsilon}\right)^{\frac{p}{p-1}} \frac{p-1}{p} \|\boldsymbol{\omega}(t)\|_{L^p}^p,\end{aligned}$$

where we used ε -version of the Young's inequality and $\varepsilon = \varepsilon(p)$. By integration over time we get

$$\|\boldsymbol{\omega}(t)\|_{L^p}^p \leq \int_0^T \varepsilon^p \|\mathbf{S}(t)\|_{W^{2,p}}^p + \left(\frac{1}{\varepsilon}\right)^{\frac{p}{p-1}} (p-1) \|\boldsymbol{\omega}(t)\|_{L^p}^p \, dt + \|\boldsymbol{\omega}(0)\|_{L^p}^p.$$

Let us recall the estimate of the velocity gradient by vorticity, see Yudovic [65]

Proposition 2. *For any $p > 1$, the following estimate holds:*

$$\|\nabla \mathbf{v}\|_p \leq \frac{Cp^2}{p-1} \|\omega\|_p. \quad (2.41)$$

Proposition 2 yields

$$\|\mathbf{v}\|_{W^{1,p}}^p \leq c_Y^p \int_0^T \varepsilon^p \|\mathbf{S}\|_{W^{2,p}}^p + \left(\frac{1}{\varepsilon}\right)^{\frac{p}{p-1}} (p-1) \|\mathbf{v}\|_{W^{1,p}}^p dt + c_v(0),$$

where $c_Y = c_Y(p) = \frac{Cp^2}{p-1}$ and $c_v(0) = \|\omega(0)\|_{L^p}^p$.

Further we focus on the stress evolution equation (2.40d), we integrate over time and take p -th power of L^p -norm

$$\|\mathbf{S} - \Delta \mathbf{S}\|_{L^p}^p \leq \left\| \int_0^T \mathbf{D} - \mathbf{v} \nabla \mathbf{S} - \mathbf{W} \mathbf{S} + \mathbf{S} \mathbf{W} dt + \mathbf{S}(0) - \Delta \mathbf{S}(0) \right\|_{L^p}^p.$$

By the Jensen's inequality we get

$$\|\mathbf{S} - \Delta \mathbf{S}\|_{L^p}^p \leq \int_0^T \|\mathbf{D}\|_{L^p}^p + \|\mathbf{v} \nabla \mathbf{S}\|_{L^p}^p + 2\|\nabla \mathbf{v} \mathbf{S}\|_{L^p}^p dt + \|\mathbf{S}(0) - \Delta \mathbf{S}(0)\|_{L^p}^p.$$

For the left hand side we use

$$\|\mathbf{S}\|_{W^{2,p}}^p \leq c_0 \|\mathbf{S} - \Delta \mathbf{S}\|_{L^p}^p,$$

which follows from the maximal regularity of the problem $f = \mathbf{S} - \Delta \mathbf{S}$.

By Hölder inequality we obtain

$$\|\mathbf{S}\|_{W^{2,p}}^p \leq c_0 \int_0^T \|\mathbf{v}\|_{W^{1,p}}^p + \|\mathbf{v}\|_{L^{2p}}^p \|\nabla \mathbf{S}\|_{L^{2p}}^p + 2\|\nabla \mathbf{v}\|_{L^p}^p \|\mathbf{S}\|_{L^\infty}^p dt + \|\mathbf{S}(0) - \Delta \mathbf{S}(0)\|_{L^p}^p.$$

Moreover, embedding $W^{1,2} \hookrightarrow L^{2p}$, $\mathbf{v} \in L^\infty(0, T; W^{1,2})$ and $\mathbf{S} \in L^\infty(0, T; W^{2,2})$ provide

$$\|\mathbf{S}\|_{W^{2,p}}^p \leq c_0 \int_0^T \|\mathbf{v}\|_{W^{1,p}}^p + c_e \|\mathbf{v}\|_{W^{1,2}}^p \|\mathbf{S}\|_{W^{2,2}}^p + 2c \|\nabla \mathbf{v}\|_{L^p}^p dt + \|\mathbf{S}(0) - \Delta \mathbf{S}(0)\|_{L^p}^p,$$

$$\|\mathbf{S}\|_{W^{2,p}}^p \leq c_0 \int_0^T \|\mathbf{v}\|_{W^{1,p}}^p + c c_e + 2c \|\nabla \mathbf{v}\|_{L^p}^p dt + c_S(0).$$

We conclude

$$\|\mathbf{S}\|_{W^{2,p}}^p + \|\mathbf{v}\|_{W^{1,p}}^p \leq \int_0^T (c_Y^p \varepsilon^p) \|\mathbf{S}\|_{W^{2,p}}^p + \left(c_Y^p \left(\frac{1}{\varepsilon}\right)^{\frac{p}{p-1}} (p-1) + c_0 + 2c \right) \|\mathbf{v}\|_{W^{1,p}}^p dt + c_v(0) + c_S(0).$$

$$\|\mathbf{S}\|_{W^{2,p}}^p + \|\mathbf{v}\|_{W^{1,p}}^p \leq \tilde{C}(p)^0 \int_0^T (\|\mathbf{S}\|_{W^{2,p}}^p + \|\mathbf{v}\|_{W^{1,p}}^p + c) dt + c(0), \quad (2.42)$$

$$\text{where } \tilde{C}(p) = \max \left\{ \frac{c\varepsilon p^2}{p-1}, \frac{cp^2}{p-1} \left(\left(\frac{1}{\varepsilon}\right)^{\frac{p}{p-1}} (p-1) + c \right)^{\frac{1}{p}} \right\}.$$

Our idea was to try to control this constant by a proper choice of $\varepsilon(p)$. This is a negative result that shows that the presented approach does not lead to the bound formulated by Yudovich (2.7). Constant $\tilde{C}(p)$ grows at least linearly with respect to p and is not admissible by the Yudovich uniqueness theory, see [64].

2.3.7 Higher order local estimates

In this section we provide the higher order local estimates to system (2.13), namely the estimates on the third spatial derivatives of both \mathbf{v} and \mathbf{S} . We apply D^3 to (2.13b) and multiply by $D^3\mathbf{v}$:

$$\begin{aligned} \int_{\Omega} D^3 \frac{\partial \mathbf{v}}{\partial t} \cdot D^3 \mathbf{v} \, dx + \int_{\Omega} D^3(\mathbf{v} \nabla \mathbf{v}) \cdot D^3 \mathbf{v} \, dx + \int_{\Omega} D^3 \nabla p \cdot D^3 \mathbf{v} \, dx &= \int_{\Omega} D^3 \operatorname{div} \mathbf{S} \cdot D^3 \mathbf{v} \, dx, \\ \frac{1}{2} \frac{d}{dt} \|D^3 \mathbf{v}\|_{L^2}^2 + \int_{\Omega} D^3(\mathbf{v} \nabla \mathbf{v}) \cdot D^3 \mathbf{v} \, dx &= \int_{\Omega} D^3 \operatorname{div} \mathbf{S} \cdot D^3 \mathbf{v} \, dx. \end{aligned}$$

Analogously, we apply D^3 to (2.13c) and multiply by $D^3\mathbf{S}$. This leads to

$$\begin{aligned} \int_{\Omega} D^3 \frac{\partial \mathbf{S}}{\partial t} : D^3 \mathbf{S} \, dx + \int_{\Omega} D^3(\mathbf{v} \nabla \mathbf{S}) : D^3 \mathbf{S} \, dx - \int_{\Omega} D^3 \frac{\partial}{\partial t} \Delta \mathbf{S} : D^3 \mathbf{S} \, dx \\ + \int_{\Omega} D^3(\mathbf{S} \mathbf{W} - \mathbf{W} \mathbf{S}) : D^3 \mathbf{S} \, dx &= \int_{\Omega} D^3 \mathbf{D} : D^3 \mathbf{S} \, dx, \\ \frac{1}{2} \frac{d}{dt} (\|D^3 \mathbf{S}\|_{L^2}^2 + \|D^4 \mathbf{S}\|_{L^2}^2) + \int_{\Omega} D^3(\mathbf{v} \nabla \mathbf{S}) : D^3 \mathbf{S} \, dx \\ + \int_{\Omega} D^3(\mathbf{S} \mathbf{W} - \mathbf{W} \mathbf{S}) : D^3 \mathbf{S} \, dx &= \int_{\Omega} D^3 \mathbf{D} : D^3 \mathbf{S} \, dx. \end{aligned}$$

The convective terms are estimated in the standard way. Important feature is the cancellation of the highest order term, as in (2.20)

$$\begin{aligned} \int_{\Omega} D^3(\mathbf{v} \nabla \mathbf{v}) \cdot D^3 \mathbf{v} \, dx &\leq \|D^3 \mathbf{v}\|_{L^2}^3, \\ \int_{\Omega} D^3(\mathbf{v} \nabla \mathbf{S}) : D^3 \mathbf{S} \, dx &\leq \|D^3 \mathbf{v}\|_{L^2} \|D^3 \mathbf{S}\|_{L^2}^2. \end{aligned}$$

The co-rotational term

$$\left| \int_{\Omega} D^3(\mathbf{S} \mathbf{W} - \mathbf{W} \mathbf{S}) : D^3 \mathbf{S} \, dx \right| = \left| \int_{\Omega} D^2(\mathbf{S} \mathbf{W} - \mathbf{W} \mathbf{S}) : D^4 \mathbf{S} \, dx \right|$$

reads as follows

$$\begin{aligned} \left| \int_{\Omega} D^2(\mathbf{S} \mathbf{W} - \mathbf{W} \mathbf{S}) : D^4 \mathbf{S} \, dx \right| &\leq c \|\nabla \mathbf{v}\|_{L^2} \|D^2 \mathbf{S}\|_{L^\infty} \|D^4 \mathbf{S}\|_{L^2} + c \|D^2 \mathbf{v}\|_{L^2} \|D \mathbf{S}\|_{L^\infty} \|D^4 \mathbf{S}\|_{L^2} \\ &\quad + c \|D^3 \mathbf{v}\|_{L^2} \|\mathbf{S}\|_{L^\infty} \|D^4 \mathbf{S}\|_{L^2}. \end{aligned}$$

Therefore

$$\left| \int_{\Omega} D^3(\mathbf{S} \mathbf{W} - \mathbf{W} \mathbf{S}) : D^3 \mathbf{S} \, dx \right| \leq c \|D^3 \mathbf{v}\|_{L^2} \|D^4 \mathbf{S}\|_{L^2}^2 \leq c (\|D^3 \mathbf{v}\|_{L^2}^2 + \|D^4 \mathbf{S}\|_{L^2}^4).$$

Finally we obtain the estimate which provides the local in time bounds for higher order derivatives of \mathbf{v} and \mathbf{S}

$$\frac{d}{dt} (\|D^3 \mathbf{v}\|_{L^2}^2 + \|D^3 \mathbf{S}\|_{L^2}^2 + \|D^4 \mathbf{S}\|_{L^2}^2) \leq C (\|D^3 \mathbf{v}\|_{L^2}^2 + \|D^3 \mathbf{S}\|_{L^2}^2 + \|D^4 \mathbf{S}\|_{L^2}^2)^2.$$

2.4 Regularization by $\Delta \mathbf{S}$

The second regularization to the system (2.1), namely $\Delta \mathbf{S}$, gives us local in time existence and global in time existence for small initial data. We investigate the following system:

$$\operatorname{div} \mathbf{v} = 0, \quad (2.43a)$$

$$\frac{\partial \mathbf{v}}{\partial t} + \mathbf{v} \nabla \mathbf{v} + \nabla p = \operatorname{div} \mathbf{S}, \quad (2.43b)$$

$$\frac{\partial \mathbf{S}}{\partial t} + \mathbf{v} \nabla \mathbf{S} + \mathbf{W} \mathbf{S} - \mathbf{S} \mathbf{W} - \Delta \mathbf{S} = \mathbf{D}. \quad (2.43c)$$

2.4.1 A priori estimates

Let us now present formal a priori estimates for system (2.43) on a two dimensional periodic domain Ω . We mainly focus on the differences between regularization presented in Section 2.3.1.

The first a priori estimate reads

$$\begin{aligned} \frac{1}{2} \int_0^T \frac{d}{dt} \|\mathbf{v}\|_{L^2}^2 dt &= - \int_0^T \int_{\Omega} \mathbf{D} : \mathbf{S} dx dt, \\ \frac{1}{2} \int_0^T \frac{d}{dt} \|\mathbf{S}\|_{L^2}^2 dt + \int_0^T \|\nabla \mathbf{S}\|_{L^2}^2 dt &= \int_0^T \int_{\Omega} \mathbf{D} : \mathbf{S} dx dt. \end{aligned}$$

The integration over time yields

$$\sup_{t \in [0, T]} \|\mathbf{v}(t)\|_2^2 + \sup_{t \in [0, T]} \|\mathbf{S}(t)\|_2^2 + 2 \int_0^T \|\nabla \mathbf{S}\|_2^2 dt = \|\mathbf{v}(0)\|_2^2 + \|\mathbf{S}(0)\|_2^2 \text{ a.e. } t \in (0, T). \quad (2.44)$$

Equation (2.44) indicates, by the Gronwall inequality, that

$$\mathbf{v} \in L^\infty(0, T; L^2(\Omega)), \quad \mathbf{S} \in L^\infty(0, T; L^2(\Omega)) \cap L^2(0, T; W^{1,2}(\Omega)).$$

The second estimate, yield

$$\frac{1}{2} \int_0^T \frac{d}{dt} \|\nabla \mathbf{v}\|_{L^2}^2 dt = \int_0^T \int_{\Omega} \nabla(\operatorname{div} \mathbf{S}) : \nabla \mathbf{v} dx dt, \quad (2.45)$$

$$\begin{aligned} \frac{1}{2} \int_0^T \frac{d}{dt} (\|\nabla \mathbf{S}\|_{L^2}^2) dt + \int_0^T \|\Delta \mathbf{S}\|_{L^2}^2 dt &= - \int_0^T \underbrace{\int_{\Omega} ([\nabla \mathbf{v}] \nabla \mathbf{S}) : \nabla \mathbf{S} dx}_{\text{A}} dt \\ &\quad + \int_0^T \underbrace{\int_{\Omega} (\mathbf{W} \mathbf{S} - \mathbf{S} \mathbf{W}) : \Delta \mathbf{S} dx}_{\text{B}} dt \\ &\quad + \int_0^T \int_{\Omega} \nabla \mathbf{D} : \nabla \mathbf{S} dx dt. \end{aligned} \quad (2.46)$$

Estimation of convective and co-rotational terms, differs from the previous case.

Term A

$$\begin{aligned}
\int_{\Omega} ([\nabla \mathbf{v}] \nabla \mathbf{S}) : \nabla \mathbf{S} \, dx &\leq \|\nabla \mathbf{v}\|_{L^2} \|\nabla \mathbf{S}\|_{L^4} \|\nabla \mathbf{S}\|_{L^4} \leq \|\nabla \mathbf{v}\|_{L^2} \|\mathbf{S}\|_{W^{1,4}}^2 \underbrace{\leq}_{\text{embedding}} \|\nabla \mathbf{v}\|_{L^2} \|\mathbf{S}\|_{W^{\frac{3}{2},2}}^2 \\
\|\nabla \mathbf{v}\|_{L^2} \|\mathbf{S}\|_{W^{\frac{3}{2},2}}^2 &\underbrace{\leq}_{\text{interpolation}} \|\nabla \mathbf{v}\|_{L^2} \|\mathbf{S}\|_{W^{1,2}} \|\mathbf{S}\|_{W^{2,2}} \leq c \left(\frac{1}{\varepsilon} \right) \|\nabla \mathbf{v}\|_{L^2}^2 \|\nabla \mathbf{S}\|_{L^2}^2 + c(\varepsilon) \|\Delta \mathbf{S}\|_{L^2}^2
\end{aligned} \tag{2.47}$$

Term B

$$\begin{aligned}
\int_{\Omega} (\mathbf{W} \mathbf{S} - \mathbf{S} \mathbf{W}) : \Delta \mathbf{S} \, dx &\leq 2 \|\nabla \mathbf{v}\|_{L^2} \|\mathbf{S}\|_{L^\infty} \|\Delta \mathbf{S}\|_{L^2} \underbrace{\leq}_{\text{Agmon's ineq.}} c \|\nabla \mathbf{v}\|_{L^2} \|\mathbf{S}\|_{W^{1,2}}^{\frac{1}{2}} \|\mathbf{S}\|_{W^{2,2}}^{\frac{1}{2}} \|\Delta \mathbf{S}\|_{L^2} \\
&\leq \|\nabla \mathbf{v}\|_{L^2} \|\nabla \mathbf{S}\|_{L^2}^{\frac{1}{2}} \|\Delta \mathbf{S}\|_{L^2}^{\frac{3}{2}} \underbrace{\leq}_{\text{Young's ineq.}} c \left(\frac{1}{\varepsilon} \right) \|\nabla \mathbf{v}\|_{L^2}^4 \|\nabla \mathbf{S}\|_{L^2}^2 + c(\varepsilon) \|\Delta \mathbf{S}\|_{L^2}^2
\end{aligned} \tag{2.48}$$

Let us now sum up (2.45), (2.46), (2.47) and (2.48)

$$\frac{1}{2} \frac{d}{dt} (\|\nabla \mathbf{v}\|_{L^2}^2 + \|\nabla \mathbf{S}\|_{L^2}^2) + c \|\Delta \mathbf{S}\|_{L^2}^2 \leq c (\|\nabla \mathbf{v}\|_{L^2}^2 + \|\nabla \mathbf{v}\|_{L^2}^4) \|\nabla \mathbf{S}\|_{L^2}^2 \leq c (\|\nabla \mathbf{v}\|_{L^2}^2 + \|\nabla \mathbf{S}\|_{L^2}^2)^2. \tag{2.49}$$

ODE

Option 1 Let us denote $X = (\|\nabla \mathbf{v}\|_{L^2}^2 + \|\nabla \mathbf{S}\|_{L^2}^2)$ and $Y = c \|\Delta \mathbf{S}\|_{L^2}^2$, thus (2.49) became

$$\frac{d}{dt} X + Y \leq X^2,$$

$$\frac{d}{dt} X \leq X^2 \implies X(t) \leq \frac{1}{\frac{1}{X(0)} - ct},$$

so

$$X(t) + \int_0^T Y \leq CT \left(\frac{X(0)}{1 - cTX(0)} \right)^2.$$

Thus, we conclude that for $T < \frac{1}{cX(0)}$

$$\mathbf{v} \in L^\infty(0, T; W^{1,2}(\Omega)), \quad \mathbf{S} \in L^\infty(0, T; W^{1,2}(\Omega)) \cap L^2(0, T; W^{2,2}(\Omega)).$$

Remark 1. One can show that (2.49) holds for arbitrary exponent greater than one

$$\frac{d}{dt} (\|\nabla \mathbf{v}\|_{L^2}^2 + \|\nabla \mathbf{S}\|_{L^2}^2) + c \|\Delta \mathbf{S}\|_{L^2}^2 \leq c (\|\nabla \mathbf{v}\|_{L^2}^2 + \|\nabla \mathbf{S}\|_{L^2}^2)^\alpha \text{ for } \alpha > 1.$$

What gives us a clue concerning global in time existence.

Option 2 Using slightly different inequality than (2.49), namely

$$\begin{aligned} \frac{d}{dt} (\|\nabla \mathbf{v}\|_{L^2}^2 + \|\nabla \mathbf{S}\|_{L^2}^2) + c\|\Delta \mathbf{S}\|_{L^2}^2 &\leq c (\|\nabla \mathbf{v}\|_{L^2}^2 + \|\nabla \mathbf{v}\|_{L^2}^4) \|\nabla \mathbf{S}\|_{L^2}^2 \\ &\leq c (\|\nabla \mathbf{v}\|_{L^2}^2 + \|\nabla \mathbf{S}\|_{L^2}^2)^2 \|\nabla \mathbf{S}\|_{L^2}^2 \leq c (\|\nabla \mathbf{v}\|_{L^2}^2 + \|\nabla \mathbf{S}\|_{L^2}^2)^2 \|\Delta \mathbf{S}\|_{L^2}^2, \end{aligned} \quad (2.50)$$

with the notation introduced for previous case, we obtain

$$\begin{aligned} \frac{d}{dt} X + Y &\leq X^2 Y, \\ \frac{d}{dt} X + (1 - X^2) Y &\leq 0. \end{aligned} \quad (2.51)$$

Let us assume that the initial data are small, namely

$$1 - \delta > X^2 = (\|\nabla \mathbf{v}\|_{L^2}^2 + \|\nabla \mathbf{S}\|_{L^2}^2)^2.$$

Proposition 3. *Let $1 - \delta > X^2$, then $\forall t, 1 - X^2(t) > \delta$*

Proof. We assume by contradiction that $\exists t^*$ such that $1 - X^2(t^*) = \delta$. Integrating (2.51) over time on $(0, t^*)$ yields

$$X(t^*) - X(0) + \int_0^{t^*} (1 - X^2) Y \, dt \leq 0.$$

From the assumption we get estimate

$$X(t^*) + \delta \int_0^{t^*} Y \, dt \leq X(0).$$

Therefore

$$X(t^*) \leq X(0) \Rightarrow 1 - X(t^*)^2 \geq 1 - X(0)^2 > \delta.$$

What completes the proof. □

Proposition 3 provides global in time estimates for $\|\nabla \mathbf{v}\|_{L^2}^2$ and $\|\nabla \mathbf{S}\|_{L^2}^2$ under the small initial data assumption. Knowing that $(\|\nabla \mathbf{v}\|_{L^2}^2 + \|\nabla \mathbf{S}\|_{L^2}^2)$ is globally bounded in time, we can show that $\|\Delta \mathbf{S}\|_{L^2}^2$ is also bounded independently of time.

Further steps: Galerkin approximation, uniform estimates, estimates of time derivative, and limit passage, proceed in a standard way.

Chapter 3

Finite Element Formulation

In the last 25 years, the Crystal Plasticity Finite Element Method (CPFEM) has been extensively studied. The recent overview by Roters et al. [71, 72] summarize applications of the CPFEM method. Authors cover simulation of: shear band formation, shape memory, non-uniform deformation texture formation, anisotropy, among others. Most of the methods that have been developed are structural, formulated in Lagrangian coordinates and based on the virtual work principle. Even for large deformations the increments of the deformation gradient are computed, what is typical for Lagrangian description, see [73].

In this chapter we present fully Eulerian finite element study of crystal plasticity. To solve the full system of equations (3.1) we discretize it in time with an implicit second order θ -scheme and in space with proper finite element method. We propose a monolithic method/solver .

An Eulerian approach in the context of crystal plasticity was studied by Cazacu and Ionescu [74, 75] where authors confine to rigid body motions and plane strains. Moreover, by using fluid-like approach we can overcome typical Lagrangian bounds and simulate very large deformation as well as topology changes like contact, see [76, 77].

Simplicial elements are used to discretize the system in space. The finite element discretization of the rate type visco-elasto-plastic models leads to several numerical problems. The proper choice of elements to satisfy the discrete Ladyzhenskaya, Babuška and Brezzi (LBB) condition [78] on a velocity-pressure-stress $(\mathbf{v}, p, \mathbf{S})$. The mixed formulation containing the stress tensor result in a twofold saddle point type problems, which were studied in [79, 80]. The presence of convective term in the differential constitutive law reflects the hyperbolic nature of this equation. It can be solved by using appropriate stabilization technique, such as streamline upwind Petrov Galerkin (SUPG) [81] or discontinuous finite elements [82]. Moreover, we have to deal with problems arising from the strong non-linear nature of the model. The review of the finite element methods for visco-elastic flow can be found in [83].

Let us recall the strong form of the incompressible system that we discretize into the Galerkin system and consequently solve using finite element method

$$\operatorname{div} \mathbf{v} = 0, \tag{3.1a}$$

$$\frac{\partial}{\partial t} \mathbf{v} + \mathbf{v} \nabla \mathbf{v} - \operatorname{div} \mathbf{S} + \nabla p = 0, \tag{3.1b}$$

$$\frac{\partial}{\partial t} \mathbf{S} + \mathbf{v} \nabla \mathbf{S} + \mathbf{S} \mathbf{W} - \mathbf{W} \mathbf{S} = 2\mu_e(\mathbf{D}), \tag{3.1c}$$

$$\frac{\partial}{\partial t} \mathbf{a}_i = [\nabla \mathbf{v}] \mathbf{a}_i. \tag{3.1d}$$

The system is satisfied inside the domain Ω , the boundary $\partial\Omega$ consists of two non-intersecting parts Γ_D and Γ_N corresponding to the Dirichlet and the Neumann boundary conditions, respectively. It holds that $\mathbf{v} = \mathbf{v}_D$ on Γ_D and $\mathbf{S}\mathbf{n} = \mathbf{t}$ on Γ_N . Moreover, the initial condition reads, $\mathbf{v}(x, 0) = \mathbf{v}_0(x)$, $\mathbf{S}(x, 0) = \mathbf{S}_0(x)$, $p(x, 0) = p_0(x)$ and $\mathbf{a}_i(x, 0) = \mathbf{a}_{i0}(x)$.

The implementation is done in the software package FEniCS [84, 85]. The FEniCS is a collection of open source finite element software for automated solution of differential equations. Computational examples are given in Chapter 4.

3.1 The mesh

The domain $\Omega \in \mathbb{R}^d$ is approximated by a simplicial triangulation \mathcal{T}_h . We introduce the partition of the domain as a finite set of cells \mathcal{T}_h with disjoint interiors such that

$$\bigcup_{K \in \mathcal{T}_h} K = \Omega. \quad (3.2)$$

We define $h_K := \text{diam}(K)$ and $\varrho_K := \sup\{\text{diam}(B) : B \text{ is a ball with } B \subset K\}$ and require that the triangles are shape regular, namely there exists a positive real number $\alpha \in \mathbf{R}$, independent of h_K , $K \in \mathcal{T}_h$, such that for all $K \in \mathcal{T}_h$

$$\frac{h_K}{\varrho_K} \leq \alpha. \quad (3.3)$$

3.2 Space discretization

To discretize (3.1) by the means of finite elements we test the strong formulation with arbitrary functions, which are called test functions, and integrate over the domain Ω .

$$\mathbb{V} = H_0^1(\Omega, \mathbf{R}^d) = \{\mathbf{v} \in H^1(\Omega, \mathbf{R}^d); \mathbf{v} = 0 \text{ on } \Gamma_D\}, \quad (3.4a)$$

$$\mathbb{P} = L_0^2(\Omega) = \{q \in L^2(\Omega); \int_{\Omega} q \, dx = 0\}, \quad (3.4b)$$

$$\mathbb{S} = L^2(\Omega, \mathbf{R}_{sym}^{d \times d}), \quad (3.4c)$$

$$\mathbb{A} = L^2(\Omega, \mathbf{R}). \quad (3.4d)$$

We denote test functions by \mathbf{z}_v , z_p , \mathbf{Z}_S , and \mathbf{z}_{a_i} . We call

$$(\mathbf{v}, p, \mathbf{S}, \mathbf{a}_1, \dots, \mathbf{a}_d) \in \mathbb{V} \times \mathbb{P} \times \mathbb{S} \times \mathbb{A} \times \dots \times \mathbb{A}$$

a weak solution to (3.1) when the following system holds

$$\int_{\Omega} \text{div } \mathbf{v} \, z_p \, dx = 0, \quad (3.5a)$$

$$\int_{\Omega} \left(\frac{\partial}{\partial t} \mathbf{v} + \mathbf{v} \nabla \mathbf{v} - \text{div } \mathbf{S} + \nabla p \right) \cdot \mathbf{z}_v \, dx = 0, \quad (3.5b)$$

$$\int_{\Omega} \left(\frac{\partial}{\partial t} \mathbf{S} + \mathbf{v} \nabla \mathbf{S} + \mathbf{S} \mathbf{W}_e - \mathbf{W}_e \mathbf{S} \right) : \mathbf{Z}_S \, dx = \int_{\Omega} 2\mu_e \mathbf{D}_e : \mathbf{Z}_S \, dx, \quad (3.5c)$$

$$\int_{\Omega} \frac{\partial}{\partial t} \mathbf{a}_i \cdot \mathbf{z}_{a_i} \, dx = \int_{\Omega} \mathbf{L}_e \mathbf{a}_i \cdot \mathbf{z}_{a_i} \, dx. \quad (3.5d)$$

We integrate by parts the following terms,

$$\begin{aligned} \int_{\Omega} \nabla p \cdot \mathbf{z}_v \, dx &= - \int_{\Omega} p \mathbf{I} : \nabla \mathbf{z}_v \, dx, \\ - \int_{\Omega} \operatorname{div} \mathbf{S} \cdot \mathbf{z}_v \, dx &= \int_{\Omega} \mathbf{S} : \nabla \mathbf{z}_v \, dx - \int_{\Gamma_N} \mathbf{t} \cdot \mathbf{z}_v \, dS. \end{aligned}$$

Finite element method is based on the weak formulation (3.5). Let us introduce finite dimensional spaces $\mathbb{V}_h \subset \mathbb{V}, \mathbb{P}_h \subset \mathbb{P}, \mathbb{S}_h \subset \mathbb{S}, \mathbb{A}_h \subset \mathbb{A}$ and corresponding bases $\{\phi_{v_j}\}_{j=1}^{N_v}, \{\phi_{p_j}\}_{j=1}^{N_p}, \{\phi_{S_j}\}_{j=1}^{N_S}, \{\phi_{a_j}\}_{j=1}^{N_a}$. The finite element expansion of the discrete solutions reads

$$\mathbf{v}_h - \mathbf{v}_{D_h} = \sum_{j=1}^{N_v} v_j(t) \phi_{v_j}, \text{ for } \mathbf{v}_{D_h} = \mathbf{v}_D \text{ on } \Gamma_D, \quad (3.6a)$$

$$p_h = \sum_{j=1}^{N_p} p_j(t) \phi_{p_j}, \quad (3.6b)$$

$$\mathbf{S}_h = \sum_{j=1}^{N_S} S_j(t) \phi_{S_j}, \quad (3.6c)$$

$$\mathbf{a}_{ih} = \sum_{j=1}^{N_a} a_{ij}(t) \phi_{a_j}, \quad i \in \{1, 2, 3\}, \quad (3.6d)$$

where v_j, p_j, S_j, a_{ij} are the nodal values and $\phi_{v_j}, \phi_{p_j}, \phi_{S_j}, \phi_{a_j}$ are basis functions. We denote vectors of coefficients by

$$\mathbf{V} = (v_1, v_2, \dots, v_{N_v}), \quad (3.7a)$$

$$\mathbf{P} = (p_1, p_2, \dots, p_{N_p}), \quad (3.7b)$$

$$\mathbf{S} = (S_1, S_2, \dots, S_{N_S}), \quad (3.7c)$$

$$\mathbf{A} = (a_{11}, a_{12}, \dots, a_{1N_a}, a_{21}, a_{22}, \dots, a_{2N_a}, a_{31}, a_{32}, \dots, a_{3N_a}). \quad (3.7d)$$

We define the Galerkin approximation system. Find

$$(\mathbf{v}_h, p_h, \mathbf{S}_h, \mathbf{a}_{1h}, \mathbf{a}_{2h}, \mathbf{a}_{3h}) \in \mathbb{V}_h \times \mathbb{P}_h \times \mathbb{S}_h \times \mathbb{A}_h \times \mathbb{A}_h \times \mathbb{A}_h$$

satisfying

$$\int_{\Omega} \operatorname{div} \mathbf{v}_h z_p \, dx = 0, \quad (3.8a)$$

$$\int_{\Omega} \left(\frac{\partial}{\partial t} \mathbf{v}_h + \mathbf{v}_h \nabla \mathbf{v}_h \right) \cdot \mathbf{z}_v \, dx + \int_{\Omega} (\mathbf{S}_h - p_h \mathbf{I}) : \nabla \mathbf{z}_v \, dx = \int_{\Gamma_N} \mathbf{t}_h \cdot \mathbf{z}_v \, dS, \quad (3.8b)$$

$$\int_{\Omega} \left(\frac{\partial}{\partial t} \mathbf{S}_h + \mathbf{v}_h \nabla \mathbf{S}_h + \mathbf{S}_h \mathbf{W}_{eh} - \mathbf{W}_{eh} \mathbf{S}_h - 2\mu_e \mathbf{D}_{eh} \right) : \mathbf{Z}_S \, dx = 0, \quad (3.8c)$$

$$\int_{\Omega} \left(\frac{\partial}{\partial t} \mathbf{a}_{ih} - \mathbf{L}_{eh} \mathbf{a}_{ih} \right) \cdot \mathbf{z}_{a_i} \, dx = 0, \quad i \in \{1, 2, 3\}. \quad (3.8d)$$

3.3 Time discretization

The time interval $[0, T]$ is divided into a set of discrete points $\{t_k\}$ such that $t_0 = 0$ and $t_K = T$. The time increment

$$\Delta t = t_{k+1} - t_k \quad \forall k. \quad (3.9)$$

We are looking for a solution u^{k+1} at a time level $k+1$ with given solution u^k . Problem is solved using FEM described in the rest of the Chapter.

We employ implicit time schemes, namely for $\theta \in (0, 1]$

$$\frac{u^{k+1} - u^k}{\Delta t} + \theta A(u^{k+1}) + (1 - \theta)A(u^k) = 0. \quad (3.10)$$

For $\theta = 1$ we obtain the first order unconditionally stable backward Euler scheme:

$$\frac{u^{k+1} - u^k}{\Delta t} + A(u^{k+1}) = 0. \quad (3.11)$$

For $\theta = \frac{1}{2}$ the second order conditionally stable Crank-Nicolson scheme:

$$\frac{u^{k+1} - u^k}{\Delta t} + \frac{1}{2}A(u^{k+1}) + \frac{1}{2}A(u^k) = 0. \quad (3.12)$$

Visco-elastic problems are often solved with more exact time schemes i.e. fractional step θ -scheme which is second order unconditionally stable time scheme or implicit Glowinski three-step scheme for $\theta = 1 - \sqrt{2}/2$, almost the third order conditionally stable time scheme. For reference see [86, 87].

We discretize (3.8) with one step backward Euler scheme. For given $(\mathbf{v}_h^k, p_h^k, \mathbf{S}_h^k, \mathbf{a}_{1h}^k, \mathbf{a}_{2h}^k, \mathbf{a}_{3h}^k)$ and the time step Δt find a solution $(\mathbf{v}_h, p_h, \mathbf{S}_h, \mathbf{a}_{1h}, \mathbf{a}_{2h}, \mathbf{a}_{3h})$ satisfying

$$\int_{\Omega} \operatorname{div} \mathbf{v}_h z_p \, dx = 0, \quad (3.13a)$$

$$\int_{\Omega} \left(\frac{\mathbf{v}_h - \mathbf{v}_h^k}{\Delta t} + \mathbf{v}_h \nabla \mathbf{v}_h \right) \cdot \mathbf{z}_v \, dx + \int_{\Omega} \mathbf{S}_h : \nabla \mathbf{z}_v \, dx - \int_{\Omega} p_h \operatorname{div} \mathbf{z}_v \, dx = \int_{\Gamma_N} \mathbf{t}_h \cdot \mathbf{z}_v \, dS, \quad (3.13b)$$

$$\int_{\Omega} \left(\frac{\mathbf{S}_h - \mathbf{S}_h^k}{\Delta t} + \mathbf{v}_h \nabla \mathbf{S}_h + \mathbf{S}_h \mathbf{W}_{eh} - \mathbf{W}_{eh} \mathbf{S}_h - 2\mu_e \mathbf{D}_{eh} \right) : \mathbf{Z}_S \, dx = 0, \quad (3.13c)$$

$$\int_{\Omega} \left(\frac{\mathbf{a}_{ih} - \mathbf{a}_{ih}^k}{\Delta t} - \mathbf{L}_{eh} \mathbf{a}_{ih} \right) \cdot \mathbf{z}_{\mathbf{a}_i} \, dx = 0, \quad i \in \{1, 2, 3\}, \quad (3.13d)$$

where

$$\mathbf{L}_{eh} = \nabla \mathbf{v}_h - \mathbf{L}_{ph} = \nabla \mathbf{v}_h - \sum_{\alpha=1}^N \operatorname{sgn}(\mathbf{S}_h : \mathbf{s}_h^{(\alpha)} \otimes \mathbf{m}_h^{(\alpha)}) \left(|\mathbf{S}_h : \mathbf{s}_h^{(\alpha)} \otimes \mathbf{m}_h^{(\alpha)}| \right)^{1/m} \mathbf{s}_h^{(\alpha)} \otimes \mathbf{m}_h^{(\alpha)}.$$

3.4 The discrete problem

We have not specified the test functions yet, let us put

$$\mathbf{z}_v = \phi_{v_l} \text{ for } l = 1, \dots, N_v, \quad (3.14a)$$

$$z_p = \phi_{p_l} \text{ for } l = 1, \dots, N_p, \quad (3.14b)$$

$$\mathbf{Z}_S = \phi_{S_l} \text{ for } l = 1, \dots, N_S, \quad (3.14c)$$

$$\mathbf{z}_a = \phi_{a_l} \text{ for } l = 1, \dots, N_a. \quad (3.14d)$$

Substituting (3.6) and (3.14) into (3.13) yields

$$\begin{aligned}
& \sum_j v_j \underbrace{\int_{\Omega} \operatorname{div} \phi_{v_j} \phi_{p_l} \, dx}_{B_{jl}} = 0, \text{ for } l \in 1, \dots, N_p \\
& \sum_j v_j \underbrace{\int_{\Omega} \phi_{v_j} \phi_{v_l} \, dx}_{A_{jl}} - \underbrace{\int_{\Omega} \mathbf{v}_h^k \phi_{v_j} \, dx}_{F_{1l}} + \Delta t \underbrace{\int_{\Omega} \sum_j v_j \phi_{v_j} \left[\sum_j v_j \nabla \phi_{v_j} \right] \phi_{v_l} \, dx}_{N_1(V)_{jl}} + \\
& \Delta t \sum_j S_j \underbrace{\int_{\Omega} \phi_{S_j} \nabla \phi_{v_l} \, dx}_{C_{jl}} - \Delta t \sum_j p_j \underbrace{\int_{\Omega} \phi_{p_j} \operatorname{div} \phi_{v_l} \, dx}_{-B_{lj}} = 0, \text{ for } l \in 1, \dots, N_v, \\
& \sum_j S_j \underbrace{\int_{\Omega} \phi_{S_j} \phi_{S_l} \, dx}_{E_{jl}} - \underbrace{\int_{\Omega} \mathbf{S}_h^k \phi_{S_l} \, dx}_{F_{2l}} + \Delta t \underbrace{\int_{\Omega} \left(\sum_j v_j \phi_{v_j} \left[\sum_j S_j \nabla \phi_{S_j} \right] \right) \phi_{S_l} \, dx}_{N_2(V,S)_{jl}} \\
& + \Delta t \underbrace{\int_{\Omega} \left(\sum_j S_j \phi_{S_j} \left(\sum_j v_j \operatorname{skew}(\nabla \phi_{v_j}) - \mathbf{L}_{p_h} \right) - \left(\sum_j v_j \operatorname{skew}(\nabla \phi_{v_j}) - \mathbf{L}_{p_h} \right) \sum_j S_j \phi_{S_j} \right) : \phi_{S_l} \, dx}_{N_3(V,S)_{jl}} \\
& - 2\mu_e \Delta t \sum_j v_j \underbrace{\int_{\Omega} (\operatorname{sym}(\nabla \phi_{v_j})) \phi_{S_l} \, dx}_{G_{ij}} = 0, \text{ for } l \in 1, \dots, N_S, \\
& \sum_j a_{ij} \underbrace{\int_{\Omega} \phi_{a_j} \phi_{a_l} \, dx}_{H_{jl}} - \underbrace{\int_{\Omega} \mathbf{a}_i^k \phi_{a_l} \, dx}_{F_{3l}} \\
& - \Delta t \sum_j v_j \underbrace{\int_{\Omega} \left(\sum_j v_j (\nabla \phi_{v_j}) - \mathbf{L}_{p_h} \right) \phi_{a_l} \, dx}_{K_{jl}} = 0, \text{ for } l \in 1, \dots, N_a, \quad i \in \{1, 2, 3\},
\end{aligned}$$

where

$$\mathbf{L}_{p_h} = \sum_{\alpha=1}^N \operatorname{sgn}(\mathbf{S}_h : \mathbf{s}_h^{(\alpha)} \otimes \mathbf{m}_h^{(\alpha)}) \left(|\mathbf{S}_h : \mathbf{s}_h^{(\alpha)} \otimes \mathbf{m}_h^{(\alpha)}| \right)^{1/m} \mathbf{s}_h^{(\alpha)} \otimes \mathbf{m}_h^{(\alpha)}.$$

Let us denote the solution vector by $\mathbf{U} = (\mathbf{V}, \mathbf{P}, \mathbf{S}, \mathbf{A})$, the above system can be rewritten as a system of $N_t = N_v + N_p + N_S + dN_a$ nonlinear algebraic equations

$$\mathbf{A}(\mathbf{U})\mathbf{U} = \begin{pmatrix} A + \Delta t N_1(V) + B^T + \Delta t C \\ \Delta t B \\ \Delta t (N_2(V, S) + N_3(V, S)) - 2\mu_e \Delta t G + E \\ H - \Delta t K \end{pmatrix} \begin{pmatrix} \mathbf{V} \\ \mathbf{P} \\ \mathbf{S} \\ \mathbf{A} \end{pmatrix} = \begin{pmatrix} F_1 \\ 0 \\ F_2 \\ F_3 \end{pmatrix}, \quad (3.15)$$

where we denote the right hand side by $\mathcal{B} = (F_1, 0, F_2, F_3)^T$.

For brevity we reformulate (3.15)

$$F(\mathbf{U}) = \mathcal{A}(\mathbf{U})\mathbf{U} - \mathcal{B}. \quad (3.16)$$

Note that residuum equals

$$\mathcal{R} = -F(\mathbf{U}) = \mathcal{B} - \mathcal{A}\mathbf{U}.$$

3.4.1 The Newton solver

We formulate the Newton's method for the system

$$F_i(U_1, \dots, U_{N_t}) = 0, \text{ for } i = 1, \dots, N_t,$$

where by F_i we understand

$$F_i = F(U_1, \dots, U_{N_t}; \varphi_i),$$

where φ_i is a test function from a mixed space.

To solve nonlinear system we define Jacobian of $F(\mathbf{U})$

$$J = \frac{DF(\mathbf{U})}{D\mathbf{U}}$$

and solve linear system of equations using the Newton's method for an unknown $\tilde{\mathbf{U}} = \sum_{j=1}^{N_t} \tilde{U}_j \varphi_j$,

$$\sum_{j=1}^{N_t} \frac{DF_i}{DU_j} \tilde{U}_j = -F_i, \text{ for } i = 1, \dots, N_t.$$

We finish the k -th Newton iteration by update of a solution

$$\mathbf{U}^{k+1} = \mathbf{U}^k + \omega \tilde{\mathbf{U}},$$

where $\omega \in (0, 1]$ is a relaxation parameter. The original Newton's method has $\omega = 1$, but to improve the convergence, one can adaptively choose a smaller step ω .

To start the Newton's method an initial guess \mathbf{U}^0 have to be provided. Moreover, stopping criterion on the absolute and relative L_2 -norm of the residual is applied. The implementation details are given in the following Chapter.

3.5 The choice of finite element space

The choice of proper set of finite elements is crucial to obtain reliable numerical approximation.

Let us recall the well known Ladyzhenskaya, Babuška and Brezzi (LBB) velocity-pressure stability condition [78, 88] to the Navier-Stokes system, given in a discrete form,

$$\exists \beta \in \mathbf{R} \text{ such that } 0 < \beta \leq \inf_{p_h \in \mathbb{P}_h} \sup_{\mathbf{v}_h \in \mathbb{V}_h} \frac{\int_{\Omega} \operatorname{div} \mathbf{v}_h p_h \, dx}{\|p_h\|_{\mathbb{P}_h} \|\mathbf{v}_h\|_{\mathbb{V}_h}}. \quad (3.17)$$

Moreover, we require

$$\operatorname{div} \mathbf{v}_h \in \mathbb{P}_h.$$

The velocity-pressure-stress approximations

Working with a stress as an additional variable in a weak formulation requires further compatibility constraints onto the choice of the discrete spaces for the triple velocity-pressure-stress [80]

$$\exists \beta \in \mathbf{R} \text{ such that } 0 < \beta \leq \inf_{\mathbf{v}_h \in \mathbb{V}_h} \sup_{\mathbf{S}_h \in \mathbb{S}_h} \frac{\int_{\Omega} \operatorname{div} \mathbf{S}_h \mathbf{v}_h \, dx}{\|\mathbf{S}_h\|_{\mathbb{S}_h} \|\mathbf{v}_h\|_{\mathbb{V}_h}}. \quad (3.18)$$

We refer to a paper of Fortin and Pierre [89], because authors consider a case without a viscous contribution as in the system (3.1). It is shown that the following conditions must be satisfied:

- The velocity-pressure spaces must be compatible with classical LBB condition (3.17).
- Discontinuous approximation of the stress imposes condition

$$\operatorname{sym}(\nabla \mathbf{v}_h) \in \mathbb{S} \text{ for all } \mathbf{v}_h \in \mathbb{V}. \quad (3.19)$$

- Continuous approximation of the stress requires that the number of local degrees of freedom must be larger than that used for the velocity space.

To satisfy condition (3.17) we choose the continuous $\mathcal{P}_2 - \mathcal{P}_1$ Taylor-Hood elements [90]. The requirement (3.19) can be fulfilled by using a \mathcal{P}_1 -discontinuous approximation. On the other hand, in the continuous case we put \mathcal{P}_2 for the stress space. Figure 3.1 presents $\mathcal{P}_2\mathcal{P}_1\mathcal{P}_1$ -disc and $\mathcal{P}_2\mathcal{P}_1\mathcal{P}_2$ velocity-pressure-stress triples.

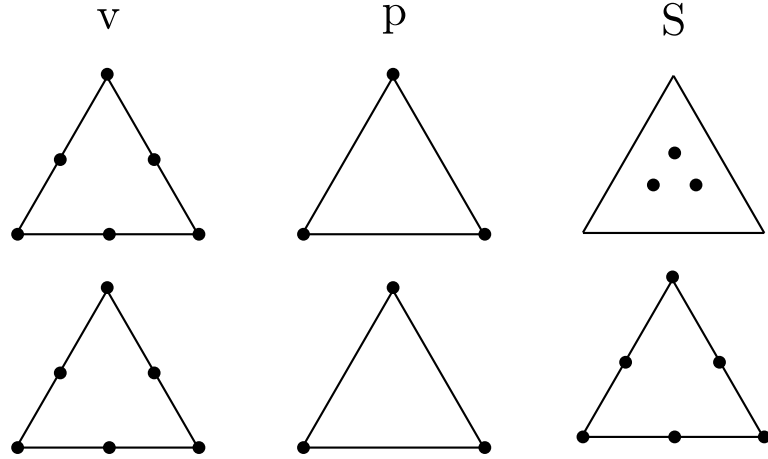


Figure 3.1: Discretization schemes

Finite element spaces are given by

$$\begin{aligned} \mathbb{V}_h &= \{\mathbf{v}_h \in W^{1,2}(\Omega; \mathbf{R}^d); \mathbf{v}|_K \in \mathcal{P}_2(K)^d \forall K \in \mathcal{T}_h\}, \\ \mathbb{P}_h &= \{\varrho_h \in L_0^2(\Omega) \cap C^0(\Omega; \mathbf{R}); \varrho_h|_K \in \mathcal{P}_1(K) \forall K \in \mathcal{T}_h\}, \\ \mathbb{S}_h &= \{\mathbf{S}_h \in L^2(\Omega; \mathbf{R}_{\operatorname{sym}}^{d \times d}); \mathbf{S}_h|_K \in \mathcal{P}_1(K)^{d \times d} \forall K \in \mathcal{T}_h\}, \\ \mathbb{S}_h &= \{\mathbf{S}_h \in H_0^1(\Omega; \mathbf{R}_{\operatorname{sym}}^{d \times d}); \mathbf{S}_h|_K \in \mathcal{P}_2(K)^{d \times d} \forall K \in \mathcal{T}_h\}. \end{aligned}$$

For admissible discretizations on quadrilateral elements we refer to triples, such as bi-quadratic velocity, discontinuous linear pressure, and discontinuous quadratic stress elements of Fortin and Fortin [91] or bi-quadratic velocity, bi-linear pressure, and bi-linear stress sub-elements of Marchal and Croche [81].

Moreover, when viscous contribution is present, the LBB condition (3.18) does not need to be satisfied, see [92].

Crystal plasticity basis

What remains is to specify the discrete space for crystal plasticity basis \mathbb{A}_h . Working with system (3.13) we discretize equation (3.13d) in a monolithic setting by \mathcal{P}_1 elements

$$\mathbb{A}_h = \{\mathbf{a}_h \in L^2(\Omega)^d \cap C^0(\Omega; \mathbb{R}^d); \mathbf{a}_h|_K \in \mathcal{P}_1(K) \forall K \in \mathcal{T}_h\}.$$

It is worth to mention that instead of computing (3.13d) namely set of vectorial equations, one can replace that by one tensorial equation (1.116)

$$\int_{\Omega} \left(\nabla \mathbf{v}_h - \sum_{i=1}^d \nu_h^{(\alpha)} \dot{\mathbf{a}}_{ih} \otimes \mathbf{a}_h^i - \sum_{\alpha=1}^N \mathbf{s}_h^{(\alpha)} \otimes \mathbf{m}_h^{(\alpha)} \right) : \mathbf{Z}_a \, dx = 0, \quad (3.20)$$

where

$$\nu_h^{(\alpha)} = \nu_0 \operatorname{sgn}(\mathbf{S}_h : \mathbf{s}_h^{(\alpha)} \otimes \mathbf{m}_h^{(\alpha)}) \left(|\mathbf{S}_h : \mathbf{s}_h^{(\alpha)} \otimes \mathbf{m}_h^{(\alpha)}| \right)^{1/m}$$

and the test function

$$\mathbf{Z}_a = \begin{pmatrix} z_{a1} \\ \vdots \\ z_{ad} \end{pmatrix}.$$

On the other hand, since the discrete system of equations is relatively large, for the sake of computational cost, we can perform the explicit update of the lattice basis vectors

$$\mathbf{a}_{ih} = \mathbf{a}_{ih}^k + \Delta t \mathbf{L}_{e_h^k} \mathbf{a}_{ih}^k, \text{ for } i = 1, \dots, d, \quad (3.21)$$

where

$$\mathbf{L}_{e_h^k} = \nabla \mathbf{v}_h^k - \sum_{\alpha=1}^N \operatorname{sgn}(\mathbf{S}_h^k : \mathbf{s}_h^{(\alpha)k} \otimes \mathbf{m}_h^{(\alpha)}) \left(|\mathbf{S}_h^k : \mathbf{s}_h^{(\alpha)k} \otimes \mathbf{m}_h^{(\alpha)k}| \right)^{1/m} \mathbf{s}_h^{(\alpha)k} \otimes \mathbf{m}_h^{(\alpha)k}.$$

This approach is used to the channel die compression, where slip systems $(\mathbf{s}^{(\alpha)}, \mathbf{m}^{(\alpha)})$ were updated explicitly after each time step, see Section 4.1.

Moreover, in the case of two dimensional 2-turn equal channel angular extrusion, instead of introducing crystal plasticity basis, we reduced number of unknowns to one angle. Description of the evolution of three slip systems is equivalent to the evolution of the lattice orientation, see Section 4.3.

3.5.1 Stress evolution stabilization

Let us rewrite system (3.13) in a compact way

$$(\operatorname{div} \mathbf{v}_h, z_p) = 0, \quad (3.22a)$$

$$\left(\frac{\mathbf{v}_h - \mathbf{v}_h^k}{\Delta t} + \mathbf{v}_h \nabla \mathbf{v}_h, \mathbf{z}_v \right) + (\mathbf{S}_h, \nabla \mathbf{z}_v) - (p_h, \operatorname{div} \mathbf{z}_v) = (\mathbf{t}_h, \mathbf{z}_v)_{\Gamma_N}, \quad (3.22b)$$

$$\left(\overset{\nabla}{\mathbf{S}}_h - 2\mu_e \mathbf{D}_{eh}, \mathbf{Z}_S \right) = 0, \quad (3.22c)$$

$$\left(\frac{\mathbf{a}_{ih} - \mathbf{a}_{ih}^k}{\Delta t} - \mathbf{L}_{eh} \mathbf{a}_{ih}, \mathbf{z}_{a_i} \right) = 0, \quad i \in \{1, 2, 3\}. \quad (3.22d)$$

The need for stabilizing the stress comes from the hyperbolic nature of equation (3.22c). We would like to present two possible ways, how to overcome this problem.

First we mention streamline-upwind/Petrov-Galerkin method of Brooks and Hughes [93], first applied in the context of viscoelastic fluids in [81]

$$\left(\overset{\nabla}{\mathbf{S}}_h - 2\mu_e \mathbf{D}_{eh}, \mathbf{Z}_S + \alpha \mathbf{z}_v \nabla \mathbf{Z}_S \right) = 0, \quad (3.23)$$

where α stands for a parameter that is of the form $\alpha = \frac{h}{U}$ with characteristic mesh size h and characteristic velocity U .

The second method was proposed by Marchal and Crochet [81]. The idea is to apply stabilization only to the convective term

$$\left(\overset{\nabla}{\mathbf{S}}_h - 2\mu_e \mathbf{D}_{eh}, \mathbf{Z}_S \right) + (\mathbf{v}_h \nabla \mathbf{S}_h, \alpha \mathbf{z}_v \nabla \mathbf{Z}_S) = 0. \quad (3.24)$$

3.6 Arbitrary Lagrangian-Eulerian approach

We devote this section to the introduction of the arbitrary Lagrangian Eulerian (ALE) method, for details we refer to [94, 95, 96]. We employ ALE to deal with free boundary and avoid mesh damages, see Chapter 4.

The arbitrary Lagrangian Eulerian (ALE) is a finite element formulation in which the computational system is not a priori fixed in space (Eulerian) or attached to material (Lagrangian). In fact we can formulate our problem on an arbitrary domain defined Ω_x (i.e. moving, time dependent domain) and define ALE mapping ϕ between fixed computational domain Ω_a and an arbitrary domain Ω_x , $\phi : \Omega_a \rightarrow \Omega_x$. ALE mapping is the key to transform our system to the fixed computational domain. For this sake proper definition of the ALE mapping is of a great importance. The class of ALE methods is widely applied, e.g. to fluid structure interaction problems.

As shown in Figure 3.2 we define arbitrary configuration in between Lagrangian and Eulerian coordinates. Let us introduce following dependencies and notation:

$$x = \chi(X, t) = \phi(a, t) = \phi(\psi(X, t), t), \quad \chi = \phi \circ \psi. \quad (3.25)$$

The ALE displacement, the ALE velocity, and the ALE deformation gradient read as follows

$$\mathbf{u}_a(a, t) = x - a, \quad \mathbf{v}_a(a, t) = \frac{\partial \phi}{\partial t}, \quad \mathbf{F}_a = \frac{\partial \phi}{\partial a}. \quad (3.26)$$

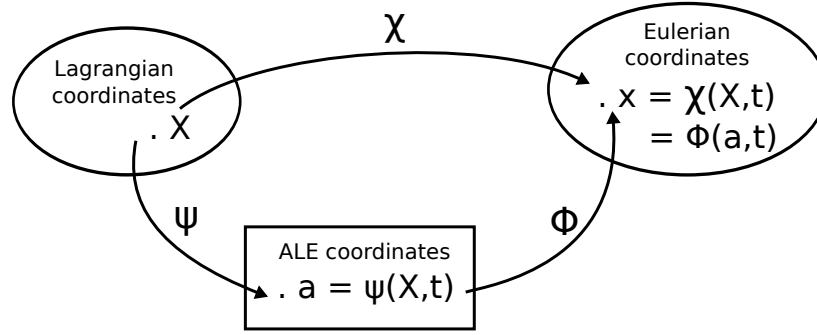


Figure 3.2: ALE formulation

Similarly to Section 1.1.2 we present a correspondence between the Eulerian and the ALE coordinates

$$\nabla_a \varphi = \mathbf{F}_a^T \nabla \varphi, \quad \nabla_a \varphi = \nabla \varphi \mathbf{F}_a. \quad (3.27)$$

Let us derive a relation between time derivatives

$$\mathbf{v} = \frac{\partial \chi(X, t)}{\partial t} = \frac{\partial \phi(\psi(X, t), t)}{\partial t} = \frac{\partial \phi}{\partial t} + \frac{\partial \phi(a, t)}{\partial a} \frac{\partial \psi(X, t)}{\partial t} = \mathbf{v}_a + \mathbf{F}_a \frac{\partial \psi(X, t)}{\partial t}.$$

Let us define the convective velocity \mathbf{c} and \mathbf{w} by

$$\mathbf{c} = \mathbf{v} - \mathbf{v}_a = \mathbf{F}_a \mathbf{w} = \mathbf{F}_a \frac{\partial \psi}{\partial t}. \quad (3.28)$$

For any function φ we have

$$\frac{\partial \varphi}{\partial t_a} = \frac{\partial \varphi(a, t)}{\partial t} = \frac{\partial \varphi(\phi(a, t), t)}{\partial t} = \frac{\partial \varphi}{\partial t} \Big|_x + \frac{\partial \varphi}{\partial x} \frac{\partial \phi}{\partial t} = \frac{\partial \varphi}{\partial t} \Big|_x + \mathbf{v}_a \nabla \varphi. \quad (3.29)$$

Thus we obtain

$$\begin{aligned} \frac{d}{dt} \varphi &= \frac{\partial \varphi}{\partial t_x} + \mathbf{v} \nabla \varphi = \frac{\partial \varphi}{\partial t_a} + (\mathbf{v} - \mathbf{v}_a) \nabla \varphi \\ &= \frac{\partial \varphi}{\partial t_a} + (\mathbf{v} - \mathbf{v}_a) \nabla_a \varphi \mathbf{F}_a^{-1} \\ &= \frac{\partial \varphi}{\partial t_a} + \mathbf{F}_a^{-1} \mathbf{c} \nabla_a \varphi \\ &= \frac{\partial \varphi}{\partial t_a} + \mathbf{w} \nabla_a \varphi. \end{aligned}$$

3.6.1 Balance equations in the ALE coordinates

In Section 1.7 we formulated the system of equations (1.136). Note that, in contrary to previous systems in this Chapter, the system (3.30) describes compressible material. Now we are ready to rewrite it into the ALE framework

$$\frac{\partial \varrho}{\partial t_a} + (\mathbf{v} - \mathbf{v}_a) \cdot \nabla_a \varrho \mathbf{F}_a^{-1} + \varrho \operatorname{tr}(\nabla_a \mathbf{v} \mathbf{F}_a^{-1}) = 0, \quad (3.30a)$$

$$\varrho \left(\frac{\partial \mathbf{v}}{\partial t_a} + (\mathbf{v} - \mathbf{v}_a) \cdot \nabla_a \mathbf{v} \mathbf{F}_a^{-1} \right) - (\nabla_a \varrho \mathbf{S}) \mathbf{F}_a^{-T} = 0, \quad (3.30b)$$

$$\frac{\partial \mathbf{S}}{\partial t_a} + (\mathbf{v} - \mathbf{v}_a) \cdot \nabla_a \mathbf{S} \mathbf{F}_e^{-1} - \nabla \mathbf{v} \mathbf{F}_a^{-1} \mathbf{S} - \mathbf{S} \mathbf{F}_a^{-T} \nabla \mathbf{v}^T = \mathbf{L}_e \mathbf{F}_a^{-1} + \mathbf{F}_a^{-T} \mathbf{L}_e^T \quad (3.30c)$$

$$\nabla_a \mathbf{v} \mathbf{F}_a^{-1} = \sum_{\alpha=1}^N \nu^{(\alpha)} \left(\mathbf{s}^{(\alpha)} \otimes \mathbf{m}^{(\alpha)} \right) + \sum_{i=1}^d \dot{\mathbf{a}}_i \otimes \mathbf{a}^i. \quad (3.30d)$$

To obtain a weak formulation we need to transform the integrals over Ω_x to the integrals over Ω_a . Important point in application of the integral substitution theorem is to use the Piola identity that states

$$\operatorname{div}_a ((\det \mathbf{F}_a) \mathbf{F}_a^{-T}) = 0.$$

3.7 Implementation

The methods described in this chapter are implemented as a FEniCS based Python module [85, 97]. We use following linear algebra backends: PETSc - Portable, Extensible Toolkit for Scientific Computation [98] and MUMPS: a MULTifrontal Massively Parallel sparse direct Solver [99].

Chapter 4

Numerical examples

We give a detailed description of performed numerical simulations. Two different deformation settings were considered: uniaxial compression and channel extrusion. The first case consist of an uniaxial compression of a pillar-shaped sample and plane strain compression in a channel die. The second focuses on 2-turn equal channel angular extrusion in two and three dimensions.

Similar – an Eulerian approach to crystal plasticity has been presented in Cazacu and Ionescu [74]. Viscoplastic law is obtained from Schmid law by using an overstress approach, in contrary to our research where the power law is adopted (1.120). To describe the lattice evolution authors consider only one differential equation. Analogous approach is studied in [100], however extended compressible materials and the 2-turn ECAP setting.

Moreover in [75] authors proposed a numerical algorithm that is refereed to as Augmented Lagrangian method. A mixed finite element – finite volume strategy was used: the equation for the velocity field is discretized using the finite element method while a finite volume method, with an upwind choice of the flux, is adopted for the hyperbolic equation related to the lattice orientation. The results of two-dimensional numerical simulations of equal-channel die extrusion and channel die compression are reported.

The algorithms presented in this chapter differs from the Augmented Lagrangian method described above. We provide thermodynamic derivation of the complete system (1.136) and solve a fully coupled problem by means of finite elements. Furthermore we do not confine to plain strains, see Section 4.2.

We argue that the Eulerian formulation is very well suited for flow-like problems, as for the 2-turn Equal Channel Angular Extrusion experiment [100], and with little adjustments for compression of single crystal [101].

4.1 Plane strain compression of a single crystal

4.1.1 Channel-die compression

We consider a rectangular-shaped single crystal with two or three slip systems, that is subjected to channel-die compression under plane strain conditions as shown in Figure 4.1.

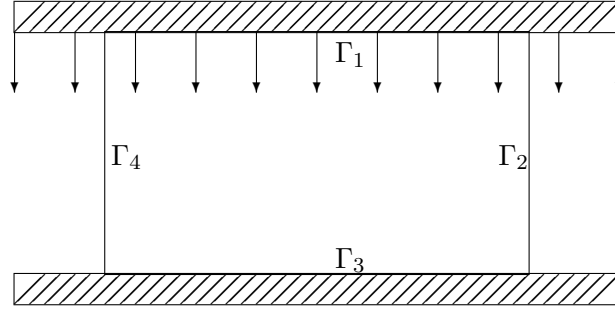


Figure 4.1: Channel-die compression scheme

Three slip systems are oriented as in Figure 4.2, where $\varphi = 55^\circ$. In the case of two slip systems we omit the third slip system, perpendicular to compression axis.

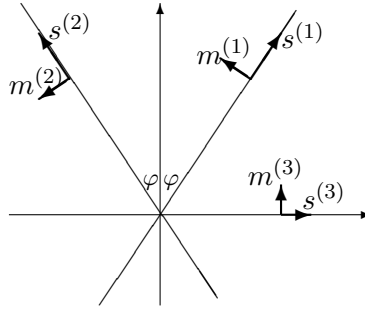


Figure 4.2: Scheme of slip systems

The initial boundary conditions are taken as in (4.4), with $\Gamma_D = \Gamma_1 \cup \Gamma_3$ and $\Gamma_N = \Gamma_2 \cup \Gamma_4$. Namely, for the velocity ($\mathbf{v} = (v_1, v_2)$) and the Cauchy stress are assumed to be

$$v_2 = V \text{ on } \Gamma_1, \quad v_2 = 0 \text{ on } \Gamma_3, \quad \mathbf{T}\mathbf{n} = \mathbf{0} \text{ on } \Gamma_2 \cup \Gamma_4.$$

Characteristic values are set to satisfy following ratios

$$\frac{E}{\tau_0} = 1000, \quad \frac{\nu_0 L}{V} = 1, \quad (4.1)$$

where E stands for Young's modulus and V , L , ν_0 are reference: velocity, length and slip rate, respectively. Note, that τ_0 was defined in (1.121).

The set of value of parameters of compressed material, which satisfies (4.1), were chosen following numerical studies in [27], namely: the density $\varrho_0 = 3000 \text{ kg/m}^3$, the velocity $V = 10^{-5} \text{ m/s} = 10 \mu\text{m/s}$, the length $L = 10^{-2} \text{ m}$, the reference slip rate $\nu_0 = 10^{-3} \text{ 1/s}$, the reference stress $\tau_0 = 123 \text{ MPa}$, the Poisson's ratio $\nu_{\text{pois}} = 0.3$, and the rate sensitivity parameter is between $m \in [0.005, 0.05]$ that is $1/m \in [20, 200]$. The rotation of the slip systems are described by the angles of lattice rotation α^i , with initial values $(\alpha_0^1, \alpha_0^2, \alpha_0^3) = (\alpha_0 + \varphi, \alpha_0 - \varphi, \alpha_0 + \frac{\pi}{2})$, where $\varphi = 54.74^\circ$. In double slip case third slip system is omitted.

In the case of plane strain compression we formulate the system of equations consist of (1.53a), (1.53b), (D.8) and the evolution of slip systems. The unknowns are density ϱ , the velocity \mathbf{v} , the Cauchy stress tensor \mathbf{T} , the slip directions $\mathbf{s}^{(\alpha)}$, and the normal to slip planes $\mathbf{m}^{(\alpha)}$, which is given by the system of equations

$$\dot{\varrho} + \varrho \operatorname{div} \mathbf{v} = 0, \quad (4.2a)$$

$$\varrho \dot{\mathbf{v}} - \operatorname{div} \mathbf{T} = 0, \quad (4.2b)$$

$$\dot{\mathbf{T}} + \mathbf{T} \operatorname{div} \mathbf{v} - \mathbf{L}_e \mathbf{T} - \mathbf{T} \mathbf{L}_e^T = \varrho \mathcal{C}(\mathbf{D} - \mathbf{D}_p), \quad (4.2c)$$

$$\dot{\mathbf{s}}^{(\alpha)} = \left(\nabla \mathbf{v} - \sum_{\alpha=1}^N \nu^{(\alpha)} \mathbf{s}^{(\alpha)} \otimes \mathbf{m}^{(\alpha)} \right) \mathbf{s}^{(\alpha)}, \quad (4.2d)$$

$$\dot{\mathbf{m}}^{(\alpha)} = \left(\nabla \mathbf{v} - \sum_{\alpha=1}^N \nu^{(\alpha)} \mathbf{s}^{(\alpha)} \otimes \mathbf{m}^{(\alpha)} \right)^{-T} \mathbf{m}^{(\alpha)}, \quad (4.2e)$$

where

$$\nu^{(\alpha)} = \nu_0 \operatorname{sgn}(\tau^{(\alpha)}) \left(\frac{|\tau^{(\alpha)}|}{\tau_c^{(\alpha)}} \right)^{1/m}, \quad \text{with } \dot{\tau}_c^{(\alpha)} = \sum_{\beta=1}^N H_{\alpha\beta} |\nu^{(\beta)}|, \quad \tau_c^{(\alpha)}|_{t=0} = \tau_0. \quad (4.3)$$

In the two dimensional case the evolution of the slip systems is computed directly. In contrary to three dimensional case where we used the lattice basis. Note that in two dimensions we consider up to three slip systems, thus the number of unknown will not increase when you compare number of slip system with lattice basis vectors.

The system (4.2) holds for all $x \in \Omega$ and all $t \in [0, \infty)$ and is endowed with the initial and boundary conditions

$$\begin{aligned} \varrho(x, 0) &= \varrho_0(x) \text{ for } x \in \Omega, \\ \mathbf{s}^{(\alpha)}(x, 0) &= (\cos(\alpha_0^{(\alpha)}(x)), \sin(\alpha_0^{(\alpha)}(x))), \text{ for } x \in \Omega, \\ \mathbf{m}^{(\alpha)}(x, 0) &= (-\sin(\alpha_0^{(\alpha)}(x)), \cos(\alpha_0^{(\alpha)}(x))), \text{ for } x \in \Omega, \\ \mathbf{T}(x, 0) &= \mathbf{0} \text{ for } x \in \Omega, \\ \mathbf{v}(x, t) &= \mathbf{v}_0(x, t) \text{ for } x \in \Gamma_D \times [0, \infty), \\ \mathbf{T}(x, t) \mathbf{n} &= \mathbf{0} \text{ for } x \in \Gamma_N \times [0, \infty), \end{aligned} \quad (4.4)$$

where $\partial\Omega = \Gamma_D \cup \Gamma_N$ and $\varrho_0, \mathbf{v}_0, \alpha_0^{(\alpha)}$ are given functions.

Moreover, we specify right hand side of (4.2c), i.e. fourth order elasticity tensor \mathcal{C} as

$$\mathcal{C}(\mathbf{D} - \mathbf{D}_p) = \lambda_e (\operatorname{tr}(\mathbf{D} - \mathbf{D}_p)) \mathbf{I} + 2\mu_e (\mathbf{D} - \mathbf{D}_p),$$

where the Lamé coefficients take following values

$$\lambda_e = 576.92\tau_0 \text{ and } \mu_e = 384.62\tau_0.$$

After rescaling the system (4.2) we notice that characteristic number, which multiplies the dynamic term in the momentum equilibrium $\varrho \dot{\mathbf{v}}$, reads $R_1 = \frac{\varrho_0 V^2}{\tau_0} \approx 3 \times 10^{-5}$. Thus, quasi-static assumption would be justified in that case. Although we keep this term for computational purposes.

In what follows by strain we understand the nominal strain $e = \frac{h-H_0}{H_0}$, where h and H_0 stand for current and initial height of the specimen, respectively. All the results were computed up to nominal strain 0.3.

Simulations were conducted on a structured triangular mesh consists of 37688 vertices (74800 cells).

4.1.2 Finite element formulation

The time is discretized by a one step finite difference and a mixed finite element discretization is used in space. The choice of the approximations of each variable consists of \mathcal{P}_2 elements for the velocity, \mathcal{P}_1 for the density and the lattice rotations (all continuous) and \mathcal{P}_1 -discontinuous for the Cauchy stress and the slip rates. This leads to the following definitions of the finite-dimensional spaces

$$\begin{aligned}\mathbb{V}_h &= \{v_h \in W^{1,2}(\Omega; \mathbf{R}^2); \quad \mathbf{v}|_{\Gamma_1} = (0, -1), \mathbf{v}|_{\Gamma_3} = (0, 0) \mathbf{v}|_K \in \mathcal{P}_2(K)^2 \forall K \in \mathcal{T}_h\}, \\ \mathbb{R}_h &= \{\varrho_h \in W^{1,2}(\Omega; \mathbf{R}); \quad \varrho_h|_{\Gamma_1} = 1, \varrho_h|_K \in \mathcal{P}_1(K) \forall K \in \mathcal{T}_h\}, \\ \mathbb{T}_h &= \{\mathbf{T}_h \in L^2(\Omega; \mathbf{R}_{\text{sym}}^{2 \times 2}); \quad \mathbf{T}_h|_K \in \mathcal{P}_1(K)^{2 \times 2} \forall K \in \mathcal{T}_h\}, \\ \mathbb{N}_h &= \{\nu_h \in L^2(\mathbf{R}); \quad \nu_h|_K \in \mathcal{P}_1(K) \forall K \in \mathcal{T}_h\}, \\ \mathbb{A}_h &= \{\varphi_h \in W^{1,2}(\Omega; \mathbf{R}); \quad \varphi_h|_{\Gamma_1} = 0, \varphi_h|_K \in \mathcal{P}_1(K) \forall K \in \mathcal{T}_h\}.\end{aligned}$$

Here, \mathcal{T}_h is the triangulation of our domain with h representing the discretization parameter, for example the characteristic size of the triangles. The time interval $(0, T)$ is divided into steps of length Δt and by superscript k we denote the variables at the time level t_k .

4.1.3 Three step algorithm

For the solution algorithm of the system (4.2) at each timestep the set of the equations is decomposed into two parts which are solved subsequently in three sub-steps. Given \mathbf{v}^{k-1} , ϱ^{k-1} , \mathbf{T}^{k-1} , $\mathbf{s}^{(i)k-1}$, $\mathbf{m}^{(i)k-1}$, $\nu^{(i)k-1}$ and $g^{(i)k-1}$ from previous time level we proceed as follows:

Step 1: Solve problem for \mathbf{v}^k , ϱ^k , \mathbf{T}^k , and $\nu^{(i)k}$

$$\begin{aligned}\frac{\varrho^k - \varrho^{k-1}}{\Delta t} + \operatorname{div}(\varrho^k \mathbf{v}^k) &= 0, \\ \varrho^k \left(\frac{\mathbf{v}^k - \mathbf{v}^{k-1}}{\Delta t} + \left(\mathbf{v}^k - \mathbf{v}_{\text{mesh}}^{k-1} \right) \nabla \mathbf{v}^k \right) - \operatorname{div} \mathbf{T}^k &= 0, \\ \frac{\mathbf{T}^k - \mathbf{T}^{k-1}}{\Delta t} + \left(\mathbf{v}^k - \mathbf{v}_{\text{mesh}}^{k-1} \right) \nabla \mathbf{T}^k + \mathbf{T}^k \operatorname{div} \mathbf{v}^k \\ - \mathbf{L}_e^{k,k-1} \mathbf{T}^k - \mathbf{T}^k (\mathbf{L}_e^{k,k-1})^T - \varrho^k \mathcal{C}(\mathbf{D}^k - \mathbf{D}_p^{k,k-1}) &= 0, \\ \nu^{(i)k} - \operatorname{sgn}(\mathbf{T}^k : \mathbf{s}^{(i)k-1} \otimes \mathbf{m}^{(i)k-1}) \left(\frac{|\mathbf{T}^k : \mathbf{s}^{(i)k-1} \otimes \mathbf{m}^{(i)k-1}|}{g^{(i)k-1}} \right)^{1/m} &= 0 \quad \forall i \in \{1, 2, 3\},\end{aligned}\tag{4.5}$$

where if we use $\mathbf{L}_p^{(i)k-1} = \mathbf{s}^{(i)k-1} \otimes \mathbf{m}^{(i)k-1}$, we define $\mathbf{L}_e^{k,k-1} = \nabla \mathbf{v}^k - \sum_{i=1}^N \nu^{(i)k} \mathbf{L}_p^{(i)k-1}$ and $\mathbf{D}_p^{k,k-1} = \sum_{i=1}^N \nu^{(i)k} \operatorname{sym}(\mathbf{L}_p^{(i)k-1})$.

Step 2: Move the mesh by $\mathbf{u}^k = \mathbf{v}_{\text{mesh}}^k \Delta t$. The velocity of the mesh motion $\mathbf{v}_{\text{mesh}}^k$ can be taken as the material velocity \mathbf{v}^k which in fact leads to a Lagrangian description or it can be chosen arbitrary with restriction that $\mathbf{v}_{\text{mesh}}^k | \partial\Omega = \mathbf{v}^k | \partial\Omega$ which leads to the ALE description.

Step 3: Compute the new critical stress, the slip directions, and the new normal to the slip planes

$$\begin{aligned}
\frac{\mathbf{s}^{(i)k} - \mathbf{s}^{(i)k-1}}{\Delta t} + \left(\mathbf{v}^k - \mathbf{v}_{\text{mesh}}^k \right) \nabla \mathbf{s}^{(i)k} &= \mathbf{L}_e^k \mathbf{s}^{(i)k}, \\
\frac{\mathbf{m}^{(i)k} - \mathbf{m}^{(i)k-1}}{\Delta t} + \left(\mathbf{v}^k - \mathbf{v}_{\text{mesh}}^k \right) \nabla \mathbf{m}^{(i)k} &= (\mathbf{L}_e^k)^{-T} \mathbf{m}^{(i)k}, \\
\frac{g^{(i)k} - g^{(i)k-1}}{\Delta t} + \left(\mathbf{v}^k - \mathbf{v}_{\text{mesh}}^k \right) \nabla g^{(i)k} &= \sum_{j=1}^N h_{ij} |\nu^{(j)}|,
\end{aligned} \tag{4.6}$$

where $\mathbf{L}_e^k = \nabla \mathbf{v}^k - \sum_{i=1}^N \text{sgn}(\mathbf{T}^k : \mathbf{s}^{(i)k} \otimes \mathbf{m}^{(i)k}) \left(\frac{|\mathbf{T}^k : \mathbf{s}^{(i)k} \otimes \mathbf{m}^{(i)k}|}{g^{(i)k}} \right)^{1/m} \mathbf{s}^{(i)k} \otimes \mathbf{m}^{(i)k}$.

The systems (4.5) and (4.6) are formulated in standard weak sense, discretized by means of the mixed FE spaces mentioned above. To solve the systems we employ a non-linear Newton-Raphson solver with an analytic evaluation of the Jacobian and use sparse direct solver MUMPS for solving the linear systems. Implementation is done in the software package FEniCS [84].

4.1.4 Comparison with experimental data

To verify the ability of the proposed algorithm to model crystal plasticity phenomena the simulation results are compared with Harren et al. experiments [27]. X-ray measurements were carried out by them to determine the lattice reorientation of the single crystals of various initial crystallographic orientations in plane strain compression (PSC) in a channel die before macroscopic shear bands appeared, i.e. to the engineering strain ≈ 0.3 - 0.9 . It was observed that except for crystals oriented symmetrically with respect to the compression and extension axes, the crystals exhibited an overall common behavior. After yield, all these crystals started to reorient in such a way that their crystallographic direction [110] approached the compression axis and the direction [001] became parallel to the extension axis along the channel, i.e. these reorientations tend to bring the crystals toward the (110)[001] orientation. The (110)[001] geometry coincides with a stable state of symmetric slip on four slip systems: (111)[10 $\bar{1}$], (111)[01 $\bar{1}$] and (11 $\bar{1}$)[101], (11 $\bar{1}$)[011]. The net shearing systems associated with this symmetric state are then [11 $\bar{2}$] in (111) and [112] in (11 $\bar{1}$), and hence the resulting deformation of this symmetric state is aligned with the channel; the state of the plane strain crystallographic deformation is approached. In order to simulate the compression tests of single crystals, Harren et al. [27] employed two-dimensional single crystal model with two considered slip systems (111)[11 $\bar{2}$] and (11 $\bar{1}$)[112]. The orientation of the slip systems with respect to compression axis is $\phi = \arccos \approx 55^\circ$. The experimental observations and the computed deformation response are in a close agreement. To test the present approach we use the same two-dimensional single crystal plane strain compression.

4.1.5 The influence of the rate sensitivity

In [27] the imperfection of the specimen was introduced by perturbation of the right-hand side of the boundary, namely

$$x_1|_{\Gamma_2} = x_1 + 5 \times 10^{-6} \cos\left(\frac{\pi x_2}{L_0}\right). \tag{4.7}$$

The method presented in Section 4.1.2 was employed to solve initial boundary value problem (4.2) with the rate sensitivity parameter $m = 0.005$ and Γ_2 given by (4.7).

The values of the magnitude of the velocity, the density, and the slip rates for three different strains are presented in Figure 4.3.

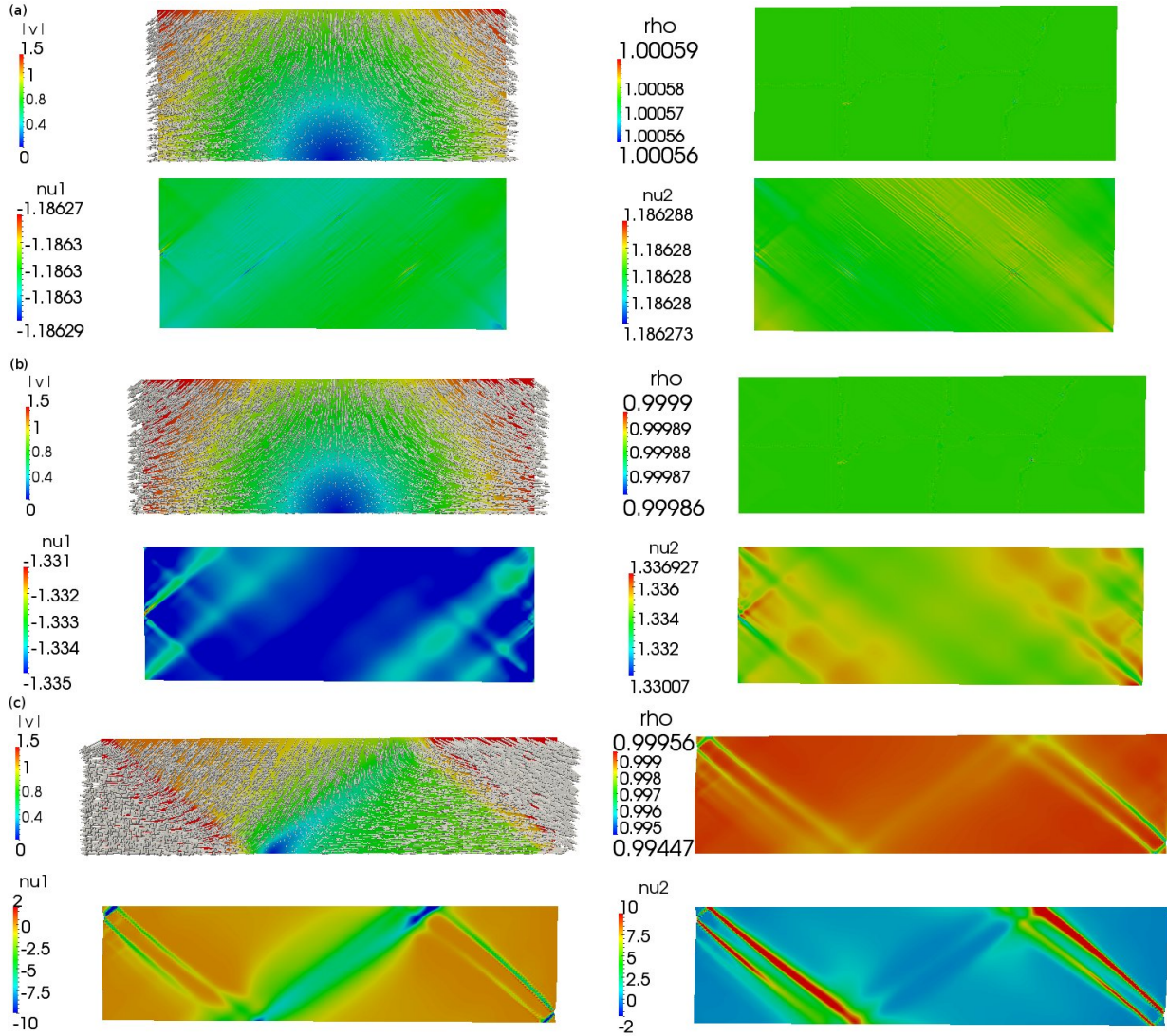


Figure 4.3: The evolution of the velocity (top-left), the density (top-right), and the slip rates (bottom) for nominal strains 0.1 (a), 0.2 (b), and 0.3 (c).

4.1.6 Influence of initial angle of lattice rotation

In this section we address the problem of the compression of double-slip single crystal with the non zero initial angle of the lattice rotation. The presented method is not able to capture the case presented in Section 4.1.5 for initial angle different than zero. Thus to investigate the influence of initial angle of lattice rotation we consider the rate sensitivity parameter significantly smaller than 0.005, namely 0.05. In Figure 4.4 we present result of simulations with different initial orientation for square and rectangular shaped domains. Initial orientations were set at $0.2 \text{ rad} = 11.46^\circ$ and $0.4 \text{ rad} = 22.9^\circ$.

We observe that the angle of lattice rotation has a tendency to decrease, namely during die-compression orientation of slip systems approaches the symmetric orientation.

For similar computational studies we refer to [74], where authors consider 3 slip systems with initial orientation of 0.417 rad .

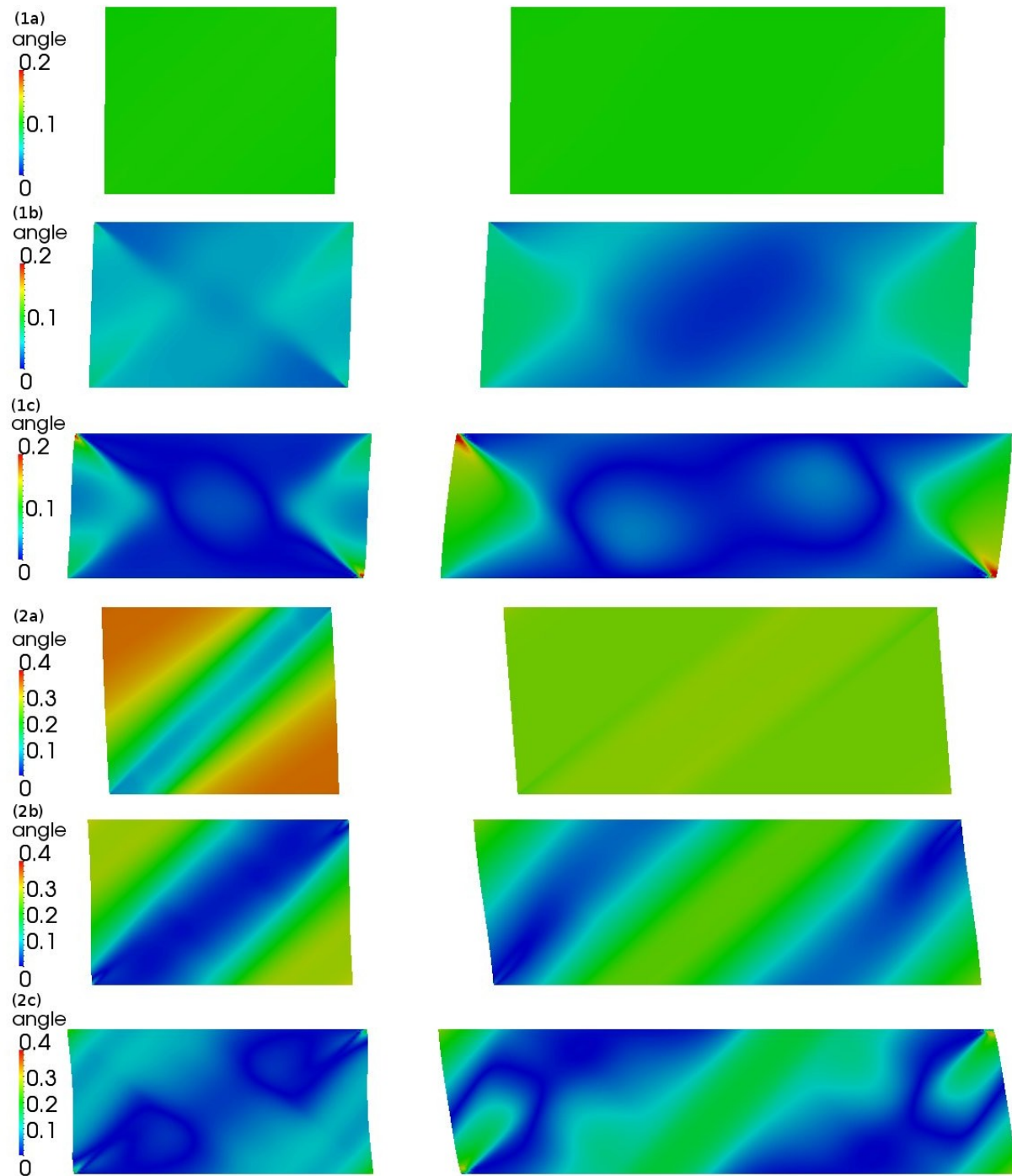


Figure 4.4: The evolution of the angle of the lattice rotation of double-slip single crystal for initial lattice rotation 0.2 rad (1) and 0.4 rad (2) for nominal strains 0.1 (a), 0.2 (b), and 0.3 (c).

4.1.7 Activity of slip systems

Figure 4.5 shows the behaviour of individual slip systems. There is a measurable difference between the alignment of slip activity regions (shear bands) between square and rectangle shaped domains. It is also worth of noticing that the third slip system is almost inactive.

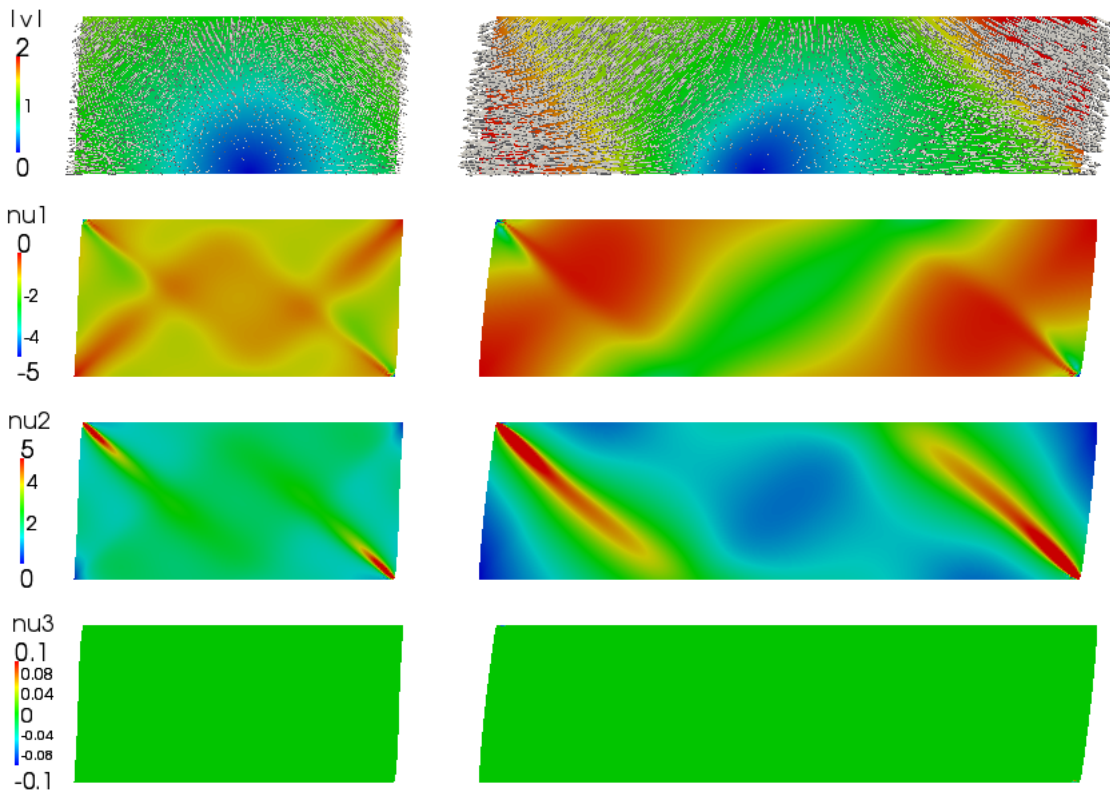


Figure 4.5: Velocity field and slip rates on individual slip systems for single crystal with initial lattice rotation 0.2 rad at nominal strain 0.3.

4.1.8 Stress-strain behaviour

Nominal stress reads $n = \mathbf{T}_{22}$. In Figure 4.1.8 we present stress strain dependency.

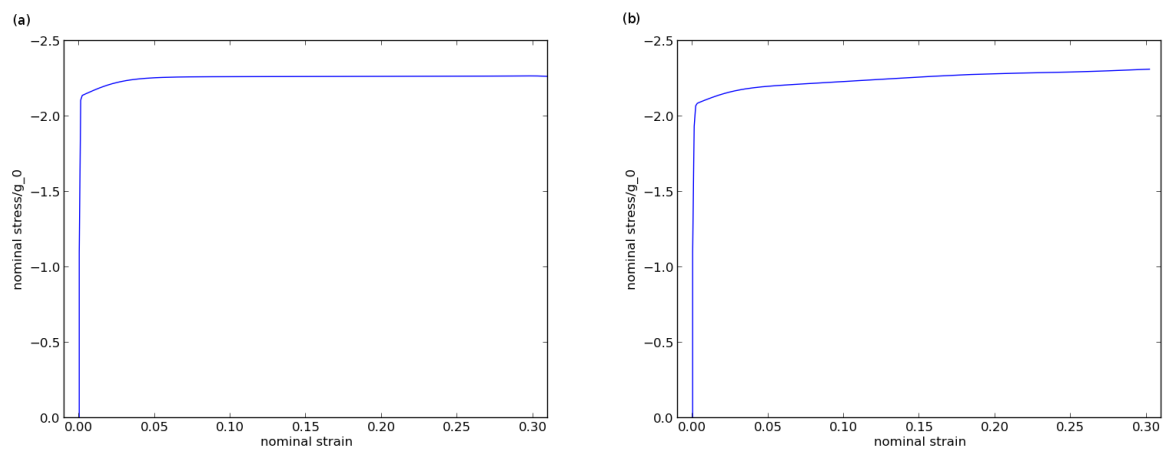


Figure 4.6: Nominal stress vs. nominal strain, for numerical simulations described in Section 4.1.5 (a) and Section 4.1.6 (b).

4.2 Micropillar compression

In the case of simple compression we deal with a free boundary problem. Here we employ the Arbitrary Lagrangian Eulerian (ALE) approach in the sense that we use our Eulerian formulation on a moving mesh which captures the free boundary. ALE method was introduced in Section 3.6.

The compression testing methodology is shown schematically in Figure 4.7. The setting mimics the compression experiment commonly performed on macroscopic samples [102, 103], [26].

We recall the system of equations (1.136). Unknowns are the density ϱ , the velocity \mathbf{v} , the Kirchhoff stress \mathbf{S} , and the lattice vectors $\mathbf{a}_1, \mathbf{a}_2, \mathbf{a}_3$ ($\mathbf{s}^{(\alpha)}$ and $\mathbf{m}^{(\alpha)}$ are given through lattice vectors)

$$\dot{\varrho} + \varrho \operatorname{div} \mathbf{v} = 0, \quad (4.8a)$$

$$\varrho \dot{\mathbf{v}} = \operatorname{div} (\varrho \mathbf{S}), \quad (4.8b)$$

$$\overset{\nabla}{\mathbf{S}} = \mathbf{C} \left(\mathbf{D} - \sum_{\alpha=1}^N \nu^{(\alpha)} \operatorname{sym} \left(\mathbf{s}^{(\alpha)} \otimes \mathbf{m}^{(\alpha)} \right) \right), \quad (4.8c)$$

$$\nabla \mathbf{v} = \sum_{\alpha=1}^N \nu^{(\alpha)} \left(\mathbf{s}^{(\alpha)} \otimes \mathbf{m}^{(\alpha)} \right) + \sum_{i=1}^d \dot{\mathbf{a}}_i \otimes \mathbf{a}^i, \quad (4.8d)$$

$$\nu^{(\alpha)} = \nu_0 \operatorname{sgn} \left(\mathbf{s}^{(\alpha)} : \mathbf{S} \mathbf{m}^{(\alpha)} \right) \left(\mathbf{s}^{(\alpha)} : \mathbf{S} \mathbf{m}^{(\alpha)} \right)^{\frac{1}{m}}. \quad (4.8e)$$

The rate sensitivity parameter m is taken to be 0.05, the hardening effects are neglected. The system (4.8) is equipped with the following initial and boundary conditions:

$$\begin{aligned} \varrho(x, 0) &= 1 \text{ for } x \in \Omega, \\ \mathbf{v}(x, t) &= \mathbf{v}_0(x, t) \text{ for } x \in \Gamma_D \times [0, \infty), \\ \mathbf{S}(x, t) \mathbf{n} &= \mathbf{0} \text{ for } x \in \Gamma_N \times [0, \infty), \\ \mathbf{S}(x, 0) &= \mathbf{0} \text{ for } x \in \Omega, \\ \mathbf{a}_1(x, 0) &= (1, 0, 0), \text{ for } x \in \Omega, \\ \mathbf{a}_2(x, 0) &= (0, 1, 0), \text{ for } x \in \Omega, \\ \mathbf{a}_3(x, 0) &= (0, 0, 1), \text{ for } x \in \Omega, \end{aligned}$$

where $\partial\Omega = \Gamma_D \cup \Gamma_N$ and \mathbf{v}_0 is a given functions.

The set of value of parameters of compressed material, corresponds to the experimental and numerical works [104, 26]. The ratio between the height L_0 and diameter D is selected to be 2.3. The elastic constants are chosen to be $c_{11} = 280.5\text{GPa}$, $c_{12} = 188.5\text{MPa}$, and $c_{44} = 133.5\text{GPa}$, see (1.104). The reference values reads: the length $l_0 = 10\mu\text{m}$, the velocity $\mathbf{v}_0 = 1\mu\text{m/s}$, the reference slip rate $\nu_0 = 0.1\text{s}$, the stress $\tau_0 = 420\text{MPa}$.

Although the values do not refer to any specific material, these material parameters are those for a single-crystal Ni-base superalloy, i.e. Rene N5, a Ni-base superalloy commonly used in turbine blade applications, which has a nominal composition of Ni-8Co-7Cr-7Ta-6.2Al-5W-3Re-2Mo-0.2Hf, see [26].

Two kinds of the top velocity boundary condition are considered, see Figure 4.8. In the first case we fix the velocity on the top boundary Γ_1 , $\mathbf{v}_0(x, t)|_{\Gamma_1} = (0, 0, -1)$. This condition is refer to as constrained and setting mimics the case where the loading axis is very stiff and the friction between the top surface and the plunger is extremely high. The second case is

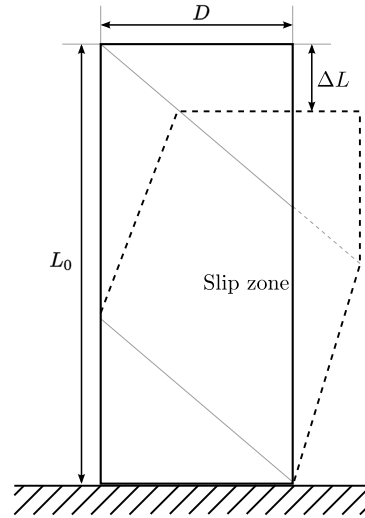


Figure 4.7: Scheme of micropillar compression, dashed lines represent the shape of compressed sample

called unconstrained and we allow the top surface to move in the plane perpendicular to z -axis, $\mathbf{v}_{0_z}(x, t)|_{\Gamma_3} = -1$. This simply mimics the case where there is no friction between the top surface and the plunger.

In rest of the Dirichlet boundary, namely Γ_3 the velocity is fixed $\mathbf{v}_0(x, t)|_{\Gamma_3} = (0, 0, 0)$. Moreover, we put the Neumann boundary condition $\mathcal{S}(x, t)\mathbf{n} = \mathbf{0}$ on the lateral surface Γ_2 .

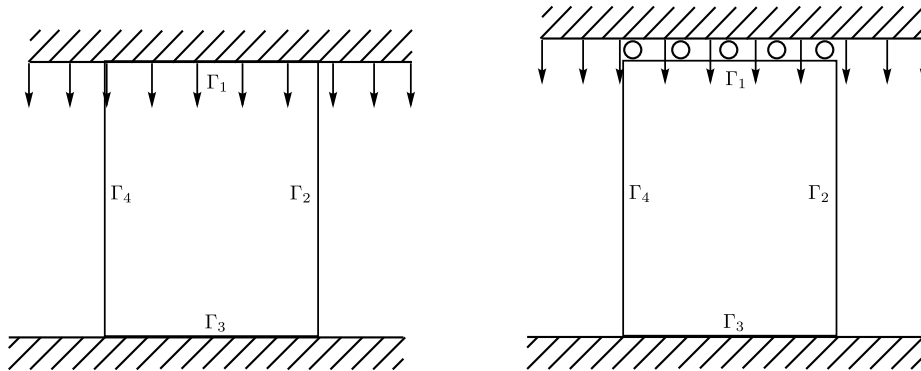


Figure 4.8: Scheme of micropillar compression boundary conditions, constrained (left) and unconstrained (right)

4.2.1 Slip systems

The crystal orientation is relative to the fixed sample coordinates in the reference configuration. The lattice basis vectors coincide with the systems of coordinates axis. The definitions of slip systems are given in Table 4.2.1. The primary slip system is number 2, $(111)[10\bar{1}]$.

α	Slip direction $\sqrt{2}\mathbf{s}^{(\alpha)}$	Slip plane normal $\sqrt{3}\mathbf{m}^{(\alpha)}$
1	$[\bar{1}10]$	(111)
2	$[10\bar{1}]$	(111)
3	$[0\bar{1}1]$	(111)
4	$[\bar{1}\bar{1}0]$	$(1\bar{1}\bar{1})$
5	$[101]$	$(1\bar{1}\bar{1})$
6	$[01\bar{1}]$	$(1\bar{1}\bar{1})$
7	$[110]$	$(\bar{1}1\bar{1})$
8	$[\bar{1}01]$	$(\bar{1}1\bar{1})$
9	$[0\bar{1}\bar{1}]$	$(\bar{1}1\bar{1})$
10	$[1\bar{1}0]$	$(\bar{1}\bar{1}1)$
11	$[\bar{1}0\bar{1}]$	$(\bar{1}\bar{1}1)$
12	$[011]$	$(\bar{1}\bar{1}1)$

Table 4.1: Slip systems for three dimensional micropillar compression

4.2.2 Finite element formulation

The time is discretized by a one step finite difference and a mixed finite element discretization is used in space. The choice of the approximations of each variable consists of \mathcal{P}_2 elements for the velocity, \mathcal{P}_1 for the density and the lattice basis vectors, and \mathcal{P}_2 for the Kirchhoff stress. This leads to the following definitions of the finite-dimensional spaces

$$\begin{aligned} \mathbb{V}_h &= \{\mathbf{v}_h \in W^{1,2}(\Omega; \mathbf{R}^d); \mathbf{v}|_{\Gamma_1} = (0, 0, -1), \mathbf{v}|_{\Gamma_3} = (0, 0, 0), \mathbf{v}|_K \in \mathcal{P}_2(K)^d \forall K \in \mathcal{T}_h\}, \\ \mathbb{P}_h &= \{\varrho_h \in L^2_0(\Omega) \cap C^0(\Omega; \mathbf{R}); \varrho_h|_K \in \mathcal{P}_1(K) \forall K \in \mathcal{T}_h\}, \\ \mathbb{S}_h &= \{\mathbf{S}_h \in H^1_0(\Omega; \mathbf{R}_{\text{sym}}^{d \times d}); \mathbf{S}_h|_K \in \mathcal{P}_2(K)^{d \times d} \forall K \in \mathcal{T}_h\} \\ \mathbb{A}_h &= \{\mathbf{a}_h \in L^2(\Omega)^d \cap C^0(\Omega; \mathbb{R}^d); \mathbf{a}_h|_K \in \mathcal{P}_1(K) \forall K \in \mathcal{T}_h\}. \end{aligned}$$

Here, \mathcal{T}_h is the triangulation of our domain with h representing the discretization parameter, for example the characteristic size of tetrahedra. The time interval $(0, T)$ is divided in to steps of length Δt and by superscript k we denote the variables at the time level t_k .

4.2.3 Two step algorithm

For the solution algorithm of the system (4.8) at each time step we perform two actions. Given $\mathbf{v}^k, \varrho^k, \mathbf{S}^k, \mathbf{a}_i^k$ from previous time level we proceed as follows:

Step 1: Solve problem for $\mathbf{v}^{k+1}, \varrho^{k+1}, \mathbf{S}^{k+1}$, and \mathbf{a}_i^{k+1}

$$\left(\frac{\varrho^{k+1} - \varrho^k}{\Delta t} + \text{div}(\varrho^{k+1} \mathbf{v}^{k+1}), z_\varrho \right) = 0,$$

$$\begin{aligned} \left(\frac{\mathbf{v}_h^{k+1} - \mathbf{v}_h^k}{\Delta t} + (\mathbf{v}_h^{k+1} - v_{mesh}^k) \nabla \mathbf{v}_h^{k+1}, \mathbf{z}_v \right) + (\mathbf{S}_h^{k+1}, \nabla \mathbf{z}_v) &= 0, \\ \left(\mathbf{S}_h^{k+1} - 2\mu_e \mathbf{D}_{e_h}^{k+1}, \mathbf{Z}_S \right) &= 0, \\ \left(\frac{\mathbf{a}_{i_h}^{k+1} - \mathbf{a}_{i_h}^k}{\Delta t} - \mathbf{L}_{e_h}^{k+1} \mathbf{a}_{i_h}^{k+1}, \mathbf{z}_{a_i} \right) &= 0, \quad i \in \{1, 2, 3\}. \end{aligned}$$

Step 2: Move the mesh by $\mathbf{u}^k = \mathbf{v}_{mesh}^k \Delta t$. The velocity of the mesh motion \mathbf{v}_{mesh}^k can be taken as the material velocity \mathbf{v}^k which in fact leads to a Lagrangian description or it can be chosen arbitrary with restriction that $\mathbf{v}_{mesh}^k|_{\partial\Omega} = \mathbf{v}^k|_{\partial\Omega}$ which leads to the ALE description.

4.2.4 Experimental Results

We present the experimental results by Shade et al. [26]. Authors performed uni-axial mechanical tests on micrometer-scale specimens that can operate inside a scanning electron microscope (SEM). Figure 4.9 (A) shows SEM images at various strain levels during a representative constrained experiment. By comparison, images at various strain levels from an unconstrained experiment are shown in Figure 4.9 (B).

In the next section we present numerical simulations of micropillar compression under constrained and unconstrained boundary conditions.

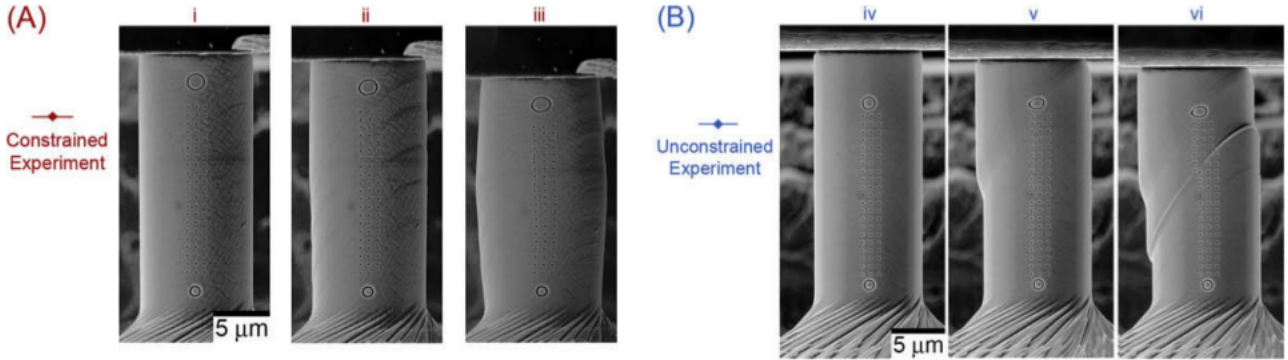


Figure 4.9: The results of compression experiments on Rene N5 microcrystals [26]. Three SEM images at various strain levels for constrained and unconstrained experiments and corresponding stress–strain curves.

4.2.5 Results

Since computations are conducted in the Eulerian coordinates primary variable is the velocity. In Figure 4.10 we present the velocity field in the whole sample together with an x –axis cross-section. There is a measurable difference between the alignment of slip activity regions (shear bands) between constrained and unconstrained domains, see Figure 4.11. Figures 4.13 and 4.12 show the behaviour of individual slip systems, constrained and unconstrained boundary conditions. It is also worth of noticing that some of the slip system are almost inactive.

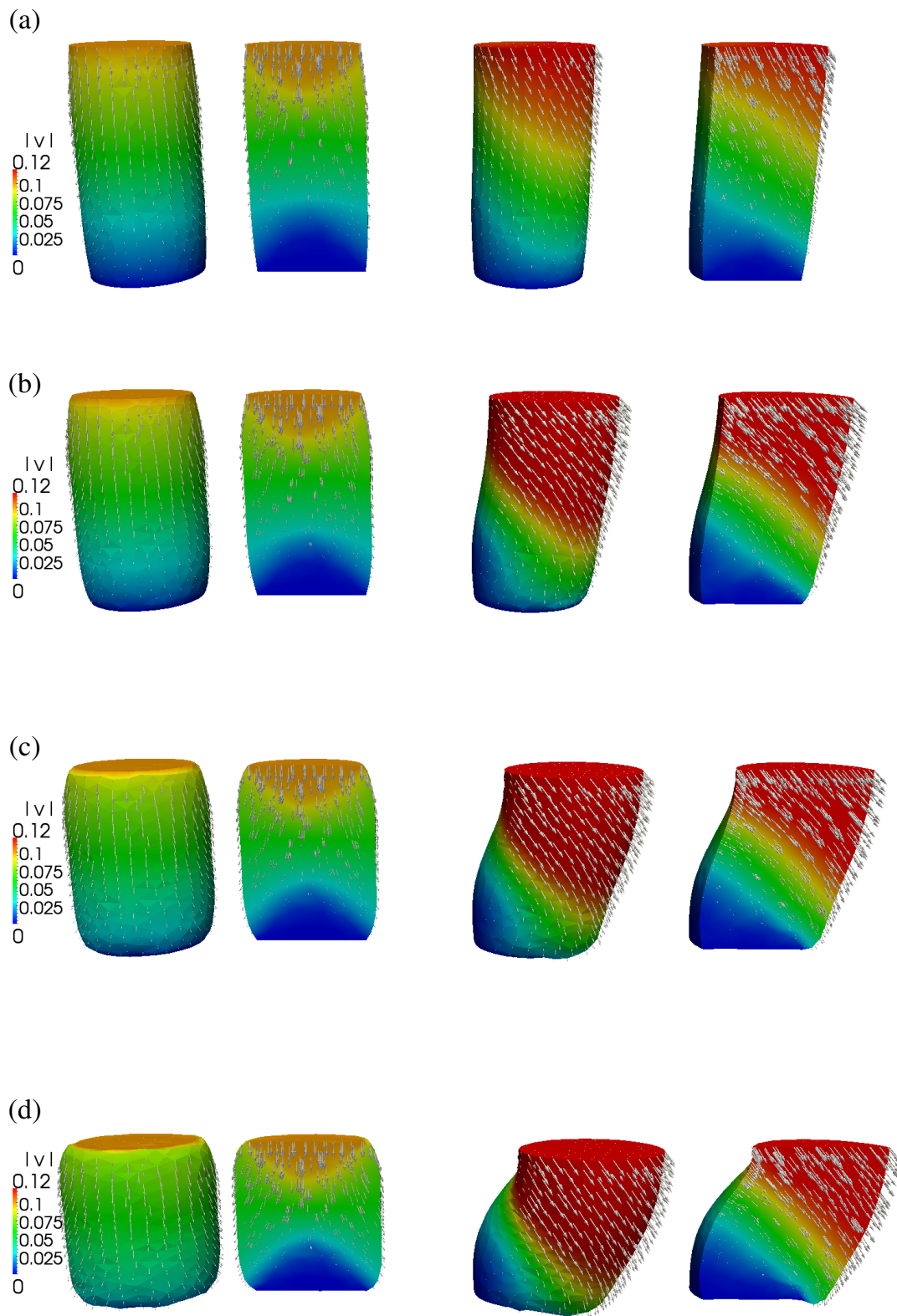


Figure 4.10: The evolution of the velocity, the whole sample and cross-section for nominal strains 0.1 (a), 0.2 (b), 0.3 (c), and 0.4 (d), constrained domain (left), unconstrained (right).

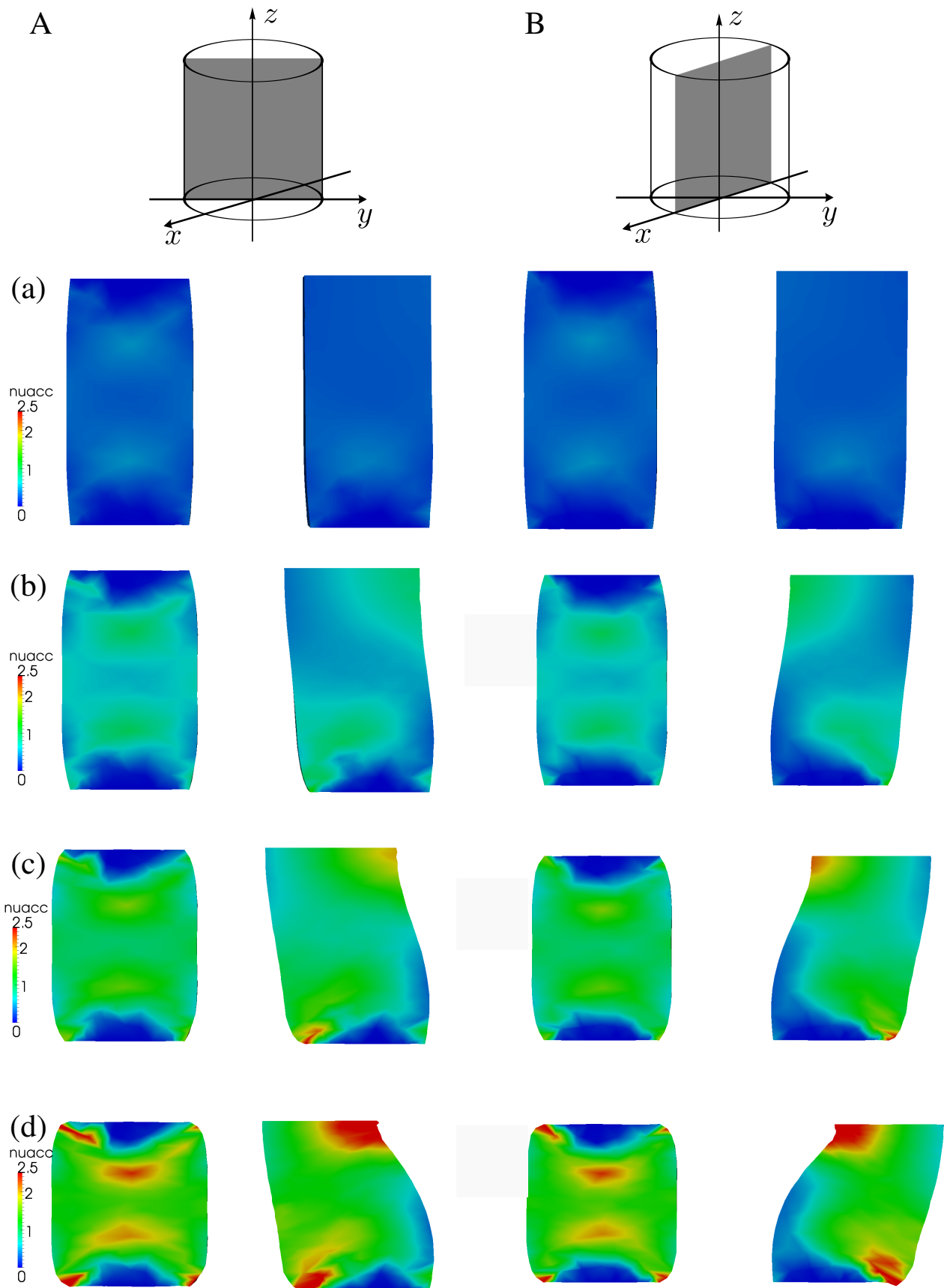


Figure 4.11: The evolution of the accumulated slip for two cross-sections A and B, for nominal strains 0.1 (a), 0.2 (b), 0.3 (c), and 0.4 (d), constrained domain (left), unconstrained (right).

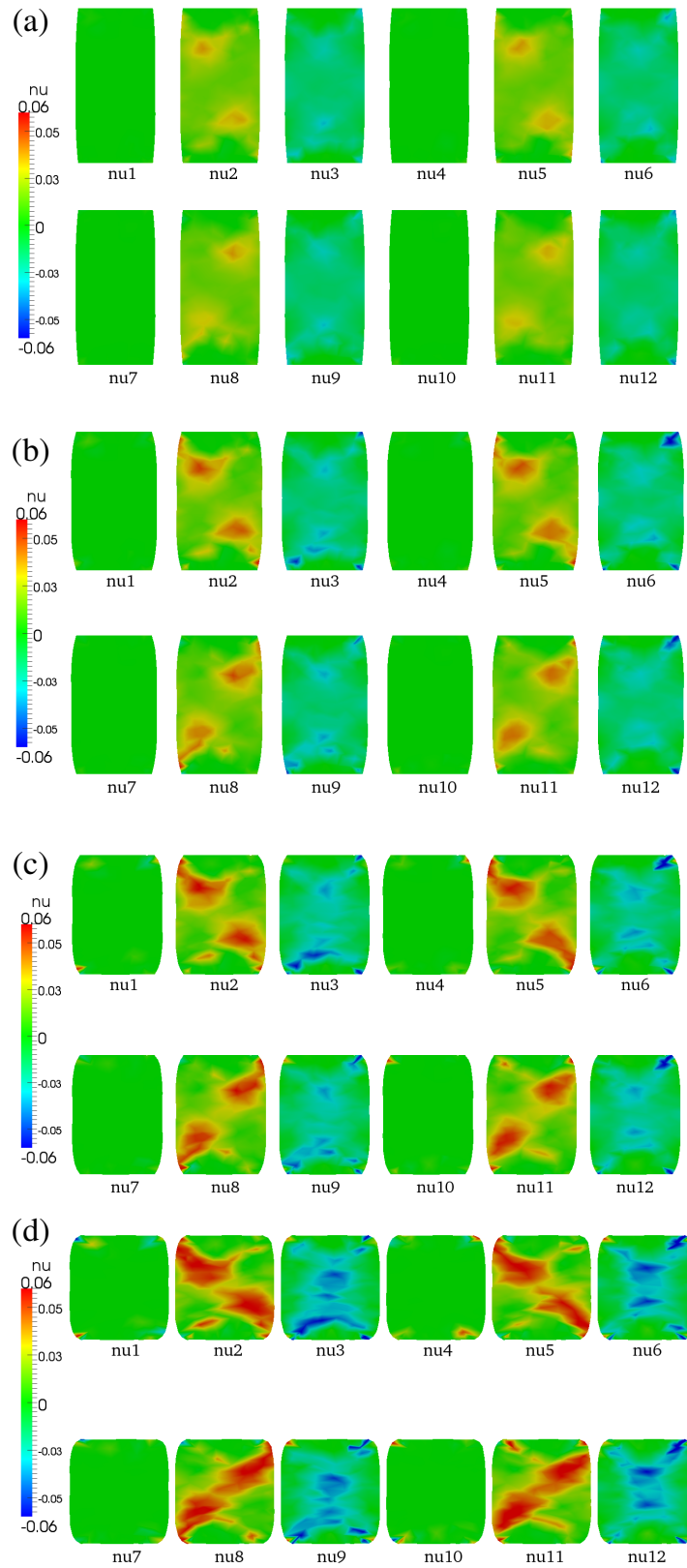


Figure 4.12: The evolution of the accumulated slip for two cross-sections A and B, for nominal strains 0.1 (a), 0.2 (b), 0.3 (c), and 0.4 (d), constrained domain (left), unconstrained (right).

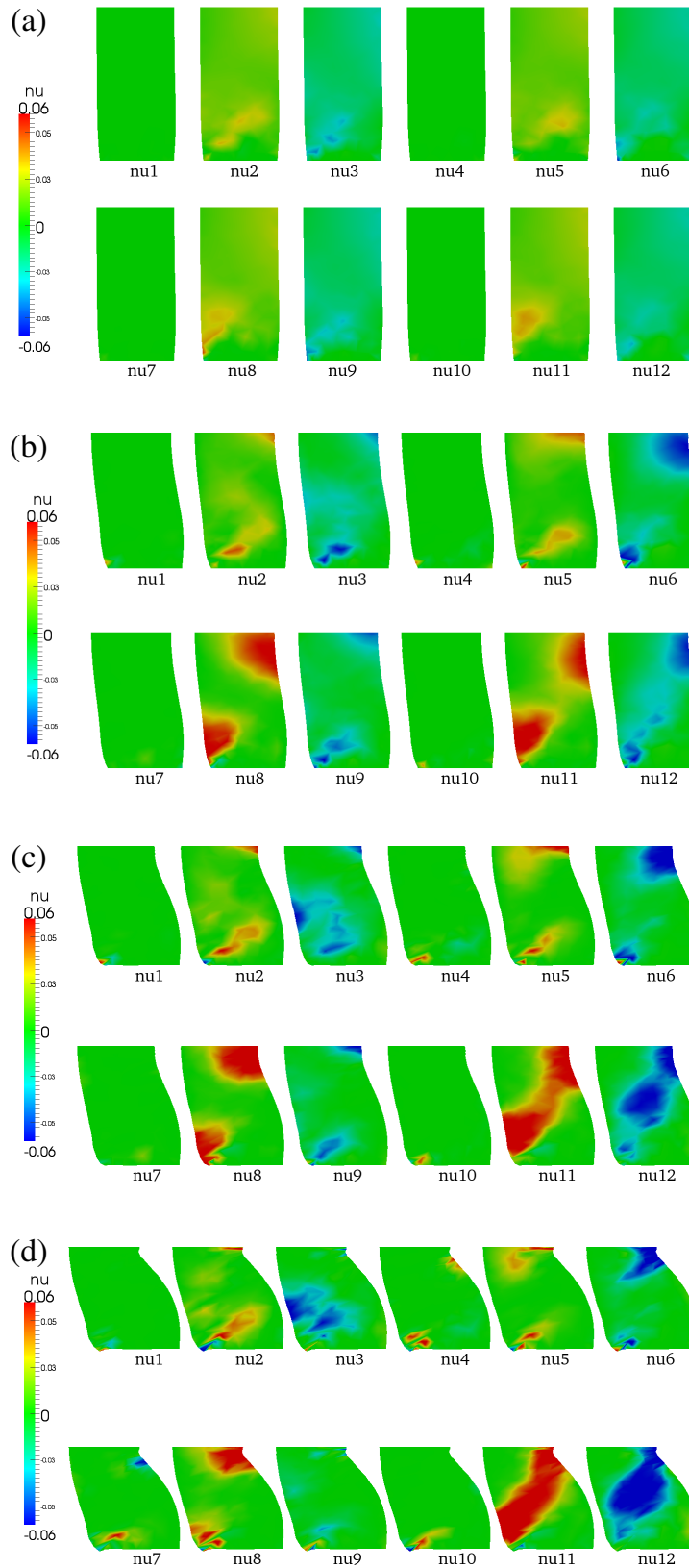


Figure 4.13: The evolution of the accumulated slip for two cross-sections A and B, for nominal strains 0.1 (a), 0.2 (b), 0.3 (c), and 0.4 (d), constrained domain (left), unconstrained (right).

4.3 2-turn Equal Channel Angular Extrusion

ECAE is based on forcing a specimen through an L-shape channel of a constant cross-section. Simple shear takes place in the thin layer at the channel turn. The process is repeated a couple of times (typically up to 10) in order to obtain a very large (severe) plastic deformation and a fine grain structure. The description of the ECAE facility is given in Section 0.2.1. The first report on the use of a 2-turn channel is due to [105]. Later the idea was extended to multi-pass ECAE by [106].

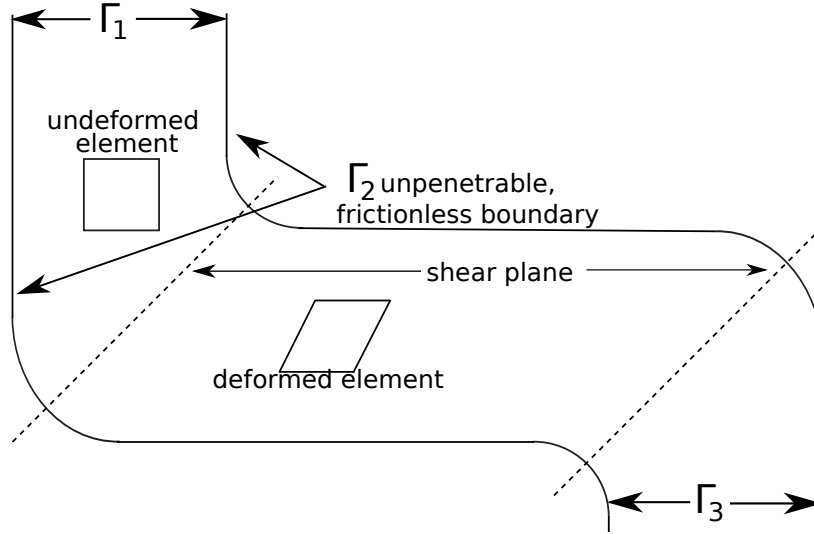


Figure 4.14: Scheme of 2-turn ECAE experiment

The Eulerian system of equations that consists of (1.53a), (1.53b), (1.95) and the evolution of slip systems, allows us to consider more than one turn in a single domain. We chose a 2-turn channel to show the main features of the presented approach. For experimental and numerical studies of a 2-turn ECAE we refer to [28, 29].

4.3.1 Evolution of slip systems

By taking the time derivative of the relation $\mathbf{s}^{(\alpha)} = \mathbf{F}_e \mathbf{s}_0^{(\alpha)}$ and substituting $\dot{\mathbf{F}}_e$ from (1.75), we obtain the equation that describes the evolution of the slip directions

$$\dot{\mathbf{s}}^{(\alpha)} = \left(\nabla \mathbf{v} - \sum_{\alpha} \nu^{(\alpha)} \mathbf{s}^{(\alpha)} \otimes \mathbf{m}^{(\alpha)} \right) \mathbf{s}^{(\alpha)}. \quad (4.9)$$

In Section 4.3 we will restrict ourselves to the plane strain case. We consider projections of three dimensional slip systems onto the plane. Due to the geometrical restrictions of the in-plane model of FCC crystal, we will consider only three slip systems (for detailed discussion see [74]). Two dimensional vectors corresponding to the α -th slip system can be described by their angle of lattice rotation φ_{α} and the scalars s_{α} , m_{α} responsible for elastic stretching. Since all three slip systems are rotating together, we can characterise the rotation by specifying the angles φ_{α} for $\alpha \in \{1, 2, 3\}$ as $\varphi_1 = \varphi + \phi$, $\varphi_2 = \varphi$, and $\varphi_3 = \varphi - \phi$, where $\phi = 54.7^{\circ}$,

$$\mathbf{s}^{(\alpha)} = s_{\alpha} (\cos \varphi_{\alpha}, \sin \varphi_{\alpha}), \quad \mathbf{m}^{(\alpha)} = m_{\alpha} (-\sin \varphi_{\alpha}, \cos \varphi_{\alpha}). \quad (4.10)$$

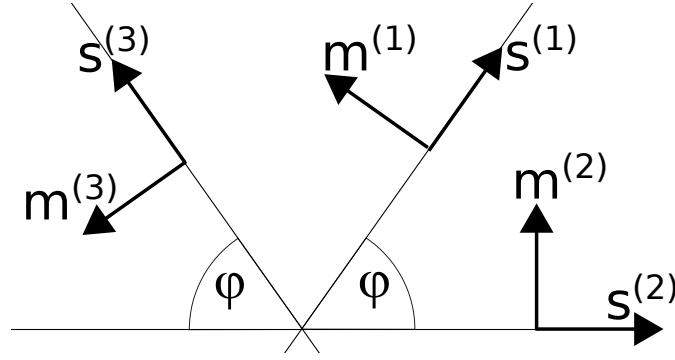


Figure 4.15: Scheme of slip systems

We reformulate the vectorial equations (4.9) in terms of the scalar unknowns $(\varphi, s_1, m_1, s_2, m_2, s_3, m_3)$, for $\alpha \in \{1, 2, 3\}$ we have

$$\dot{\varphi} = (-\sin \varphi, \cos \varphi) \cdot \left(\nabla \mathbf{v} - \sum_{\alpha=1}^3 \nu^{(i)} \mathbf{s}^{(\alpha)} \otimes \mathbf{m}^{(\alpha)} \right) s_2(\cos \varphi, \sin \varphi), \quad (4.11)$$

$$\dot{s}_\alpha = (\cos \varphi_\alpha, \sin \varphi_\alpha) \cdot \left(\nabla \mathbf{v} - \sum_{\alpha=1}^3 \nu^{(\alpha)} \mathbf{s}^{(\alpha)} \otimes \mathbf{m}^{(\alpha)} \right) s_\alpha(\cos \varphi_\alpha, \sin \varphi_\alpha), \quad (4.12)$$

$$\dot{m}_\alpha = (-\sin \varphi_\alpha, \cos \varphi_\alpha) \cdot \left(\nabla \mathbf{v} - \sum_{\alpha=1}^3 \nu^{(\alpha)} \mathbf{s}^{(\alpha)} \otimes \mathbf{m}^{(\alpha)} \right) m_\alpha(-\sin \varphi_\alpha, \cos \varphi_\alpha). \quad (4.13)$$

4.3.2 Initial-boundary Value Problem

Our domain Ω is the 2-turn channel (see Figure 4.14). In the Eulerian description of plane-strain crystal plasticity the unknowns are: the velocity $\mathbf{v}(x, t)$, the Cauchy stress $\mathbf{T}(x, t)$, the density $\varrho(x, t)$, and the orientation of the lattice $\varphi(x, t)$. The boundary of the domain is divided into three parts: the inflow boundary Γ_1 , the impenetrable boundary Γ_2 and the outflow boundary Γ_3 . The boundary conditions are set to be: the Dirichlet inflow condition on the velocity and the lattice orientation, $\mathbf{v}|_{\Gamma_1} = \mathbf{v}_{in} = (0, -1)$, $\varphi|_{\Gamma_1} = \varphi_{in} = 0$, the perfect-slip on Γ_2 , and the stress free condition on Γ_3 . The material parameters and characteristic values are taken to be: the density $\varrho_0 = 3000 \frac{\text{kg}}{\text{m}^3}$, the velocity $V = 10^{-5} \frac{\text{m}}{\text{s}} = 10 \frac{\mu\text{m}}{\text{s}}$, the length $L = 10^{-2} \text{m}$, the reference slip rate $\nu_0 = 10^{-3} \frac{1}{\text{s}}$, the reference stress $\tau_0 = 70 \text{MPa}$, the Young's modulus $E = 1000\tau_0$, the Poisson's ratio $\nu_{pois} = 0.35$, and the rate sensitivity parameter $m = 0.05$ ($1/m = 20$). The material parameters correspond to aluminium and the characteristic values reflect ECAE experiments. As initial values we put $\mathbf{v}(x, 0) = 0$, $\mathbf{T}(x, 0) = 0$, $\tau_c(x, 0) = \tau_0$, $\varrho(x, 0) = 1$, $\varphi(x, 0) = 0$ and $m_\alpha(x, 0) = s_\alpha(x, 0) = 1$, $\forall \alpha \in \{1, 2, 3\}$.

After rescaling of the system we get the following set of equations

$$\begin{aligned} \varrho_{,t} + \text{div}(\varrho \mathbf{v}) &= 0, \\ R_1 \varrho \dot{\mathbf{v}} - \text{div} \mathbf{T} &= 0, \\ \dot{\mathbf{T}} + \mathbf{T} \text{div} \mathbf{v} + \mathbf{W} \mathbf{T} - \mathbf{T} \mathbf{W} &= \varrho \mathcal{C}(\mathbf{D} - \mathbf{D}_p), \\ \dot{\varphi} &= (-\sin \varphi, \cos \varphi) \cdot \left(\nabla \mathbf{v} - R_2 \sum_{\alpha=1}^3 \nu^{(\alpha)} \mathbf{s}^{(\alpha)} \otimes \mathbf{m}^{(\alpha)} \right) s_2(\cos \varphi, \sin \varphi), \end{aligned} \quad (4.14)$$

where \mathbf{D}_* , $\nu^{(\alpha)}$, m_α , s_α and $\dot{\tau}_c^{(\alpha)}$ are given by (1.114), (1.120), (4.12), (4.13) and (1.121), respectively.

Two characteristic numbers appear in the system, $R_1 = \frac{\rho_0 V^2}{L\tau_0} \approx 10^{-12}$ and $R_2 = \frac{L\nu_0}{V} = 1$. The very small value of R_1 justifies the restriction to the quasi-static case, which is common in plasticity. However we keep the time derivative in the balance equation (1.53).

Moreover, we specify the hardening matrix $H_{ij} = H = H_0 \text{sech}^2\left(\frac{H_0 \nu_{acc}}{\tau_s - \tau_0}\right)$, where the initial hardening rate $H_0 = 8.9\tau_0$, the saturation strength $\tau_s = 1.8\tau_0$ and the accumulated slip $\nu_{acc}(t) = \sum_{\alpha} \int_0^t |\nu^{(\alpha)}| dt$, see [21].

4.3.3 Finite Element Formulation

Inspired by the numerical methods of fluid dynamics, a finite element Eulerian representation is formulated and applied to a solution of the flow adjustment initial-boundary value problem for the 2-turn equal channel angular extrusion, see Section 4.3.2.

The domain Ω is approximated by a simplicial triangulation \mathcal{T}_h . Time is discretized by a one step finite difference. The discretization in space consists of P2 elements for the velocity, P1 for the density and the lattice rotations (all continuous) and P1-discontinuous for the Cauchy stress and the slip rates. We define the finite-dimensional spaces

$$\begin{aligned} \mathbb{V}_h &= \{v_h \in W^{1,2}(\Omega; \mathbf{R}^2); \mathbf{v}|_{\Gamma_1} = (0, -1), \mathbf{v}|_K \in \mathcal{P}_2(K)^2 \forall K \in \mathcal{T}_h\}, \\ \mathbb{R}_h &= \{\varrho_h \in W^{1,2}(\Omega; \mathbf{R}); \varrho_h|_{\Gamma_1} = 1, \varrho_h|_K \in \mathcal{P}_1(K) \forall K \in \mathcal{T}_h\}, \\ \mathbb{T}_h &= \{\mathbf{T}_h \in W^{1,2}(\Omega; \mathbf{R}_{sym}^{2 \times 2}); \mathbf{T}_h|_K \in \mathcal{P}_1(K)^{2 \times 2} \forall K \in \mathcal{T}_h\}, \\ \mathbb{N}_h &= \{\nu_h \in L^2(\mathbf{R}); \nu_h|_1 \in \mathcal{P}_1(K) \forall K \in \mathcal{T}_h\}, \\ \mathbb{A}_h &= \{\varphi_h \in W^{1,2}(\Omega; \mathbf{R}); \varphi_h|_{\Gamma_1} = 0, \varphi_h|_K \in \mathcal{P}_1(K) \forall K \in \mathcal{T}_h\}. \end{aligned}$$

The slip rates are added to the system (4.14) as variables. We discretize the system (4.14) in a mixed finite element space and solve the following problem. Find

$$(\mathbf{v}_h, \varrho_h, \mathbf{T}_h, \nu_{1h}, \nu_{2h}, \nu_{3h}, \varphi_h) \in \mathbb{V}_h \times \mathbb{R}_h \times \mathbb{T}_h \times \mathbb{N}_h \times \mathbb{N}_h \times \mathbb{N}_h \times \mathbb{A}_h,$$

such that

$$\begin{aligned} (\varrho_{h,t}, z_\varrho) + (\mathbf{v}_h \nabla \varrho_h, z_\varrho) + (\varrho_h \text{div}(\mathbf{v}_h), z_\varrho) &= 0 \quad \forall z_\varrho \in \mathbb{R}_{h0}, \\ R_1 (\varrho_h \dot{\mathbf{v}}_h, \mathbf{z}_v) + (\mathbf{T}_h, \nabla(\mathbf{z}_v)) + (\mathbf{T}_h \mathbf{n} \cdot \mathbf{n}, \mathbf{z}_v \cdot \mathbf{n})_{\Gamma_2} + \frac{\beta}{h} (\mathbf{v}_h \cdot \mathbf{n}, \mathbf{z}_v \cdot \mathbf{n})_{\Gamma_2} &= 0 \quad \forall \mathbf{z}_v \in \mathbb{V}_{h0}, \\ \left(\dot{\mathbf{T}}_h + \mathbf{T}_h \text{div} \mathbf{v}_h + \mathbf{W}_h \mathbf{T}_h - \mathbf{T}_h \mathbf{W}_h, \mathbf{Z}_T \right) - (\varrho \mathcal{C}(\mathbf{D}_h - \mathbf{D}_{*h}), \mathbf{Z}_T) + (\mathbf{Z}_T \mathbf{n} \cdot \mathbf{n}, \mathbf{v}_h \cdot \mathbf{n})_{\Gamma_2} &= 0 \quad \forall \mathbf{Z}_T \in \mathbb{T}_h, \\ \left(\nu_h^{(\alpha)} - \text{sgn}(\mathbf{T}_h : \mathbf{s}_h^{(\alpha)} \otimes \mathbf{m}_h^{(\alpha)}) \left(\frac{|\mathbf{T}_h : \mathbf{s}_h^{(\alpha)} \otimes \mathbf{m}_h^{(\alpha)}|}{\tau_c^{(\alpha)}} \right)^{20}, z_{\nu\alpha} \right) &= 0 \quad \forall z_{\nu\alpha} \in \mathbb{N}_h \text{ and } \alpha \in \{1, 2, 3\}, \\ \left(\dot{\varphi}_h - (-\sin \varphi_h, \cos \varphi_h)^T \left(\nabla \mathbf{v}_h - R_2 \sum_{i=1}^3 \nu_h^{(\alpha)} \mathbf{s}_h^{(\alpha)} \otimes \mathbf{m}_h^{(\alpha)} \right) s_{2h}(\cos \varphi_h, \sin \varphi_h), z_\varphi \right) &= 0 \quad z_\varphi \in \mathbb{A}_h, \end{aligned} \tag{4.15}$$

where (\cdot, \cdot) is the standard L_2 inner product. The boundary conditions on the impenetrable, frictionless boundary Γ_2 are imposed by the Nitsche's method:

$$(\mathbf{Z}_T \mathbf{n} \cdot \mathbf{n}, \mathbf{v} \cdot \mathbf{n})_{\Gamma_2} + (\mathbf{T} \mathbf{n} \cdot \mathbf{n}, \mathbf{z}_v \cdot \mathbf{n})_{\Gamma_2} + \frac{\beta}{h} (\mathbf{v} \cdot \mathbf{n}, \mathbf{z}_v \cdot \mathbf{n})_{\Gamma_2} \text{ with } \beta = 10, \text{ see [107].}$$

To solve the system (4.15) we employ a non-linear Newton-Ralphson solver with an analytic Jacobian. Implementation is done in the software package FEniCS [84]. A linear system is solved by a direct solver.

Moreover, the critical resolved shear stresses and the stretch of slip directions are updated after each time step according to (1.121), (4.12), and (4.13).

4.3.4 Results

We present the results of computations at the moment when a steady state is reached (see Figure 4.16). We treat the plastic material as a fluid so it fills the entire domain, as opposed to models where empty zones (close to outer turn) are reported [29]. The velocity profile is typical of flow problems.

We can observe that plastic slip occurs only in the vicinity of shear planes where the channel turns. The accumulated slip has its highest values close to the inner turns. Its density is almost constant, although it changes in the neighbourhood of the curved part of the boundary and it is higher before the first turn than in the rest of the domain. The lattice rotation also changes nearby the shear planes in the direction of turn.

In Figure 4.17 we observe the behaviour of individual slip systems. The arrangement of slip directions is presented in Figure 4.15. We notice that the activation of a particular slip system depends on its position relative to the shear plane. The second slip system is almost inactive but we need to take it into account due to compressibility.

Simulations were conducted for two different meshes: 5278 vertices (10252 cells) and 21289 vertices (41974 cells). We conclude that the problem is mesh independent. The presented results were computed with the finer mesh.

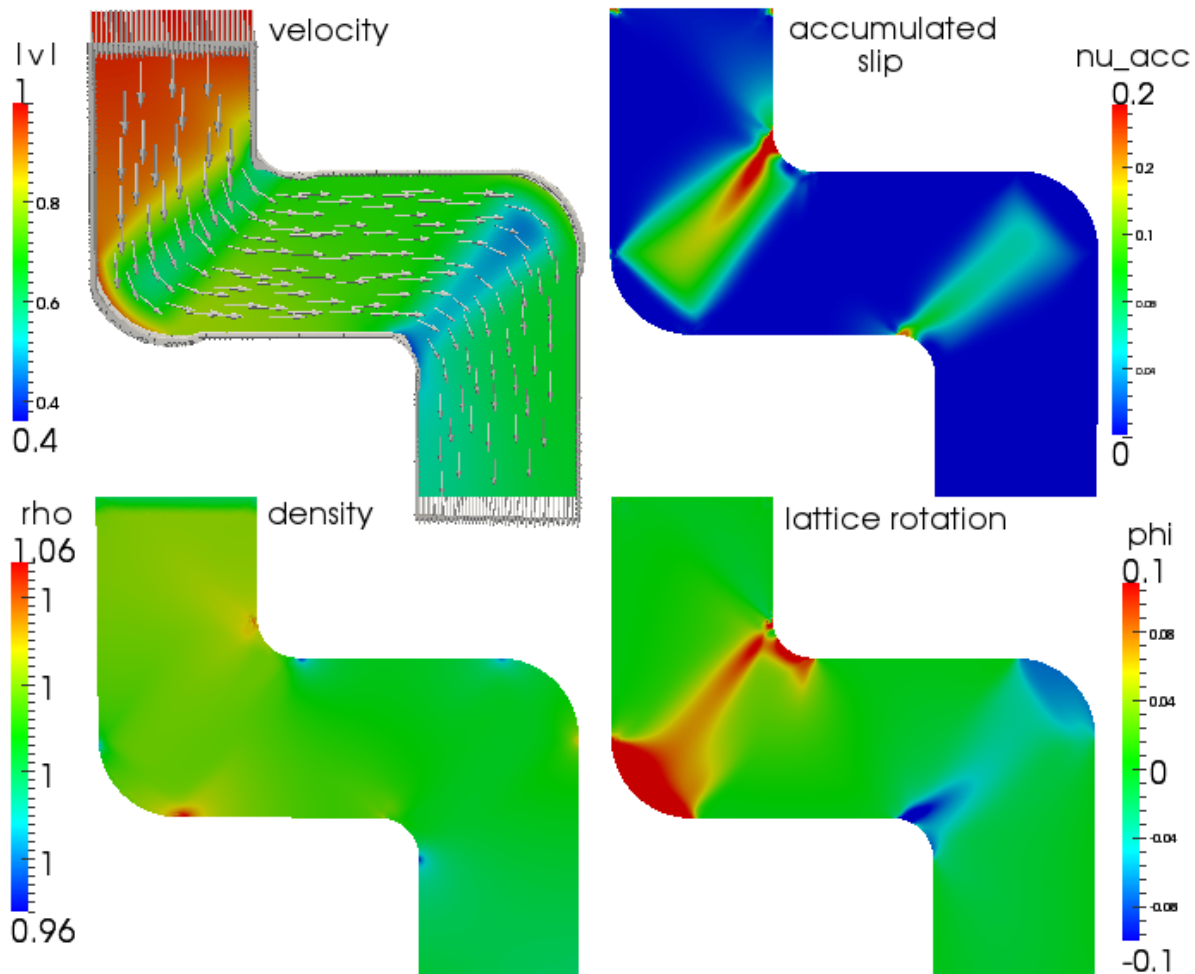


Figure 4.16: Computed variables: velocity magnitude (top-left), accumulated slip (top-right), density (bottom-left), lattice rotation (bottom-right).

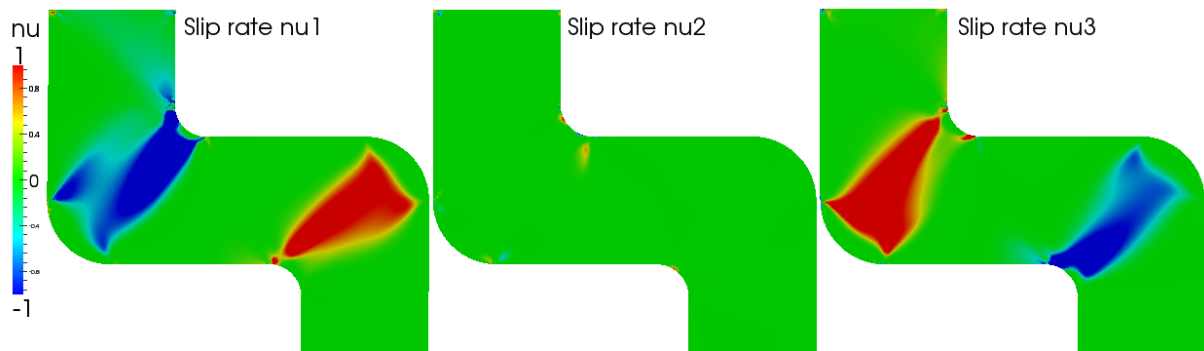


Figure 4.17: Behaviour of slip rates on individual slip systems in the 2-turn channel.

Chapter 5

Conclusions

In this chapter we discuss results obtained in the whole dissertation. We have concentrated in this study on derivation, analysis and simulations of plastic material treated as highly viscous fluid. The aim of this work was to provide an Eulerian description of crystal plasticity and prove that the proposed approach is suitable for describing large deformations in typical severe plastic deformations settings.

Modelling

In Chapter 1 we showed a new way of deriving thermodynamically compatible rate-type fluid model for crystal plastic material. The derivation is based on the multiplicative decomposition of the deformation gradient, the Gibbs potential, and the principle of maximum rate of entropy production. Main contributions read as follows:

- Two approaches to modelling large deformations plasticity has been compared. Multiplicative decomposition by Kröner and natural configuration by Rajagopal, we showed that both lead to the additive decomposition of the deformation gradient.
- We employed the Gibbs potential to derive rate-type stress-strain constitutive law. It is worth to emphasise that for an anisotropic material presented procedure gives the objective rate of stress. On the other hand, for isotropic material we can apply so called objectivity trick, see Section 1.3.4. In addition in Appendix D we discussed derivation based on the Helmholtz potential.
- The description of the evolution of crystal structure in Eulerian system of coordinates is covered. We introduced the lattice basis and provide the equation (1.113) that describes the evolution of basis vectors, see also [36]. It is important, because in crystal plasticity literature the evolution of the crystal lattice is mostly described in Lagrangian frame. To the best of our knowledge, the only Eulerian based description of crystal plasticity, by Cazacu and Ionescu [74, 75], considers evolutions of slip directions in two dimensions. This approach is equivalent but computationally inefficient in three dimensions.
- Furthermore, we propose possible extensions of the flow rule by a rate independent implicit constitutive relation, namely rewrite perfect plastic flow rule as an implicit scalar equation. Several variants of an implicit formulae and description of preliminary numerical studies are given.

- We apply the maximum rate of the dissipation principle to crystal plasticity. The method allows us to avoid single crystal hypothesis by postulating proper rate of dissipation - one scalar function. Moreover, some other entropy production functions and corresponding constitutive relation are presented in Appendix F.

Analysis

Chapter 2 addresses mathematical properties of the incompressible version of a reduced (simplified) model. We proposed regularizations to the rate type equation that enables us to prove following results:

- Global-in-time existence of a weak solution to the $\Delta \frac{\partial}{\partial t} \mathbf{S}$ -regularised system.
- Local-in-time existence and global existence for small initial data of a weak solution to the $\Delta \mathbf{S}$ -regularised system.

The proofs rely on the logarithmic Sobolev inequality and second order a priori estimates. The regularization can be arbitrary small. We were unable to prove local in time existence to the system without regularization. The reasons are explained in Appendix B.

Simulations

Chapters 3 and 4 cover numerical tools used (finite element method) and the results of numerical simulations, respectively. Three numerical examples have been considered: channel-die compression, micropillar compression, and 2-turn equal channel angular extrusion.

- We formulated a finite element discretization schemes, which has been used to solve the fully coupled problem. Our solver is monolithic.
- In the case of compression the Arbitrary Lagrangian Eulerian (ALE) approach has been used in the sense that we use the Eulerian formulation on a moving mesh which captures the free boundary. We developed new algorithms for two and three dimensional compression.
- Among the novel ingredients of the model and in consequence a numerical method is the use of an Eulerian form of the evolution of the lattice basis. This allows for efficient three dimensional computations of the material with full set of slip systems, e.g. 12 slip system in the case of FCC structure.
- To test the proposed approach based on ALE method we considered the two-dimensional single crystal plane strain compression and three-dimensional micropillar compression. Chosen settings refer to the literature, see Harren et al. [27] and Shade et al. [26] respectively.
- The results of channel-die compression simulations are in agreement with experimental observations. Our model predicts that the lattice reorientation of the single crystals of various initial crystallographic orientations tends to bring the crystals toward the geometry coincided with a stable state of symmetric slip. The simulations in the case of symmetric double slip lead to the formation of the shear bands, which corresponds to Harren's et al. results [27].
- The method is able to reproduce a solutions obtained by Lagrangian based methods, and exceed them to higher strains. In the case of compression strains up to 0.2 are reported [27, 26], however our method is able proceed up to 0.4.

- 2-turn channel enables us to introduce high strains within one ECAP pass. For this setting the introduction of the elastic stretches was important. They allow us to reduce high values of stress in the vicinity of inner turns. This result extends [29, 74], where rigid plastic material was considered.
- Since our method is based on Eulerian formulation we proved that it is capable of solving deformations with very large strains for suitably defined problems. The reason is that the priority is not the displacement and the strain but the velocity of the material flow and the distortion of the crystal lattice space.

Further work

As the direction for the future work we plan focus our efforts on the following tasks.

First is to extend the modelling part and consider higher-order gradient crystal plasticity theory, i.e. add the gradients of the geometrically necessary dislocation densities, see [108, 109, 110]. This direction seems promising to capture formation of special kinds of deformation, in particular controlling the thickness of shear bands. The modelling goal, that was not reached, is to observe grain refinement and structure formation. The applied method is macroscopic and thus unable to capture such effects. Therefore, for this purpose one need to combine a microscopic model. Interesting approach has been proposed in Kowalczyk et al. [111], where authors combine deformation paths for different initial locations of a material element that are computed for a non-hardening material by means of the Eulerian based finite element method with the self-consistent viscoplastic method of grain-to-polycrystal scale transition.

Moreover, the plastic behaviour is commonly described by a rate-dependent constitutive equation. We plan to extend Section 1.4.5 and develop numerical schemes able to capture a yield condition in perfect plastic material. In [24, 44, 45] authors developed a mathematical theory for models involving implicit constitutive relations. In the paper [46] finite element approximations of implicit power-law-like models for viscous incompressible fluids have been shown. We aim to provide rigorous numerical analysis of rate-independent crystal plasticity model.

The main perspective for the mathematical analysis is to release the regularization assumption and establish the local-in-time existence of a weak solution to the system (2.1).

Modelling of crystalline solids is challenging for numerical methods. We met this challenge by performing numerical simulations i.e. three dimensional compression of FCC crystal. To extend simulations we plan to investigate shear band localization under simple shear conditions. We aim to incorporate a discontinuous Galerkin approach. It seems that this extension would be a key factor in dealing with a yield condition. Continuous finite elements are unable to capture jumps in the velocity field.

List of Figures

1	Schematic illustration of a typical ECAP facility, showing the shearing plane within the die.	15
2	Schematic illustration of a typical HPT facility.	16
1.1	Reference and current configuration	21
1.2	Elementary rheological models	28
1.3	Visco-elastic models	29
1.4	One-dimensional frictional element	30
1.5	One-dimensional mechanical analogue of the Bingham model	30
1.6	One-dimensional mechanical analogue	30
1.7	Schematic of the Kröner decomposition	33
1.8	Schematic of the current natural configuration of the body	33
1.9	Rearrangement of atoms in elastic and plastic (slip) deformations	39
1.10	Face center cubic FCC crystal structure (a) and some example slip system, the plane along which the crystal will slide is shown in grey (b).	40
1.11	Unit cell of FCC crystal (a); unit cell of BCC crystal (b); a triangular portion of the slip plane (corresponding slip directions are parallel to the sides of the triangle).	41
1.12	Plot of three approximations of the rate independent case.	44
3.1	Discretization schemes	79
3.2	ALE formulation	82
4.1	Channel-die compression scheme	86
4.2	Scheme of slip systems	86
4.3	The evolution of the velocity (top-left), the density (top-right),	90
4.4	The evolution of the angle of the lattice rotation of double-slip single crystal for	91
4.5	Velocity field and slip rates on individual slip systems for single crystal	92
4.6	Nominal stress vs. nominal strain, for numerical simulations	92
4.7	Scheme of micropillar compression, dashed lines represent the shape of compressed sample	94
4.8	Scheme of micropillar compression boundary conditions, constrained (left) and unconstrained (right)	94
4.9	The results of compression experiments on Rene N5 microcrystals [26]. Three SEM images at various strain levels for constrained and unconstrained experiments and corresponding stress–strain curves.	96
4.10	The evolution of the velocity, the whole sample and cross-section for nominal strains 0.1 (a), 0.2 (b), 0.3 (c), and 0.4 (d), constrained domain (left), unconstrained (right).	97

4.11	The evolution of the accumulated slip for two cross-sections A and B, for nominal strains 0.1 (a), 0.2 (b), 0.3 (c), and 0.4 (d), constrained domain (left), unconstrained (right).	98
4.12	The evolution of the accumulated slip for two cross-sections A and B, for nominal strains 0.1 (a), 0.2 (b), 0.3 (c), and 0.4 (d), constrained domain (left), unconstrained (right).	99
4.13	The evolution of the accumulated slip for two cross-sections A and B, for nominal strains 0.1 (a), 0.2 (b), 0.3 (c), and 0.4 (d), constrained domain (left), unconstrained (right).	100
4.14	Scheme of 2-turn ECAE experiment	101
4.15	Scheme of slip systems	102
4.16	Computed variables: velocity magnitude (top-left), accumulated slip (top-right), density (bottom-left), lattice rotation (bottom-right).	104
4.17	Behaviour of slip rates on individual slip systems in the 2-turn channel.	105

Appendix A

Functional spaces and technical lemmas

In this appendix we provide statements of well known lemmas and theorems, which were used in proofs of the previous results.

A.1 Definition of functional spaces

Let $s \geq 0$, $p > 1$ and $\Omega \in \mathbb{R}^d$ be a bounded Lipschitz domain, let us define

$$\mathcal{V} = \{\varphi \in C_{per}^\infty(\Omega)^d, \quad \operatorname{div} \varphi = 0, \quad \int_{\Omega} \varphi \, dx = 0\}, \quad (\text{A.1a})$$

$$\tilde{\mathcal{V}} = \{\Sigma \in C_{per}^\infty(\Omega)^{d \times d}, \quad \Sigma = \Sigma^T, \quad \int_{\Omega} \Sigma \, dx = 0\}, \quad (\text{A.1b})$$

$$H = \text{the closure of } \mathcal{V} \text{ in the } L_2(\Omega)^d \text{-norm}, \quad (\text{A.1c})$$

$$\tilde{H} = \text{the closure of } \tilde{\mathcal{V}} \text{ in the } L_2(\Omega)^{d \times d} \text{-norm}, \quad (\text{A.1d})$$

$$V_p = \text{the closure of } \mathcal{V} \text{ in } W^{1,p}(\Omega)^d \text{ with } \|\nabla(\cdot)\|_p \text{-norm}, \quad (\text{A.1e})$$

$$\tilde{V}_p = \text{the closure of } \tilde{\mathcal{V}} \text{ in } W^{1,p}(\Omega)^{d \times d} \text{ with } \|\nabla(\cdot)\|_p \text{-norm}, \quad (\text{A.1f})$$

$$V^s = \text{the closure of } \mathcal{V} \text{ in } W^{s,2}(\Omega)^d \text{-norm}, \quad (\text{A.1g})$$

$$\tilde{V}^s = \text{the closure of } \tilde{\mathcal{V}} \text{ in } W^{s,2}(\Omega)^{d \times d} \text{-norm}. \quad (\text{A.1h})$$

The scalar product in H is marked by (\cdot, \cdot) while the scalar product in V^s is marked by $\langle \cdot, \cdot \rangle$.

A.2 Bases consisting of eigenfunctions of an elliptic operator

Let us consider the following spectral problem: find $\omega^r \in V^s$ and $\lambda_r \in \mathbb{R}^d$ satisfying

$$\langle \omega^r, \varphi \rangle = \lambda_r \langle \omega^r, \varphi \rangle, \quad \forall \varphi \in V^s. \quad (\text{A.2})$$

Proposition 4. *Existence of a basis. There exists a countable set $\{\lambda_r\}_{r=1}^\infty$ and a corresponding family of eigenvectors $\{\omega_r\}_{r=1}^\infty$ solving the problem (A.2) such that*

- $\langle \omega^r, \omega^s \rangle = \delta_{rs}, \quad \forall r, s \in \mathbb{N}$,
- $1 \leq \lambda_1 \leq \lambda_2 \leq \dots$ and $\lambda_r \rightarrow \infty$ as $r \rightarrow \infty$, $\forall r, s \in \mathbb{N}$,
- $\left\langle \frac{\omega^r}{\sqrt{\lambda_r}}, \frac{\omega^s}{\sqrt{\lambda_s}} \right\rangle = \delta_{rs}$,

- $\{\omega_r\}_{r=1}^\infty$ forms a basis in V^s .

Moreover, defining

$$H^N = \text{span}\{\omega^1, \dots, \omega^N\}$$

and

$$P^N(\mathbf{v}) := \sum_{i=1}^N (v, \omega^i) \omega^i : V^s \rightarrow H^N,$$

we get

$$\begin{aligned} \|P^N\|_{\mathcal{L}(V^s, V^s)} &\leq 1, \\ \|P^N\|_{\mathcal{L}((V^s)^*, (V^s)^*)} &\leq 1, \\ \|P^N\|_{\mathcal{L}(H, H)} &\leq 1. \end{aligned}$$

Proof. See Málek et al. [70] □

The same results hold if we replace V^s by \tilde{V}^s .

A.3 Embedding theorems

Proposition 5. *Sobolev's imbedding theorem.* Let $k > 0$, $1 \leq p \leq \infty$ and Ω be a bounded Lipschitz domain. Then

$$W^{k,p}(\Omega) \hookrightarrow L^q(\Omega), \text{ where } \frac{1}{q} = \frac{1}{p} - \frac{k}{N}, \text{ if } k < \frac{N}{p},$$

$$W^{k,p}(\Omega) \hookrightarrow L^q(\Omega), \text{ for all } q \in [1, \infty), \text{ if } k = \frac{N}{p},$$

$$W^{k,p}(\Omega) \hookrightarrow C^{0, k - \frac{N}{p}}(\Omega), \text{ if } \frac{N}{p} < k < \frac{N}{p} + 1,$$

$$W^{k,p}(\Omega) \hookrightarrow C^{0, \alpha}(\Omega), \text{ for all } \alpha \in (0, 1) \text{ if } k = \frac{N}{p} + 1,$$

$$W^{k,p}(\Omega) \hookrightarrow C^{0,1}(\Omega), \text{ if } k > \frac{N}{p} + 1.$$

Moreover,

$$W^{k+s,p}(\Omega) \hookrightarrow W^{s,q}(\Omega), \text{ where } \frac{1}{q} = \frac{1}{p} - \frac{k}{N}, \text{ if } k < \frac{N}{p}.$$

In particular

$$W^{\frac{3}{2}, 2}(\Omega) \hookrightarrow W^{1,4}(\Omega).$$

Proof. See Kufner et al. [112]. □

Proposition 6. *Kondrashov's theorem on compact imbedding.* Let $k > 0$, $1 \leq p \leq \infty$. Then

$$W^{k,p}(\Omega) \hookrightarrow L^q(\Omega) \text{ for all } q \in [1, p^*) \text{ with } \frac{1}{p^*} = \frac{1}{p} - \frac{k}{N}, \text{ if } k < \frac{N}{p},$$

$$W^{k,p}(\Omega) \hookrightarrow L^q(\Omega) \text{ for all } q \in [1, \infty), \text{ if } k = \frac{N}{p},$$

$$W^{k,p}(\Omega) \hookrightarrow C(\Omega), \text{ if } k > N.$$

Proof. See Kufner et al. [112]. □

A.4 Inequalities in Sobolev spaces

Proposition 7. *Interpolation inequality.* $\Omega \in \mathbb{R}^d$ be a domain and $0 \leq s_j < \infty$, $1 \leq p_j < \infty$, $j = 0, 1$, $0 \leq \theta \leq 1$, $s = (1 - \theta)s_0 + \theta s_1$, $\frac{1}{p} = \frac{1-\theta}{p_0} + \frac{\theta}{p_1}$. Then there is a constant $C > 0$ such that

$$\|u\|_{W^{s,p}} \leq C \|u\|_{W^{s_0,p_0}}^{1-\theta} \|u\|_{W^{s_1,p_1}}^{\theta}, \text{ for } u \in W^{s_0,p_0} \cap W^{s_1,p_1}.$$

In particular

$$\|u\|_{W^{\frac{3}{2},2}} \leq C \|u\|_{W^{1,2}}^{\frac{1}{2}} \|u\|_{W^{2,2}}^{\frac{1}{2}}.$$

Proof. See Triebel [113]. □

Proposition 8. *Agmon's inequality.* Let $u \in H^2(\Omega) \cap H_0^1(\Omega)$, where $\Omega \subset \mathbb{R}^3$, then there exists a constant $C > 0$, such that

$$\|u\|_{L^\infty} \leq C \|u\|_{W^{1,2}}^{\frac{1}{2}} \|u\|_{W^{2,2}}^{\frac{1}{2}}.$$

For $\Omega \subset \mathbb{R}^2$ holds

$$\|u\|_{L^\infty} \leq C \|u\|_{L^2}^{\frac{1}{2}} \|u\|_{W^{2,2}}^{\frac{1}{2}}.$$

Proposition 9. *Young's inequality.* For $a, b \geq 0$ and $p, q > 1$ such that $\frac{1}{p} + \frac{1}{q} = 1$ holds

$$ab \leq \frac{a^p}{p} + \frac{b^q}{q}.$$

A.5 Compactness result

Proposition 10. *Aubin-Lions.* Let $X \hookrightarrow B \hookrightarrow Y$ be Banach spaces and $\{f_n\}$ a sequence bounded in $L^q(I, B) \cap L^1(I, X)$, ($1 < q \leq \infty$) and $\{\frac{d}{dt} f_n\}$ bounded in $L^1(I, Y)$. Then $\{f_n\}$ is relatively compact in $L^p(I, B)$ for any $1 \leq p < q$.

Proof. See Simon [114]. □

A.6 Ordinary Differential equations

Proposition 11. *Caratheodory Theorem.* Let $c : [t_0 - \delta, t_0 + \delta] \rightarrow \mathbb{R}^d$ the system of ordinary differential equations

$$\begin{cases} \frac{d}{dt}c(t) = F(t, c(t)), t \in [t_0 - \delta, t_0 + \delta], \\ c(t_0) = c_0 \in \mathbb{R}^d. \end{cases} \quad (\text{A.3})$$

We assume that $F : [t_0 - \delta, t_0 + \delta] \times K$, where $K = \{c \in \mathbb{R}^d, |c - c_0| < \beta\}$, for some $\beta > 0$. If F satisfies the Caratheodory conditions:

1. $t \mapsto F_i(t, c)$ is measurable for all $i = 1, \dots, d$ and for all $c \in K$,
2. $c \mapsto F_i(t, c)$ is continuous for almost all $t \in [t_0 - \delta, t_0 + \delta]$,
3. there exists an integrable function $G : [t_0 - \delta, t_0 + \delta] \rightarrow \mathbb{R}$ such that

$$|F_i(t, c)| \leq G(t), \quad \forall (t, c) \in [t_0 - \delta, t_0 + \delta] \times K, \forall i = 1, \dots, d,$$

then there exists $\delta' \in (0, \delta)$ and a continuous function $c : [t_0 - \delta', t_0 + \delta'] \rightarrow \mathbb{R}^d$ such that

1. $\frac{d}{dt}c$ exists for almost all $t \in [t_0 - \delta', t_0 + \delta']$,
2. c solves (A.3).

Proof. See Walter [115]. □

Definition 5. *Osgood condition.* We say that a continuous nondecreasing function $\omega : [0, \infty) \rightarrow [0, \infty)$ with $\omega(0) = 0$ and $\omega(\xi) > 0$ for $\xi > 0$ satisfies Osgood's condition if

$$\int_0^1 \frac{1}{\omega(\xi)} d\xi = \infty.$$

Proposition 12. *Osgood criterion.* Let $U \subset \mathbf{R}$ be open. Let $f : U \times [0, T] \rightarrow \mathbf{R}$ be a continuous function and $\omega : [0, \infty) \rightarrow [0, \infty)$ be a function satisfying the Osgood condition. Assume

$$|f(x_1, t) - f(x_2, t)| \leq \omega(|x_1 - x_2|) \text{ for all } (x_1, t), (x_2, t) \in U.$$

Then, for any $x_0 \in U$ there is a $\delta > 0$ and $x : [0, \delta] \rightarrow U$ that is a unique solution to the ordinary differential equation $\dot{x}(t) = f(x(t), t)$ with $x(0) = x_0$.

Proof. See Osgood [116]. □

Note that the classical Cauchy-Lipschitz theorem gives the same conclusion under the stronger assumption that there is a constant M such that $|f(x_1, t) - f(x_2, t)| \leq M|x_1 - x_2|$. The function $f = x \ln x$ satisfies Osgood's criterion, but do not satisfy the assumptions of the Cauchy-Lipschitz theorem, and the bound

$$|f(x_1, t) - f(x_2, t)| \leq |x_1 - x_2| |\ln |x_1 - x_2||$$

holds.

Proposition 13. *Divergence theorem.* Let Ω be a closed region with smooth boundary $\partial\Omega$ and let φ , $\boldsymbol{\varphi}$, and \mathbf{A} be smooth scalar, vector, and tensor-valued fields on Ω , respectively. Then

$$\begin{aligned}\int_{\Omega} \nabla \varphi \, dx &= \int_{\partial\Omega} \varphi \mathbf{n} \, dS, \\ \int_{\Omega} \operatorname{div} \boldsymbol{\varphi} \, dx &= \int_{\partial\Omega} \boldsymbol{\varphi} \cdot \mathbf{n} \, dS, \\ \int_{\Omega} \operatorname{div} \mathbf{A} \, dx &= \int_{\partial\Omega} \mathbf{A} \mathbf{n} \, dS,\end{aligned}\tag{A.4}$$

where \mathbf{n} is the unit outward normal vector on $\partial\Omega$.

Appendix B

Analysis of two dimensional system

The aim of this appendix is to show where are, in our opinion, the fundamental difficulties that do not allow us to establish the local-in-time existence of a weak solution to the system (2.1).

Let us recall the system (2.1) that is in the center of our attention

$$\operatorname{div} \mathbf{v} = 0, \quad (\text{B.1a})$$

$$\frac{\partial \mathbf{v}}{\partial t} + \mathbf{v} \nabla \mathbf{v} + \nabla p = \operatorname{div} \mathbf{S}, \quad (\text{B.1b})$$

$$\frac{\partial \mathbf{S}}{\partial t} + \mathbf{v} \nabla \mathbf{S} + \mathbf{W} \mathbf{S} - \mathbf{S} \mathbf{W} = \mathbf{D}. \quad (\text{B.1c})$$

We are interested to solve the spatially periodic problem. We can treat the equation (B.1b) as an Euler equation with the right hand side $\operatorname{div} \mathbf{S}$. Therefore, we apply the strategy that was used to show the local-in-time existence of a weak solution to the Euler equation, namely perform first a priori estimates and the estimates for the third derivatives. The first a priori estimate is the same as in Section 2.3.1. We multiply (B.1b) by the velocity \mathbf{v} and integrate

$$\int_0^T \int_{\Omega} \frac{\partial \mathbf{v}}{\partial t} \cdot \mathbf{v} \, dx \, dt + \int_0^T \int_{\Omega} \mathbf{v} \nabla \mathbf{v} \cdot \mathbf{v} \, dx \, dt + \int_0^T \int_{\Omega} \nabla p \cdot \mathbf{v} \, dx \, dt = \int_0^T \int_{\Omega} \operatorname{div} \mathbf{S} \cdot \mathbf{v} \, dx \, dt,$$

which leads to

$$\frac{1}{2} \int_0^T \frac{d}{dt} \|\mathbf{v}\|_{L^2}^2 \, dt = - \int_0^T \int_{\Omega} \mathbf{S} : \nabla \mathbf{v} \, dx \, dt = - \int_0^T \int_{\Omega} \mathbf{S} : \mathbf{D} \, dx \, dt. \quad (\text{B.2})$$

Further, we multiply (2.13c) by \mathbf{S} and integrate over $(0, T) \times \Omega$

$$\begin{aligned} \int_0^T \int_{\Omega} \frac{\partial \mathbf{S}}{\partial t} : \mathbf{S} \, dx \, dt + \int_0^T \int_{\Omega} \mathbf{v} \nabla \mathbf{S} : \mathbf{S} \, dx \, dt + \int_0^T \int_{\Omega} (\mathbf{S} \mathbf{W} - \mathbf{W} \mathbf{S}) : \mathbf{S} \, dx \, dt &= \int_0^T \int_{\Omega} \mathbf{D} : \mathbf{S} \, dx \, dt, \\ \frac{1}{2} \int_0^T \frac{d}{dt} \|\mathbf{S}\|_{L^2}^2 \, dt &= \int_0^T \int_{\Omega} \mathbf{D} : \mathbf{S} \, dx \, dt. \end{aligned} \quad (\text{B.3})$$

We sum up (2.15) and (2.17) and obtain

$$\|\mathbf{v}(t)\|_{L^2}^2 + \|\mathbf{S}(t)\|_{L^2}^2 = \|\mathbf{v}(0)\|_{L^2}^2 + \|\mathbf{S}(0)\|_{L^2}^2 \text{ a.e. } t \in (0, T). \quad (\text{B.4})$$

Equation (2.18) gives the uniform a priori estimates on \mathbf{v} and \mathbf{S} in the following function spaces

$$\mathbf{v} \in L^\infty(0, T; L^2(\Omega)), \quad \mathbf{S} \in L^\infty(0, T; L^2(\Omega)).$$

Note that in contrary to the Oldroyd-type models the first a priori estimate did not give us a bound for a gradient of the velocity.

Next, we proceed to the estimates on the third spatial derivatives of both \mathbf{v} and \mathbf{S} . We apply D^3 to (B.1b) and multiply by $D^3\mathbf{v}$:

$$\begin{aligned} \int_0^T \int_{\Omega} D^3 \frac{\partial \mathbf{v}}{\partial t} \cdot D^3 \mathbf{v} \, dx \, dt + \int_0^T \int_{\Omega} D^3 (\mathbf{v} \nabla \mathbf{v}) \cdot D^3 \mathbf{v} \, dx \, dt \\ + \int_0^T \int_{\Omega} D^3 \nabla p \cdot D^3 \mathbf{v} \, dx \, dt = \int_0^T \int_{\Omega} D^3 \operatorname{div} \mathbf{S} \cdot D^3 \mathbf{v} \, dx \, dt, \\ \frac{1}{2} \int_0^T \frac{d}{dt} \|D^3 \mathbf{v}\|_{L^2}^2 \, dt + \int_0^T \int_{\Omega} D^3 (\mathbf{v} \nabla \mathbf{v}) \cdot D^3 \mathbf{v} \, dx \, dt = \int_0^T \int_{\Omega} D^3 \operatorname{div} \mathbf{S} \cdot D^3 \mathbf{v} \, dx \, dt. \end{aligned}$$

Analogously, we apply D^3 to (B.1c) and multiply by $D^3\mathbf{S}$. This leads to

$$\begin{aligned} \int_0^T \int_{\Omega} D^3 \frac{\partial \mathbf{S}}{\partial t} : D^3 \mathbf{S} \, dx \, dt + \int_0^T \int_{\Omega} D^3 (\mathbf{v} \nabla \mathbf{S}) : D^3 \mathbf{S} \, dx \, dt \\ + \int_0^T \int_{\Omega} D^3 (\mathbf{S} \mathbf{W} - \mathbf{W} \mathbf{S}) : D^3 \mathbf{S} \, dx \, dt = \int_0^T \int_{\Omega} D^3 \mathbf{D} : D^3 \mathbf{S} \, dx \, dt, \\ \frac{1}{2} \int_0^T \frac{d}{dt} \|D^3 \mathbf{S}\|_{L^2}^2 \, dt + \int_0^T \int_{\Omega} D^3 (\mathbf{v} \nabla \mathbf{S}) : D^3 \mathbf{S} \, dx \, dt \\ + \int_0^T \int_{\Omega} D^3 (\mathbf{S} \mathbf{W} - \mathbf{W} \mathbf{S}) : D^3 \mathbf{S} \, dx \, dt = \int_0^T \int_{\Omega} D^3 \mathbf{D} : D^3 \mathbf{S} \, dx \, dt. \end{aligned}$$

The convective terms are estimated in the standard way. Important feature is the cancellation of the highest order term, as in (2.20)

$$\begin{aligned} \int_0^T \int_{\Omega} D^3 (\mathbf{v} \nabla \mathbf{v}) \cdot D^3 \mathbf{v} \, dx \, dt \leq \int_0^T \|D^3 \mathbf{v}\|_{L^2}^3 \, dt, \\ \int_0^T \int_{\Omega} D^3 (\mathbf{v} \nabla \mathbf{S}) : D^3 \mathbf{S} \, dx \, dt \leq \int_0^T \|D^3 \mathbf{v}\|_{L^2} \|D^3 \mathbf{S}\|_{L^2}^2 \, dt. \end{aligned}$$

The obstacle is the co-rotational term $\int_0^T \int_{\Omega} D^3 (\mathbf{S} \mathbf{W} - \mathbf{W} \mathbf{S}) : D^3 \mathbf{S} \, dx \, dt$ or more precisely one of its terms $\int_0^T \int_{\Omega} (\mathbf{S} D^3 \mathbf{W} - D^3 \mathbf{W} \mathbf{S}) : D^3 \mathbf{S} \, dx \, dt$ that contains fourth derivatives of the velocity. Even if we restrict ourselves to planar flows, the difficulty sustains. Indeed, in two dimensions we have

$$\mathbf{S} = \begin{pmatrix} S_{11} & S_{12} \\ S_{12} & S_{22} \end{pmatrix}, \quad \mathbf{W} = \frac{1}{2} (\nabla \mathbf{v} - \nabla \mathbf{v}^T) = \frac{1}{2} \begin{pmatrix} 0 & \frac{\partial v_1}{\partial x_2} - \frac{\partial v_2}{\partial x_1} \\ \frac{\partial v_2}{\partial x_1} - \frac{\partial v_1}{\partial x_2} & 0 \end{pmatrix} = \frac{1}{2} \begin{pmatrix} 0 & -\omega \\ \omega & 0 \end{pmatrix},$$

where $\omega = \frac{\partial v_1}{\partial x_2} - \frac{\partial v_2}{\partial x_1}$. Hence, we get

$$\begin{aligned} \mathbf{S} \mathbf{W} &= \frac{1}{2} \omega \begin{pmatrix} S_{12} & -S_{11} \\ S_{22} & -S_{12} \end{pmatrix}, \quad \mathbf{W} \mathbf{S} = \frac{1}{2} \omega \begin{pmatrix} -S_{12} & -S_{22} \\ S_{11} & S_{12} \end{pmatrix}, \\ \mathbf{S} \mathbf{W} - \mathbf{W} \mathbf{S} &= \frac{1}{2} \omega \begin{pmatrix} 2S_{12} & -S_{11} + S_{22} \\ S_{22} - S_{11} & -2S_{12} \end{pmatrix} =: \frac{1}{2} \omega \tilde{\mathbf{S}}. \end{aligned}$$

Consequently, the most difficult term takes the form

$$(\mathbf{S}D^3\mathbf{W} - D^3\mathbf{W}\mathbf{S}) : D^3\mathbf{S} = \frac{1}{2}(D^3\omega)\tilde{\mathbf{S}} : D^3\mathbf{S}.$$

Despite our effort to incorporate the equation for ω and its third derivatives or to use stream function, we have not been able to control the last term by $D^3\mathbf{v}$ and $D^3\mathbf{S}$.

Appendix C

Lagrangian and Eulerian coordinates

We provide derivation of expressions corresponding to Lagrangian-Eulerian transformation.

Formula (1.10) reads

$$\text{Grad}\varphi = \frac{\partial\varphi}{\partial X} = \frac{\partial\varphi}{\partial x} \frac{\partial\chi(X,t)}{\partial X} = \mathbf{F}^T \nabla\varphi, \quad (\text{C.1})$$

$$\text{Grad}\varphi = \frac{\partial\varphi}{\partial X} = \frac{\partial\varphi}{\partial x} \frac{\partial\chi(X,t)}{\partial X} = \nabla\varphi \mathbf{F}. \quad (\text{C.2})$$

In particular applying (C.2) to the velocity field, yields

$$\begin{aligned} \text{Grad}\mathbf{v}(x,t) &= \frac{\partial\mathbf{v}(x,t)}{\partial X} = \frac{\partial\mathbf{v}(x,t)}{\partial x} \frac{\partial\chi(X,t)}{\partial X} = \nabla\mathbf{v}(x,t) \mathbf{F}, \\ \text{Grad}\mathbf{v}(x,t) &= \nabla\mathbf{v}(x,t) \mathbf{F}. \end{aligned}$$

By taking time derivative of (1.2) and by (C.2) we obtain

$$\dot{\mathbf{F}} = \frac{\partial}{\partial t} \text{Grad}\chi = \text{Grad} \frac{\partial}{\partial t} \chi = \nabla\mathbf{v} \mathbf{F}. \quad (\text{C.3})$$

Since \mathbf{F} is invertible, (C.3) is solved for $\nabla\mathbf{v}$, and we get (1.13)

$$\nabla\mathbf{v} = \dot{\mathbf{F}} \mathbf{F}^{-1}.$$

In the proof of the Reynolds transport theorem (1.14) we used identity

$$\frac{d}{dt} J = J \text{div } \mathbf{v}. \quad (\text{C.4})$$

To derive this expression, we apply chain rule together with identity $\frac{\partial \det \mathbf{F}}{\partial \mathbf{F}} = \det \mathbf{F} \mathbf{F}^{-T}$

$$\frac{d}{dt} J = \frac{\partial \det \mathbf{F}}{\partial \mathbf{F}} : \dot{\mathbf{F}} = J \mathbf{F}^{-T} : \nabla\mathbf{v} \mathbf{F} = J \mathbf{F} \mathbf{F}^{-T} : \nabla\mathbf{v} = J \text{div } \mathbf{v}.$$

Piola's identity

$$\text{Div}(J \mathbf{F}^{-T}) = 0. \quad (\text{C.5})$$

Appendix D

Stress–strain dependence, the Helmholtz potential approach

This section is directed to the derivation of the evolutionary equation for the Cauchy stress. Usually a stress is defined as the derivative of a Helmholtz potential with respect to a proper strain measure.

We assume that the Helmholtz potential depends on the elastic Green tensor $\Psi = \Psi(\mathbf{E}_e)$ and that the lattice based second Piola-Kirchhoff stress Σ_e ,

$$\Sigma_e = \mathbf{F}_e^{-1} \mathbf{S} \mathbf{F}_e^{-T} \quad (\text{D.1})$$

is the derivative of Ψ with respect to \mathbf{E}_e

$$\Sigma_e = \frac{\partial \Psi(\mathbf{E}_e)}{\partial \mathbf{E}_e}. \quad (\text{D.2})$$

Differentiation of (D.2) with respect to time yields

$$\dot{\Sigma}_e = \frac{\partial^2 \Psi}{\partial \mathbf{E}_e \partial \mathbf{E}_e} \dot{\mathbf{E}}_e = \mathbb{C} \dot{\mathbf{E}}_e, \text{ where } \mathbb{C} = \frac{\partial^2 \Psi}{\partial \mathbf{E}_e \partial \mathbf{E}_e}. \quad (\text{D.3})$$

Our goal is to express relation (D.3) in terms of the Kirchhoff stress \mathbf{S} and the symmetric part of the velocity gradient \mathbf{D} . Differentiating (D.1) with respect to time we get

$$\dot{\mathbf{S}} = \overline{\dot{\mathbf{F}}_e \Sigma_e \mathbf{F}_e^T} = \dot{\mathbf{F}}_e \Sigma_e \mathbf{F}_e^T + \mathbf{F}_e \dot{\Sigma}_e \mathbf{F}_e^T + \mathbf{F}_e \Sigma_e \dot{\mathbf{F}}_e^T. \quad (\text{D.4})$$

Substituting (1.86), (D.1) and (D.3) into (D.4) gives

$$\dot{\mathbf{S}} - \mathbf{L}_e \mathbf{S} - \mathbf{S} \mathbf{L}_e^T = \mathbf{F}_e (\mathbb{C} \mathbf{F}_e^T (\mathbf{D}_e) \mathbf{F}_e) \mathbf{F}_e^T = \mathbf{C} \mathbf{D}_e = \mathbf{C} (\mathbf{D} - \mathbf{D}_p), \quad (\text{D.5})$$

where \mathbb{C} is a fourth order material elasticity tensor (as a derivative of tensorial function w.r.t. second order tensor) and \mathbf{C} is a fourth order spatial elasticity tensor. They are related by

$$\mathcal{C}_{ijkl} = \mathbf{F}_{e_iK} \mathbf{F}_{e_jL} \mathbf{F}_{e_kM} \mathbf{F}_{e_lN} \mathbb{C}_{KLMN}. \quad (\text{D.6})$$

On the left hand side of the formula (D.5) we obtained Truesdell rate of the Kirchhoff stress. Equation (D.5) is equivalent to the one containing the Jaumann rate of the Kirchhoff stress

$$\dot{\mathbf{S}} - \mathbf{W}_e \mathbf{S} + \mathbf{S} \mathbf{W}_e = \mathbf{C} (\mathbf{D} - \mathbf{D}_p) + \mathbf{D}_e \mathbf{S} + \mathbf{S} \mathbf{D}_e. \quad (\text{D.7})$$

It is common to neglect term $\mathbf{D}_e \mathbf{S} + \mathbf{S} \mathbf{D}_e$ on the right hand side of (D.7), see eg. [22]. To reformulate (D.5) in terms of the Cauchy stress we substitute $\mathbf{S} = \mathbf{T}/\varrho$ and deduce

$$\dot{\mathbf{T}} + \mathbf{T} \operatorname{div} \mathbf{v} - \mathbf{L}_e \mathbf{T} - \mathbf{T} \mathbf{L}_e^T = \varrho \mathcal{C}(\mathbf{D} - \mathbf{D}_p). \quad (\text{D.8})$$

Moreover, we substitute the Helmholtz potential to the dissipation formula (1.52)

$$\begin{aligned} \mathbf{S} : \mathbf{D} - \dot{\Psi} &= \mathbf{S} : \mathbf{D} - \frac{\partial \Psi(\mathbf{E}_e)}{\partial \mathbf{E}_e} : \dot{\mathbf{E}}_e = \mathbf{S} : \mathbf{D} - \boldsymbol{\Sigma}_e : \dot{\mathbf{E}}_e \\ &= \mathbf{S} : \mathbf{D} - \boldsymbol{\Sigma}_e : \mathbf{F}_e^T (\mathbf{D} - \mathbf{D}_p) \mathbf{F}_e = \mathbf{S} : \mathbf{D} - \mathbf{F}_e \boldsymbol{\Sigma}_e \mathbf{F}_e^T : (\mathbf{D} - \mathbf{D}_p) \\ &= \mathbf{S} : \mathbf{D} - \mathbf{S} : (\mathbf{D} - \mathbf{D}_p) = \mathbf{S} : \mathbf{D}_p. \end{aligned}$$

Non-negativity of $\mathbf{S} : \mathbf{D}_p$ is provided by proper assumption on the form of \mathbf{D}_p , see Section 1.4.

This appendix shows that the phenomenological procedure of taking the time derivative of (D.2) lead to the rate type model (D.8). However, without additional assumption the Helmholtz potential approach does not leads to the Jaumann rate of the Kirchhoff stress, see [36].

Appendix E

Frame-indifference principle

The material frame-indifference says that the material response (constitutive relation) is independent of an observer.

Let us define a change of frame (change of observer) at fix time t , by an time dependent orthogonal rotation $\mathbf{Q}(t)$. Spacial points x in the observed space (the current configuration/Eulerian) change according to transformation

$$x^* = y(t) + \mathbf{Q}(t)(x - x_0), \quad (\text{E.1})$$

where $y(t)$ is a point in space and $x - x_0$ is the position vector relative to an arbitrary origin x_0 . Frame-indifference says how certain quantities transforms under the change of observer: for kinematical quantities it can be calculated from (E.1), for other it has to be postulated.

We say that a scalar-, vector- and tensor-valued quantity is objective or frame indifferent if it is invariant under all observer transformation (E.1). Scalars α , vectors \mathbf{g} , and tensors \mathbf{G} satisfying:

$$\alpha^* = \alpha, \quad \mathbf{g}^* = \mathbf{g}, \quad \mathbf{G}^* = \mathbf{Q}\mathbf{G}\mathbf{Q}^T$$

are called objective.

Note that a tensor field is frame-indifferent (objective) if for frame-indifferent vector fields holds

$$\begin{aligned} \mathbf{h} = \mathbf{G}\mathbf{g} &\implies \mathbf{h}^* = \mathbf{G}^*\mathbf{g}^*, \\ \mathbf{G}^*\mathbf{g}^* = \mathbf{h}^* = \mathbf{Q}\mathbf{h} = \mathbf{Q}\mathbf{G}\mathbf{g} = \mathbf{Q}\mathbf{G}\mathbf{Q}^T\mathbf{g}^* &\implies \mathbf{G}^* = \mathbf{Q}\mathbf{G}\mathbf{Q}^T. \end{aligned}$$

For more details concerning the change of observer and the material frame-indifference, see Martinec [117]. Moreover, recently the frame-indifference has been studied by Liu and Sampaio in [118].

Appendix F

Examples of the rate of entropy production

For the sake of completeness we present four examples of the dissipation rates and resulting models after applying the maximization of the rate of entropy production:

- $\hat{\xi} = \frac{1}{2\mu}|\mathbf{S}|^2$

We maximize $\frac{1}{2\mu}|\mathbf{S}|^2$ under the constrain $\xi = \mathbf{S} : (\mathbf{D} - \mathcal{A} \overset{\nabla}{\mathbf{S}})$, where $\overset{\nabla}{\mathbf{S}}$ denote an objective time derivative. The maximization is done using Lagrange multipliers

$$L = \hat{\xi} + \lambda(\hat{\xi} - \mathbf{S} : (\mathbf{D} - \mathcal{A} \overset{\nabla}{\mathbf{S}})), \quad \frac{\partial L}{\partial \mathbf{S}} = 0,$$

$$\frac{1 + \lambda}{\lambda} \frac{\partial \hat{\xi}}{\partial \mathbf{S}} = \frac{\partial}{\partial \mathbf{S}} \left(\mathbf{S} : (\mathbf{D} - \mathcal{A} \overset{\nabla}{\mathbf{S}}) \right),$$

$$\frac{1 + \lambda}{\lambda} \frac{\partial \hat{\xi}}{\partial \mathbf{S}} = \mathbf{D} - \mathcal{A} \overset{\nabla}{\mathbf{S}} \quad | : \mathbf{S},$$

$$\frac{1 + \lambda}{\lambda} = \frac{(\mathbf{D} - \mathcal{A} \overset{\nabla}{\mathbf{S}}) : \mathbf{S}}{\frac{\partial \hat{\xi}}{\partial \mathbf{S}} : \mathbf{S}} = \frac{\hat{\xi}}{\frac{1}{\mu} \mathbf{S} : \mathbf{S}} = \frac{1}{2}.$$

Finally we obtain rate-type stress-strain constitutive relation which is a Maxwell type model

$$\frac{1}{2\mu} \mathbf{S} + \mathcal{A} \overset{\nabla}{\mathbf{S}} = \mathbf{D}. \quad (\text{F.1})$$

- $\hat{\xi} = (1 + |\mathbf{S}|)^{\frac{p'-2}{2}} |\mathbf{S}|^2$

Following the procedure presented in Section 1.5 we obtain

$$\frac{\lambda}{1 + \lambda} = \frac{(1 + |\mathbf{S}|)^{\frac{p'-2}{2}} |\mathbf{S}|^2}{\frac{p'-2}{2} (1 + |\mathbf{S}|)^{\frac{p'-2}{2}-1} 2|\mathbf{S}|^4 + 2(1 + |\mathbf{S}|)^{\frac{p'-2}{2}} |\mathbf{S}|^2}$$

and conclude

$$(1 + |\mathbf{S}|)^{\frac{p'-2}{2}} \mathbf{S} + \mathcal{A} \overset{\nabla}{\mathbf{S}} = \mathbf{D}. \quad (\text{F.2})$$

- $\hat{\xi} = \frac{1}{\mu} |\mathbf{S}|^{p'}$

$$\frac{1}{\mu} |\mathbf{S}|^{p'-2} \mathbf{S} + \mathcal{A} \overset{\nabla}{\mathbf{S}} = \mathbf{D} \quad (\text{F.3})$$

- $\hat{\xi} = \frac{1}{2\mu(|\mathbf{D}|^2)} |\mathbf{S}|^2$

$$\frac{1}{2\mu(|\mathbf{D}|^2)} \mathbf{S} + \mathcal{A} \overset{\nabla}{\mathbf{S}} = \mathbf{D} \quad (\text{F.4})$$

Bibliography

- [1] E.O. Hall. The deformation and ageing of mild steel: III discussion of results. *Proceedings of the Physical Society. Section B*, 64(9):747, 1951.
- [2] N.J. Petch. The cleavage strength of polycrystals. *Journal of the Iron and Steel Institute*, 174:25–28, 1953.
- [3] V.M. Segal, V.I. Reznikov, A.E. Drobysheskii, and V.I. Kopylov. Plastic treatment of metals by simple shear. *Izv. Akad. Nauk SSSR, Ser. Met.*, 1:115–123, 1981.
- [4] V.M. Segal. Materials processing by simple shear. *Materials Science and Engineering: A*, 197(2):157 – 164, 1995.
- [5] V.M. Segal. Equal channel angular extrusion: from macromechanics to structure formation. *Materials Science and Engineering: A*, 271(1–2):322 – 333, 1999.
- [6] P.W. Bridgman. Effects of high shearing stress combined with high hydrostatic pressure. *Phys. Rev.*, 48:825–847, Nov 1935.
- [7] P.W. Bridgman. On torsion combined with compression. *Journal of Applied Physics*, 14:273–283, June 1943.
- [8] Y. Saito, H. Utsunomiya, and H. Suzuki. Proposal of novel continuous high straining process - development of conshearing process. *M. Geiger (Ed.), Advanced Technology of Plasticity*, 2459, 1999.
- [9] J. Richert and M. Richert. A new method for unlimited deformation of metals and alloys. *Aluminum*, 62 (8):604–607, 1986.
- [10] J.Y. Huang, Y.T. Zhu, H. Jiang, and T.C. Lowe. Microstructures and dislocation configurations in nanostructured Cu processed by repetitive corrugation and straightening. *Acta Materialia*, 49(9):1497 – 1505, 2001.
- [11] J. Wadsworth and O.D. Sherby. On the bulat—damascus steels revisited. *Progress in Materials Science*, 25(1):35 – 68, 1980.
- [12] O.D. Sherby and J. Wadsworth. Ancient blacksmiths, the Iron Age, Damascus steels, and modern metallurgy. *Journal of Materials Processing Technology*, 117(3):347 – 353, 2001. Containing keynote papers presented at the proceedings of THERMEC’2000, the International conference on Processing and manufacturing of Advanced Materials.
- [13] R.I. Kuznetsov, V.I. Bykov, V.P. Chernyshev, V.P. Pilyugin, N.A. Yefremov, and A.V. Pasheyev. Plastic deformation of solid bodies under pressure. 1: Equipment and methods. *Preprint 4/85, IFM UNTs AN SSSR, Sverdlovsk, USSR*, 1985.

- [14] E. Kröner. On the plastic deformation of polycrystals [Zur plastischen Verformung des Vielkristalls]. *Acta Metallurgica*, 9(2):155–161, 1961.
- [15] E.H. Lee and D.T. Liu. Finite strain elastic-plastic theory. In H. Parkus and L.I. Sedov, editors, *Irreversible Aspects of Continuum Mechanics and Transfer of Physical Characteristics in Moving Fluids*, IUTAM Symposia, pages 213–222. Springer Vienna, 1968.
- [16] K.R. Rajagopal and A.R. Srinivasa. Mechanics of the inelastic behavior of materials – Part I: Theoretical underpinnings. *International Journal of Plasticity*, 14(10):945–967, 1998.
- [17] K.R. Rajagopal and A.R. Srinivasa. Mechanics of the inelastic behavior of materials – Part II: Inelastic response. *International Journal of Plasticity*, 14(10–11):969–995, 1998.
- [18] K.R. Rajagopal and A.R. Srinivasa. A Gibbs-potential-based formulation for obtaining the response functions for a class of viscoelastic materials. *Proc. R. Soc. A*, 467(2125):39–58, 2011.
- [19] K.R. Rajagopal and A.R. Srinivasa. A thermodynamic frame work for rate type fluid models. *Journal of Non-Newtonian Fluid Mechanics*, 88(3):207 – 227, 2000.
- [20] D. Peirce, R.J. Asaro, and A. Needleman. An analysis of nonuniform and localized deformation in ductile single crystals. *Acta Metallurgica*, 30(6):1087–1119, 1982.
- [21] D. Peirce, R.J. Asaro, and A. Needleman. Material rate dependence and localized deformation in crystalline solids. *Acta Metallurgica*, 31(12):1951–1976, 1983.
- [22] R.J. Asaro and A. Needleman. Overview no. 42 texture development and strain hardening in rate dependent polycrystals. *Acta Metallurgica*, 33(6):923–953, 1985.
- [23] R. Hill and J.R. Rice. Constitutive analysis of elastic-plastic crystals at arbitrary strain. *Journal of the Mechanics and Physics of Solids*, 20(6):401 – 413, 1972.
- [24] K.R. Rajagopal. On implicit constitutive theories. *Applications of Mathematics*, 48(4):279–319, 2003.
- [25] K.R. Rajagopal. On implicit constitutive theories for fluids. *Journal of Fluid Mechanics*, 550:243 – 249, 2006.
- [26] P.A. Shade, R. Wheeler, Y.S. Choi, M.D. Uchic, D.M. Dimiduk, and H.L. Fraser. A combined experimental and simulation study to examine lateral constraint effects on microcompression of single-slip oriented single crystals. *Acta Materialia*, 57(15):4580 – 4587, 2009.
- [27] S.V. Harren, H.E. Dève, and R.J. Asaro. Shear band formation in plane strain compression. *Acta Metallurgica*, 36(9):2435 – 2480, 1988.
- [28] A. Rosochowski and L. Olejnik. Numerical and physical modelling of plastic deformation in 2-turn equal channel angular extrusion. *Journal of Materials Processing Technology*, 125–126(0):309 – 316, 2002.
- [29] A. Rosochowski and L. Olejnik. Finite element analysis of two-turn incremental ECAP. *International Journal of Material Forming*, 1(1):483–486, 2008.
- [30] M.E. Gurtin, E. Fried, and L. Anand. *The Mechanics and Thermodynamics of Continua*. Cambridge University Press, 2010. Cambridge Books Online.

- [31] K.R. Rajagopal. Non-linear elastic bodies exhibiting limiting small strain. *Mathematics and Mechanics of Solids*, 16(1):122–139, 2011.
- [32] A.S. Wineman and K. R. Rajagopal. *Mechanical response of polymers: An introduction*. Cambridge University Press, 2000.
- [33] K.R. Rajagopal and A.R. Srinivasa. On thermomechanical restrictions of continua. *Proceedings of the Royal Society of London. Series A: Mathematical, Physical and Engineering Sciences*, 460(2042):631–651, 2004.
- [34] R. Hill. A variational principle of maximum plastic work in classical plasticity. *Quarterly Journal of Mechanics and Applied Mathematics*, 1:18–28, 1948.
- [35] E.H. Lee. Elastic–plastic deformation at finite strains. *Journal of Applied Mechanics*, 36:1–6, 1969.
- [36] A.R. Srinivasa and S.M. Srinivasan. *Inelasticity of Single Crystals*, chapter 13, pages 455–494. World Scientific, 2009.
- [37] J. Málek, V. Průša, and K.R. Rajagopal. Generalizations of the Navier-Stokes fluid from a new perspective. *International Journal of Engineering Science*, 48(12):1907 – 1924, 2010.
- [38] G.I. Taylor. Plastic deformation of metals. *J. Inst. Metals*, 62:303, 1938.
- [39] R. Hill. Continuum micro-mechanics of elastoplastic polycrystals. *J. Mech. Phys. Solids*, 13:89–101, 1965.
- [40] J.R. Rice. Inelastic constitutive relations for solids: An internal-variable theory and its application to metal plasticity. *J. Mech. Phys. Solids*, 19:433 – 455, 1971.
- [41] R.J. Asaro. Micromechanics of crystals and polycrystals. *Advances in Applied Mechanics*, 23:1–115, 1983.
- [42] J.W. Hutchinson. Bounds and self-consistent estimates for creep of polycrystalline materials. *Proceedings of the Royal Society of London A: Mathematical, Physical and Engineering Sciences*, 348(1652):101–127, 1976.
- [43] K.R. Rajagopal and A.R. Srinivasa. On the thermodynamics of fluids defined by implicit constitutive relations. *Zeitschrift Angewandte Mathematik und Physik*, 59:715–729, July 2008.
- [44] M. Bulíček, P. Gwiazda, J. Málek, and A. Świerczewska-Gwiazda. On steady flows of incompressible fluids with implicit power-law-like rheology. *Advances in Calculus of Variations*, 2009.
- [45] P. Gwiazda, A. Świerczewska-Gwiazda, J. Málek, and M. Bulíček. On unsteady flows of implicitly constituted incompressible fluids. *SIAM J. Math. Anal.*, 44(4):2756–2801, 2012.
- [46] L. Diening, C. Kreuzer, and E. Süli. Finite element approximation of steady flows of incompressible fluids with implicit power-law-like rheology. *SIAM Journal on Numerical Analysis*, 51(2):984–1015, 2013.
- [47] M. Lukáčová-Medvid’ová, H. Mizerová, and Š. Nečasová. Global existence and uniqueness result for the diffusive Peterlin viscoelastic model. *Nonlinear Analysis: Theory, Methods & Applications*, 120(0):154 – 170, 2015.

- [48] J.W. Barrett and S. Boyaval. Existence and approximation of a (regularized) Oldroyd-B model. *Mathematical Models and Methods in Applied Sciences*, 21:1783–1837, 2011.
- [49] J.W. Barrett and E. Süli. Existence and equilibration of global weak solutions to kinetic models for dilute polymers i: Finitely extensible nonlinear bead-spring chains. *Mathematical Models and Methods in Applied Sciences*, 21(06):1211–1289, 2011.
- [50] R. Sureshkumar and A.N. Beris. Effect of artificial stress diffusivity on the stability of numerical calculations and the flow dynamics of time-dependent viscoelastic flows. *Journal of Non-Newtonian Fluid Mechanics*, 60(1):53 – 80, 1995.
- [51] C. Guillopé and J.C. Saut. Existence results for the flow of viscoelastic fluids with a differential constitutive law. *Nonlinear Anal.*, 15(9):849–869, October 1990.
- [52] E. Fernández-Cara, F. Guillén, and R.R. Ortega. Mathematical modeling and analysis of viscoelastic fluids of the Oldroyd kind. In *Handbook of Numerical Analysis*, volume 8 of *Handbook of Numerical Analysis*, pages 543 – 660. Elsevier, 2002.
- [53] P.L. Lions and N. Masmoudi. Global solutions for some Oldroyd models of non-Newtonian flows. *Chinese Annals of Mathematics. Series B*, 21(2):131–146, 2000. cited By (since 1996)99.
- [54] O. Bejaoui and M. Majdoub. Global weak solutions for some Oldroyd models. *Journal of Differential Equations*, 254(2):660 – 685, 2013.
- [55] J. Chemin and N. Masmoudi. About lifespan of regular solutions of equations related to viscoelastic fluids. *SIAM Journal on Mathematical Analysis*, 33(1):84–112, 2001.
- [56] F.-H. Lin, Ch. Liu, and P. Zhang. On hydrodynamics of viscoelastic fluids. *Communications on Pure and Applied Mathematics*, 58(11):1437–1471, 2005.
- [57] Z. Lei, Ch. Liu, and Y. Zhou. Global solutions for incompressible viscoelastic fluids. *Archive for Rational Mechanics and Analysis*, 188(3):371–398, 2008.
- [58] Z. Lei. Global existence of classical solutions for some Oldroyd-B model via the incompressible limit. *Chinese Annals of Mathematics, Series B*, 27(5):565–580, 2006.
- [59] D. Fang and R. Zi. Strong solutions of 3d compressible Oldroyd-B fluids. *Mathematical Methods in the Applied Sciences*, 36(11):1423–1439, 2013.
- [60] L. Lichtenstein. Über einige existenzprobleme der hydrodynamik homogener, unzusammen-drückbarer, reibungsloser flüssigkeiten und die helmholtzschen wirbelsätze. *Mathematische Zeitschrift*, 23(1):89–154, 1925.
- [61] N. Gunther. On the motion of fluid in a moving container. *izvestia akademii nauk ussr. Seriya Fizicheskaya-Mathematica 20*, 1323-1348:1503–1532, 1927.
- [62] W. Wolibner. Un théorème sur l’existence du mouvement plan d’un fluide parfait, homogène, incompressible, pendant un temps infiniment long. *Mathematische Zeitschrift*, 37:698–726, 1933.
- [63] T. Kato. On classical solutions of the two-dimensional non-stationary Euler equation. *Archive for Rational Mechanics and Analysis*, 25(3):188–200, 1967.

- [64] V.I. Yudovich. Non-stationary flows of an ideal incompressible fluid. *Z. Vycisl. Mat. i Mat. Fiz. (Russian)*, 3:1032–1066, 1963.
- [65] V.I. Yudovich. Uniqueness theorem for the basic nonstationary problem in the dynamics of an ideal incompressible fluid. *Math. Res. Letters*, pages 27–38, 1995.
- [66] H. Kozono and Y. Taniuchi. Limiting case of the Sobolev inequality in BMO, with application to the Euler equations. *Communications in Mathematical Physics*, 214(1):191–200, 2000.
- [67] H. Kozono, T. Ogawa, and Y. Taniuchi. The critical Sobolev inequalities in Besov spaces and regularity criterion to some semi-linear evolution equations. *Mathematische Zeitschrift*, 242(2):251–278, 2002.
- [68] H. Brezis and T. Gallouet. Nonlinear schrödinger evolution equations. *Nonlinear Analysis: Theory, Methods & Applications*, 4(4):677 – 681, 1980.
- [69] H. Brezis and S. Wainger. A note on limiting cases of Sobolev embeddings and convolution inequalities. *Communications in Partial Differential Equations*, 5(7):773–789, 1980.
- [70] J. Málek, J. Nečas, M. Rokyta, and M. Růžička. *Weak and measure-valued solutions to evolutionary PDEs*, volume 13 of *Applied Mathematics and Mathematical Computation*. Chapman and Hall, London, 1996.
- [71] F. Roters, P. Eisenlohr, L. Hantcherli, D.D. Tjahjanto, T.R. Bieler, and D. Raabe. Overview of constitutive laws, kinematics, homogenization and multiscale methods in crystal plasticity finite-element modeling: Theory, experiments, applications. *Acta Materialia*, 58(4):1152 – 1211, 2010.
- [72] F. Roters, P. Eisenlohr, T.R. Bieler, and D. Raabe. *Crystal Plasticity Finite Element Methods*. Wiley-VCH Verlag GmbH & Co. KGaA, 2010.
- [73] A. Needleman. On finite element formulations for large elastic-plastic deformations. *Computers and Structures*, 20(1–3):247 – 257, 1985. Special Issue: Advances and Trends in Structures and Dynamics.
- [74] O. Cazacu and I.R. Ionescu. Dynamic crystal plasticity: An Eulerian approach. *Journal of the Mechanics and Physics of Solids*, 58(6):844 – 859, 2010.
- [75] O. Cazacu and I.R. Ionescu. Augmented Lagrangian method for Eulerian modeling of viscoplastic crystals. *Computer Methods in Applied Mechanics and Engineering*, 199(9–12):689 – 699, 2010.
- [76] Th. Richter. A fully Eulerian formulation for fluid–structure-interaction problems. *Journal of Computational Physics*, 233(0):227 – 240, 2013.
- [77] Th. Richter and Th. Wick. Finite elements for fluid–structure interaction in ALE and fully eulerian coordinates. *Computer Methods in Applied Mechanics and Engineering*, 199(41–44):2633 – 2642, 2010.
- [78] V. Girault and P.-A. Raviart. *Finite Element Methods for Navier-Stokes Equations: Theory and Algorithms (Springer Series in Computational Mathematics)*. Springer, 1986.
- [79] J.S. Howell and N.J. Walkington. Inf–sup conditions for twofold saddle point problems. *Numerische Mathematik*, 118(4):663–693, 2011.

- [80] D. Boffi, F. Brezzi, L.F. Demkowicz, R.G. Durán, R.S. Falk, and M. Fortin. *Mixed Finite Elements, Compatibility Conditions, and Applications*. Springer, 2006.
- [81] J.M. Marchal and M.J. Crochet. A new mixed finite element for calculating viscoelastic flow. *Journal of Non-Newtonian Fluid Mechanics*, 26(1):77 – 114, 1987.
- [82] F.P.T. Baaijens. Application of low-order Discontinuous Galerkin methods to the analysis of viscoelastic flows. *Journal of Non-Newtonian Fluid Mechanics*, 52(1):37 – 57, 1994.
- [83] F.P.T. Baaijens. Mixed finite element methods for viscoelastic flow analysis: A review. *J. Non-Newtonian Fluid Mech.*, pages 361–385, 1998.
- [84] A. Logg, K.-A. Mardal, and G.N. Wells, editors. *Automated Solution of Differential Equations by the Finite Element Method*, volume 84 of *Lecture Notes in Computational Science and Engineering*. Springer, 2012.
- [85] FEniCS Project, version 1.5. Available at <http://www.fenicsproject.org>.
- [86] R. Glowinski. Viscous flow simulation by finite element methods and related numerical techniques. In E. M. Murman and S. S. Abarbanel, editors, *Progress and Supercomputing in Computational Fluid Dynamics*, volume 6 of *Progress in Scientific Computing*, pages 173–210. Birkhäuser Boston, 1985.
- [87] R. Glowinski. Finite element methods for incompressible viscous flow. *Handbook of Numerical Analysis*, 9:3–1176, 2003.
- [88] S.C. Brenner and L.R. Scott. *The mathematical theory of finite element methods*. Texts in applied mathematics. Springer, New York, Berlin, Paris, 2002.
- [89] M. Fortin and R. Pierre. On the convergence of the mixed method of Crochet and Marchal for viscoelastic flows. *Computer Methods in Applied Mechanics and Engineering*, 73(3):341 – 350, 1989.
- [90] C. Taylor and P. Hood. A numerical solution of the Navier-Stokes equations using the finite element technique. *Computers & Fluids*, 1(1):73 – 100, 1973.
- [91] M. Fortin and A. Fortin. A new approach for the FEM simulation of viscoelastic flows. *Journal of Non-Newtonian Fluid Mechanics*, 32(3):295 – 310, 1989.
- [92] J. Baranger and D. Sandri. A formulation of Stokes’s problem and the linear elasticity equations suggested by the Oldroyd model for viscoelastic flow. *ESAIM: Mathematical Modelling and Numerical Analysis - Modélisation Mathématique et Analyse Numérique*, 26(2):331–345, 1992.
- [93] A.N. Brooks and T.J.R. Hughes. Streamline upwind/Petrov-Galerkin formulations for convection dominated flows with particular emphasis on the incompressible navier-stokes equations. *Computer Methods in Applied Mechanics and Engineering*, 32(1–3):199 – 259, 1982.
- [94] C.W. Hirt, A.A. Amsden, and J.L. Cook. An Arbitrary Lagrangian-Eulerian computing method for all flow speeds. *Journal of Computational Physics*, 14(3):227–253, 1974.
- [95] T. Hughes, W.K. Liu, and T. K. Zimmermann. Lagrangian-Eulerian finite element formulation for incompressible viscous flows. *Computer Methods in Applied Mechanics and Engineering*, 29(3):329–349, 1981.

- [96] G. Scovazzi and T. Hughes. Lecture notes on continuum mechanics on arbitrary moving domains. Technical report, SAND-2007-6312P, Sandia National Laboratories, 2007.
- [97] Python Software Foundation. Python Language Reference, version 2.7. Available at <http://www.python.org>.
- [98] PETSc: Portable, Extensible Toolkit for Scientific Computation. Available at <http://www.mcs.anl.gov/petsc/>.
- [99] MUMPS: a MULTifrontal Massively Parallel sparse direct Solver. Available at <http://mumps.enseeiht.fr/>.
- [100] P. Minakowski. Fluid model of crystal plasticity: Numerical simulations of 2-turn equal channel angular extrusion. *Technische Mechanik*, 34(3-4):213–221, 2014.
- [101] P. Minakowski, J. Hron, J. Kratochvíl, M. Kružík, and J. Málek. Plastic deformation treated as material flow through adjustable crystal lattice. *IOP Conference Series: Materials Science and Engineering*, 63(1):012130, 2014.
- [102] M.D. Uchic, D.M. Dimiduk, J.N. Florando, and W.D. Nix. Sample dimensions influence strength and crystal plasticity. *Science*, 305(5686):986–989, 2004. cited By 945.
- [103] M.D. Uchic, P.A. Shade, and D.M. Dimiduk. Plasticity of micrometer-scale single crystals in compression. *Annual Review of Materials Research*, 39(1):361–386, 2009.
- [104] Y.S. Choi, M.D. Uchic, T.A. Parthasarathy, and D.M. Dimiduk. Numerical study on microcompression tests of anisotropic single crystals. *Scripta Materialia*, 57(9):849 – 852, 2007.
- [105] Z.Y. Liu, G.X. Liang, E.D. Wang, and Z.R. Wang. The effect of cumulative large plastic strain on the structure and properties of a Cu-Zn alloy. *Materials Science and Engineering: A*, 242(1–2):137 – 140, 1998.
- [106] K. Nakashima, Z. Horita, M. Nemoto, and T.G. Langdon. Development of a multi-pass facility for equal-channel angular pressing to high total strains. *Materials Science and Engineering: A*, 281(1–2):82 – 87, 2000.
- [107] J. Freund and R. Stenberg. On weakly imposed boundary conditions for second order problems. *Proceedings of the International Conference on Finite Elements in Fluids*, pages 327–336, 1995.
- [108] M. Kuroda and V. Tvergaard. On the formulations of higher-order strain gradient crystal plasticity models. *Journal of the Mechanics and Physics of Solids*, 56(4):1591–1608, 2008.
- [109] M. Kuroda and V. Tvergaard. A finite deformation theory of higher-order gradient crystal plasticity. *Journal of the Mechanics and Physics of Solids*, 56(8):2573 – 2584, 2008.
- [110] M. Kuroda. On large-strain finite element solutions of higher-order gradient crystal plasticity. *International Journal of Solids and Structures*, (48):3382–3394, 2011.
- [111] K. Kowalczyk-Gajewska, K. Szwertnia, J. Kawałko, K. Wierzbowski, M. Wronski, K. Frydrych, S. Stupkiewicz, and H. Petryk. Texture evolution in titanium on complex deformation paths: Experiment and modelling. *Materials Science and Engineering: A*, 637(0):251 – 263, 2015.

- [112] A. Kufner, O. John, and S. Fucik. *Function Spaces*, volume 3 of *Mechanics: Analysis*. Springer Netherlands, 1 edition, 1977.
- [113] H. Triebel. *Interpolation Theory, Function Spaces, Differential Operators*. North-Holland, Amsterdam, 1978.
- [114] J. Simon. Compact sets in the space $L^p(0, t; B)$. *Ann. Mat. Pura Appl.*, 146:65–96, 1987.
- [115] W. Walter. *Differential and Integral Inequalities*. Springer-Verlag, Berlin/Heidelberg/New York, 1970.
- [116] W.F. Osgood. Beweis der existenz einer losung der differentialgleichung $dy/dx = f(x, y)$ ohne hinzunahme der Cauchy-Lipschitz'schen bedingung. *Monatshefte fur Mathematik und Physik*, 9(1):331–345, 1898.
- [117] Z. Martinec. Continuum mechanics (lecture notes). <http://geo.mff.cuni.cz/vyuka/Martinec-ContinuumMechanics.pdf>, 2011.
- [118] I-S. Liu and R. Sampaio. Remarks on material frame-indifference controversy. *Acta Mechanica*, 225(2):331–348, 2014.